A STUDY OF THE POTENTIAL ADVANTAGES OF LIGHT BEAMS IN WEAK AND STRONG TURBULENT ATMOSPHERES TO SATISFY ROBUST FREE SPACE COMMUNICATION CHANNELS WITH LONGER LINK DISTANCES

ALI ABDULRAHMAN DHYEAB AL-SAJEE

JULY 2018

A STUDY OF THE POTENTIAL ADVANTAGES OF LIGHT BEAMS IN WEAK AND STRONG TURBULENT ATMOSPHERES TO SATISFY ROBUST FREE SPACE COMMUNICATION CHANNELS WITH LONGER LINK DISTANCES

A THESIS SUBMITTED TO
THE GRADUATE SCHOOL OF NATURAL AND APPLIED SCIENCES OF
ÇANKAYA UNIVERSITY

BY
ALI ABDULRAHMAN DHYEAB AL-SAJEE
IN PARTIAL FULFILLMENT OF THE REQUIREMENTS FOR THE DEGREE OF
DOCTOR OF PHILOSOPHY

IN
THE DEPARTMENT OF
ELECTRONIC AND COMMUNICATION ENGINEERING

JULY 2018

Title of Thesis: **A study of the potential advantages of light beams in weak and strong turbulent atmospheres to satisfy robust free space communication channels with longer link distances**

Submitted by **ALI ABDULRAHMAN DHYEAB AL-SAJEE**

Approval of the Graduate School of Natural and Applied Sciences, Çankaya University.

Prof. Dr. Çan ÇOĞUN
Director

I certify that this thesis satisfies all the requirements as a thesis for the degree of Doctor of Philosophy (Ph.D.).

Dr. Selma Üzaydın

Assist. Prof. Dr.Özgür ERGÜL (4)
Acting Head of Department

This is to certify that we have read this thesis and that in our opinion it is fully adequate, in scope and quality, as a thesis for the degree of Doctor of Philosophy (Ph.D.).

Prof. Dr. Halil T. EYYUBOĞLU
Supervisor

Examination Date: 06.07.2018

Examining Committee Members

Prof. Dr. Halil T. EYYUBOĞLU	(Çankaya Univ.)
Assoc. Prof. Dr. Fırat HARDALAÇ	(Gazi Univ.)
Assist. Prof. Dr. Javad RAHEBI	(THK Univ.)
Assist. Prof. Dr. Ulaş BELDEK	(Çankaya Univ.)
Assist. Prof. Dr. Barbaros PREVEZE	(Çankaya Univ.)

STATEMENT OF NON-PLAGIARISM PAGE

I hereby declare that all information in this document has been obtained and presented in accordance with academic rules and ethical conduct. I also declare that, as required by these rules and conduct, I have fully cited and referenced all material and results that are not original to this work.

Name, Last Name: **ALI ABDULRAHMAN DHYEAB AL-SAJEE**

Signature : 

Date : 06.07.2018

ABSTRACT

A STUDY OF THE POTENTIAL ADVANTAGES OF LIGHT BEAMS IN WEAK AND STRONG TURBULENT ATMOSPHERES TO SATISFY ROBUST FREE SPACE COMMUNICATION CHANNELS WITH LONGER LINK DISTANCES

ALI ABDULRAHMAN DHYEAB AL-SAJEE

PH.D., Department of Electronic and Communication Engineering

Supervisor: Prof. Dr. Halil T. Eyyuboğlu

July 2018, 112 pages

Firstly, plane phase distribution sources and receivers with multi-values of topological charge were evaluated in this study. This evaluation was implemented in a computer environment. It is expected that our results will be beneficial to optical links incorporating the use of the Gaussian vortex, Elliptical Gaussian vortex, and Laguerre-Gaussian vortex beams. Computer modeling of the phase distributions of vortex beams was investigated by numerical simulation of propagation through free space. This work will help to know the phase distribution receiver by changing the numbers of the topological charge and to estimate those receivers' messages in the photodetector device. Secondly, a scintillation index (SI) formulation was carried out for the Gaussian beam on the propagation length in a turbulent atmosphere depending on the generalized beam formulation of the field. The scintillation

methods were compared in order to determine the best method that describes the phenomenon. Three types of scintillation methods were examined: the Rytov, Huygens-Fresnel and Random Phase Screen. From our graphical outputs, it was observed that the Random Phase Screen exhibits an acceptable scintillation index value. Thirdly, the results indicate that the topological charge of the Laguerre-Gaussian beam has a greater effect than the degree of the polynomial on the SI values. Moreover, if the polynomial degree is fixed, the SI has lower values in cases of a topological charge increase. Therefore, for a good state of transmission, it is recommended that the degree of the polynomial be made equal to 1 and the topological charge numbers equal to 0, 1, 2, 3, 4, 5 and 6. Fourthly, the Gaussian, Elliptical, Laguerre and Bessel vortex beams were selected and measurements of the SI were computed for different values of the n and m parameters for their beams. Then, it was found that the Elliptical beam with topological charges equaling 7 and 3 was best. Fifthly, the Gaussian beam and Gaussian vortex beams were chosen and measurements of the scintillation index were computed for the different values of the parameters of the Gaussian vortex beams. Then, it was shown that the Gaussian vortex beams with the degree of the polynomial and the topological charge equaling values of $n = 6$, $m = 3$ and $n = 5$, $m = 6$ were better than the Gaussian beam. Despite the increasing propagation distance, the SI values of the Gaussian vortex beam remained between 0.04 and 0.14 with an increase in this propagation distance compared with the Gaussian beam, the value of whose scintillation index will increase with an increase in the propagation distance. Sixthly, receiver intensities for the Laguerre-Gaussian beam in free space are affected by changes in the polynomial parameters of the Laguerre beam. It becomes evident that when the degree of the

polynomial and the topological charge parameters are the same, the receiver intensities of the Laguerre-Gaussian beam become more separate.

Finally, we compute the Symbol Error Rate for the Gaussian vortex beam for 8-Mary against a structure constant, and it appears that the Symbol Error Rate increases with an increasing structure constant parameter. The prime idea of this study is that distribution sources and receivers are more beneficial to optical channels, and the Random Phase Screen method is an acceptable method for computing the scintillation; then the Gaussian vortex beam is better than the Gaussian beam, and we can change the values of the topology parameter and polynomial degree of the Laguerre-Gaussian beam or other beams, such as the Gaussian vortex beam, to decrease the value of the scintillation index. In the end, the symbol error rate is increased by increasing the structure constant of turbulence.

Keywords: Turbulence; Phase distribution; Scintillation index (SI); Topological Charge; Random Phase Screen (RPS); Symbol Error Rate (SER).

ÖZ

UZUN BAĞLANTI MESAFELİ SERBEST UZAY İLETİŞİM KANALINI GÜÇLENDİRMEK İÇİN DALGALI ATMOSFERDE ZAYIF VE GÜÇLÜ IŞINLARIN POTANSİYEL AVANTAJLARI ÇALIŞMAS

ALI ABDULRAHMAN DHYEAB AL-SAJEE

Yüksek Lisans, Elektronik ve Bilişim Mühendisliği Bölümü

Tez Yöneticisi: Prof. Dr. Halil T. Eyyuboğlu

Tammuz 2018, 112 sayfa

Bu çalışmada, ilk olarak, topolojik yükün çoklu-değerlerinde düzlemdeki faz dağıtım kaynakları ve alıcıları değerlendirilmiştir. Bu değerlendirme bilgisayar ortamında uygulanmıştır. Bulgularımızın, Gaussian vortex, Eliptik Gaussian vortex ve Laguerre-Gaussian vortex ışınlarının kullanılmasıyla ilgili optik bağlantılarda yararlı olması beklenmektedir. Vorteks ışınlarının faz dağılımlarının bilgisayar modellemesi, serbest uzay boyunca yayılımının sayısal simülasyonu ile incelenmiştir. Bu işlem, topolojik yükün sayılarının faz dağılımı alıcısında değişiminin bilinmesine ve bu alıcıların mesajlarının fotodetektör cihazında tahmin edilmesine yardımcı oldu, ki bu çalışmanın ilk kısmıydı. İkinci olarak, alanın genelleştirilmiş ışın formülasyonuna bağlı olarak dalgalı bir atmosferde yayılma uzunluğu üzerindeki Gaussian ışını için bir sintilasyon indeksi formülasyonu gerçekleştirilmiştir. Sintilasyon indeks yöntemleri, fenomeni en iyi nasıl tanımlayacağımızı seçmek için karşılaştırıldı. üç tip sintilasyon indeksi yöntemi incelendi: Rytov, Huygens-Fresnel ve Rastgele Faz Ekranı. Grafiksel

çıktılarımızdan, Rastgele Faz Ekranının kabul edilebilir bir sintilasyon indeksi değeri sergilediği gözlemlenmiştir. Üçüncü olarak, sonuçlar, SI değerleri üzerinde, LGVB'nin topolojik yükünün (m) polinom derecesine (n) göre daha büyük bir etkiye sahip olduğu ve topolojik yükün (m) değiştiği ve polinom derecesinin (n) sabitlendiği durumlarda, SI'nın daha düşük değerlere sahip olduğunu göstermektedir. Bu nedenle, iyi bir iletim durumu için, polinom derecesinin n = 1'e eşit olması ve topolojik yük sayısının gibi, 0, 1, 2, 3, 4, 5 ve 6'ya eşit olması önerilmektedir. Dördüncüsü, Gauss, Eliptik, Laguerre ve Bessel Vorteks Işınları seçildi ve SI'nın ölçümleri, n ve m parametrelerinin farklı değerlerindeki ışınları için hesaplandı. Daha sonra, topolojik yükü (m)'in 7 ve 3'e eşit olan Eliptik ışınının en iyisi olduğu bulunmuştur. Beşinci olarak, Gauss Işını ve Gaussian vortex Işınları seçilmiş ve Sintilasyon indeks ölçümleri GVB'nin (n) ve (m) parametrelerinin farklı değerleri için hesaplanmıştır. Daha sonra, polinom derecesi ve topolojik yükü eşitleme değerleri $n=6,\ m=3$ and $n=5,\ m=6$ olan GVB'nin, GB'den daha iyi olduğu gösterilmiştir. Her ne kadar artan bir yayılma mesafesi olsa da, GVB'nin SI değerleri 0.04 ile 0.14 arasında kalmıştır ve bu yayılma mesafesi GB'deki SI değerlerine kıyasla artmaktadır. Altıncı olarak, serbest uzaydaki LGVB için alıcı yoğunlukları, Laguerre ışınının polinom parametrelerindeki değişikliklerden etkilenmektedir. (n) ve (m) parametrelerinin aynı olduğu durumlarda, LGVB'lerin alıcı yoğunluklarının daha ayrık olduğu ve bunun da düşük Sembol Hata Oranı değerine neden olacağı açıktır. Son olarak, 8-Mary için türbülans yapı sabiti 'ye karşı Laguerr Gaussian vortex ışınları için Sembol Hata Oranı hesaplanmaktadır ve türbülans yapı sabiti parametresinin artırılmasıyla Sembol Hata Oranı arttığı açıkça görülmektedir. Bu çalışmanın önemi, dağıtım kaynakları ve alıcıları optik kanallar için daha faydalı ve RPS yönteminin, bilgisayarlı Sintilasyon indeks hesaplama için kabul edilebilir

bir yöntem, Gaussian vorteks ışınının Gaussian ışınından daha iyi olduğunun ve sintilasyon değerlerininin düşürülmesi için Gaussian ışınındaki veya diğer ışınlardaki topoloji parametresi (m) ve polinom derecesi (n) değerlerinde değişiklik yapabileceğimizin ve son olarak sembol hata oranı, türbülans yapı sabiti C_n^2'nin artışı ile artabileceğinin gösterilmesindedir.

Anhtar Kelimeler: Türbülans; Faz dağılımı; Sintilasyon indeksi (SI); Topolojik Yük; Sembol Hata Oranı (SER).

ACKNOWLEDGEMENTS

I would like to express my sincere gratitude to Prof. Dr. Halil T. Eyyuboğlu, for his supervision, special guidance, suggestions, and encouragement through the development of this thesis.

It is a pleasure to express my special thanks to my family and my wife for their care, patience, and valuable support during the years of study.

TABLE OF CONTENTS

STATEMENT OF NON-PLAGIARISM PAGE iii

ABSTRACT iv

ÖZ xviii

ACKNOWLEDGEMENTS xi

Table of Contents xii

LIST OF FIGURES xv

LIST OF TABLES xx

LIST OF ABBREVIATIONS xxi

CHAPTER 1 1

INTRODUCTION AND MOTIVATION 1

CHAPTER 2 8

LITERATURE SURVEY 8

CHAPTER 3 13

MATRIX OPTICS APPROACH 13

3.3.1 Paraxial Approximation for the ABCD Matrix 17

3.3.2 Scintillation Index using the Huygens-Fresnel Integral 21

CHAPTER 4 25

SCINTILLATION INDEX EQUATION BY USING THE RYTOV APPROACH 25

4.3.1 Computation of First-Order Field Perturbations $U_1(R)$ 29

4.3.2 Computation of Higher-Order Field Perturbations Um(r,L) 31

4.4.1 Computation of First-Order Spectral Representation. 35

4.4.2 Computation of Second-Order Spectral Representation. 37

CHAPTER 5 42

VORTEX BEAMS IN FREE-SPACE-OPTICS WITH TURBULENCE ATMOSPHERE 42

5.1 Introduction 42

5.2 Free space optics 44

5.3 Optical turbulence 47

5.4 Vortex Beams 49

5.4.1 Phase Distribution of Vortex Beams 50

5.4.2 Scintillation of Laser Beams 50

CHAPTER 6 51

THEORETICAL BACKGROUND OF GAUSSIAN BEAM AND GAUSSIAN VORTEX BEAMS 51

6.1. Introduction 51

6.2. Expression of Gaussian Beam (GB) 51

6.3. Formulation of Source and Receiver Plane Intensities for Gaussian Beam 52

6.4. The Methods for Computing Scintillation Index. 52

6.4.1 Huygens-Fresnel Method 54

6.4.2 Rytov Method 98

6.4.3 Random Phase Screen Method 98

6.5 Expression of Gaussian Vortex Source Beams 106

CHAPTER 7 110

RESULTS AND DISCUSSION 110

7.1 Introduction 110

7.2. Phase Distribution Behavior with Multi-values of Topological Charge of Vortex Beams 112

7.2.1. Gaussian Vortex Beam 112

7.2.2. Elliptical Gaussian Vortex Beam 114

7.2.3 Laguerre-Gaussian Vortex Beam 115

7.3 Computing the Scintillation Index of a Gaussian Beam Using Different Methods 117

7.3.1. SI Results with the Rytov Method 118

7.3.2. SI Results with the Huygens-Fresnel Method 121

7.3.3. SI Results using the Random Phase Screen Method 125

7.4. Results of the Scintillation Index for LGVB 132

7.4.1. Topological Charge for LGVB Being Constant 132

7.4.2. Polynomial Degree for the LGVB Being Constant 75

7.5. Comparisons between Gaussian, Elliptical, Laguerre and Bessel Vortex Beams 142

7.6 Comparison between Gaussian and Vortex Gaussian Beams 152

7.7. The effect of Turbulence on the Average Intensity of the Laguerre Beam 86

7.8. Effect of Polynomial Parameters of LGVB on Intensities of the Receiver in Free Space 156

CHAPTER 8 168

CONCLUSION AND FUTURE WORK 168

8.1 Conclusion 168

8.2 Future Work 97

REFERENCES 175

APPENDIX A1

A.1 Curriculum Vitae

LIST OF FIGURES

Figure 1: A ray is characterized by its coordinate (Y) and its angle (θ) [7]. 14

Figure 2: A ray enters an optical system at location Z_1 with position Y_1 and angle θ_1 and leaves at position Y_2 and angle θ_2 at location Z_2 14

Figure 3: Line-of-sight section of length L of optical ray 16

Figure 4: A ray-matrix optical system in cascade 18

Figure 5: Geometry of propagation of the optical ray. 19

Figure 6: Propagation path without optical elements 23

Figure 7: Two points of the optical path transverse to the axis of propagation 30

Figure 8: Random Phase Screen Model of the propagation of the beam in turbulence 106

Figure 9: Source and receiver planes phase distribution of Gaussian vortex beam with the topological charge of $m = m_{-3} = -3$, $m = m_3 = 3$, $m = m_{-5} = -5$, $m = m_5 = 5$, $m = m_{-7} = -7$ and $m = m_7 = 7$ 114

Figure 10: Source and receiver planes phase distribution of Elliptical Gaussian vortex beam with the topological charge of $m = m_{-3} = -3$, $m = m_3 = 3$, $m = m_{-5} = -5$, $m = m_5 = 5$, $m = m_{-7} = -7$ and $m = m_7 = 7$.....115

Figure 11: Source and receiver planes phase distribution of Laguerre-Gaussian vortex with the topological charge of $m = m_{-3} = -3$, $m = m_3 = 3$, $m = m_{-5} = -5$, $m = m_5 = 5$, $m = m_{-7} = -7$ and $m = m_7 = 7$.....117

Figure 12: Scintillation behavior of the Gaussian beam against the propagation distance using the Rytov method for λ = 1.35 μm.....119

Figure 13: Scintillation behavior of the Gaussian beam against the propagation distance using the Rytov method for λ = 1.55 μm.....120

Figure 14: Scintillation behavior of the Gaussian beam against the propagation distance using the Rytov method for λ = 1.35 μm and λ = 1.55 μm 121

Figure 15: Scintillation behavior of the Gaussian beam against the propagation distance using the Huygens-Fresnel method for λ = 1.35 μm 123

Figure 16: Scintillation behavior of the Gaussian beam against the propagation distance using the Huygens-Fresnel method for λ = 1.55 μm 124

Figure 17: Scintillation behavior of the Gaussian beam against the propagation distance using the Huygens-Fresnel method for λ = 1.35 μm and λ = 1.55 μm 125

Figure 18: Scintillation behavior of the Gaussian beam against the propagation distance using the Random Phase Screen method for λ = 1.35 μm.....128

Figure 19: Scintillation behavior of the Gaussian beam against the propagation distance using the Random Phase Screen method for λ = 1.55 μm.....129

Figure 20: Scintillation behavior of the Gaussian beam against the propagation distance using the Random Phase Screen method for λ = 1.35 μm and λ = 1.55 μm 130

Figure 21: Scintillation behavior of the Gaussian beam against the propagation distance using the Rytov, Huygens-Fresnel and Random Phase Screen methods for λ = 1.35 μm 131

Figure 22: Scintillation behavior of the Gaussian beam against the propagation distance using the Rytov, Huygens-Fresnel and Random Phase Screen methods for λ = 1.55 μm 132

Figure 23: Scintillation variation of the LGVB with the degree of the polynomial when the topological charge is fixed to m = 1 against the propagation distance.....137

Figure 24: Scintillation variation of the LGVB with the degree of the polynomial when the topological charge is fixed to m = 3 against the propagation distance.....138

Figure 25: Scintillation variation of the LGVB with the degree of the polynomial when the topological charge is fixed to m = 5 against the propagation distance.....139

Figure 26: Scintillation variation of the LGVB with the topological charge when the degree of the polynomial is fixed to $n = 1$ against the propagation distance 140

Figure 27: Scintillation variation of the LGVB with the topological charge when the degree of the polynomial is fixed to $n = 3$ against the propagation distance 141

Figure 28: Scintillation variation of the LGVB with the topological charge when the degree of the polynomial is fixed to $n = 5$ against the propagation distance 142

Figure 29: Aperture Averaged Scintillation variation of GVB with the topological charges equal to 3 and 6, and the degrees of the polynomial equal to 6 and 5 against the propagation distance 148

Figure 30: Aperture Averaged Scintillation variation of the Elliptic beam with the topological charges equal to 7 and 3 against the propagation distance 149

Figure 31: Aperture Averaged Scintillation variation of the LGVB with the topological charges equal to ($m = 3$) and the degrees of the polynomial equal to 11and 5 against the propagation distance 150

Figure 32: Aperture Averaged Scintillation variation of the BGVB with topological charges equal to 6 and 5 against the propagation distance (L in km). 151

Figure 33: Changes in the Aperture Averaged Scintillation taking a variety of values of the n and m parameters for multi-types of beams against the propagation distance. 152

Figure 34: Changes of the SI taking a variety of values of the *n* and *m* parameters for GB beams against the propagation distance.....85

Figure 35: Changes in the SI taking a variety of values of the *n* and *m* parameters for GVB beams against the propagation distance 154

Figure 36: Average Receiver Intensity against r_x and r_y in free space.....155

Figure 37: Average Receiver Intensity against r_x and r_y in turbulence.....156

Figure 38: A two-dimensional view of receiver plane intensities of Laguerre Gaussian vortex beam with *n* = 1 and *m* = 1, 3, 5 and 7 161

Figure 39: A two-dimensional view of receiver plane intensities of Laguerre Gaussian vortex beam with *n* = 7 and *m* = 1, 3, 5 and 7.....162

Figure 40: A two-dimensional view of receiver plane intensities of Laguerre Gaussian vortex beam with *n* = 1, 3, 5 and 7 and *m* = 1.....163

Figure 41: A two-dimensional view of receiver plane intensities of Laguerre Gaussian vortex beam with *n* = 1, 3, 5, and 7 and *m* = 7.....164

Figure 42: A two-dimensional view of receiver plane intensities of Laguerre Gaussian vortex beam with *n* = 1, 3, 5, and 7 and *m* = 1, 3, 5, and 7 165

Figure 43: Symbol error rate against the structure constant C_n^2 for 8-Mary 166

Figure 44: Symbol error rate in semi-log format plotted against the structure constant C_n^2 for 8-Mary. 167

LIST OF TABLES

Table 1: Ray Matrices for Various Optical Elements [7]. 17

Table 2: Variation of values of SI between Gaussian vortex (GVB) and Elliptical Gaussian vortex (EGVB) beams.....80

Table 3: Variation of values of SI between Laguerre Gaussian vortex (LGVB) and Bessel Gaussian vortex (BGVB) beams 81

Table 4: Effect of Laguerre polynomial parameters ($n = 1$ and $m = 1, 3, 5$ and 7) on receiver intensities in free space. 158

Table 5: Effect of Laguerre polynomial parameters (n = 7 and m = 1, 3, 5 and 7) on receiver intensities in free space 158

Table 6: Effect of Laguerre polynomial parameters (n = 1 and m = 1, 3, 5 and 7) on receiver intensities in free space 159

Table 7: Effect of Laguerre polynomial parameters (n = 7 and m = 1, 3, 5 and 7) on receiver intensities in free space 89

Table 8: Effect of Laguerre polynomial parameters (m = n = 1, 3, 5 and 7) on receiver intensities in Free Space 160

LIST OF ABBREVIATIONS

RF	Radio Frequency
FSO	Free-Space Optical
SER	Symbol Error Rate
MIT	Massachusetts Institute of Technology
OWC	Optical Wireless Communications
RONJA	Reasonable Optical Near Joint Access
LED	Light Emmitt Diode
LCD	Liquid Crystal Display
PDA	Personal Digital Assistant
RAGSM	Rectangular Array Gaussian Schell-model
MD	Multiuser Diversity
SI	Scintillation Index
IR	Infrared
GOM	Geometric Optic Method
LANs	Local Area Network
DSL	Digital Subscriber Line
FSOC	Free Space Optical Communication
LIDAR	Light Detection and Ranging
LADAR	Laser Radar
OAM	Orbital Angular Momentum
RPS	Random Phase Screen

GB	Gaussian Beam
GVB	Gaussian Vortex Beam
EGVB	Elliptical Gaussian Vortex Beam
BGVB	Bessel Gaussian Vortex Beam
LGVB	Laguerre Gaussian Vortex Beam
m	Topological Charge
n	Degree of Polynomial
l_0	Inward Size of Turbulence
L_0	Large Size of Turbulence
C_n^2	Structure Constant
σ_1^2	Irradiance Fluctuations
λ	Wavelength
K	Three-dimensional wave vector
N_s	Random Phase Screens Numbers
N_R	Number of Realizations (runs)
N_g	Number of Grid Points
L_s	Source Aperture Length
L_r	Side Length of Square Aperture Opening of the Receiver Plane
d_1	Grid Spacing of Source Plane
d_2	Grid Spacing of Receiver Plane
$b^2(r,L)$	Scintillation Index for Specific Location
$b^2(L)$	Aperture Averaged Scintillation (Power Scintillation)
ΔL	Distance Between the Two Screens
F_G	Focal Length
W_G	Aperture Radius
L	Propagation Distance

W_0	Beam radius
Φ_s	Phase distribution of source
Φ_r	Phase distribution of receive
F_0	Phase of the radius of curvature
$\Psi(r,s)$	Random Part of the Complex Phase
$\Psi_1(r,s)$	First Order Perturbations
$\Psi_2(r,s)$	Second Order Perturbations
$n_1(s,z)$	Refractive Index in 2D
$J_0(x)$	Bessel function of the first kind and order zero
$U_s(s_x,s_y)$	Source Field
$U_r(r_x,r_y,L)$	Receiver Field
$\langle\ \rangle$	Mean Value
*	Conjugate Operator
Γ	Mutual Coherence Function
$\langle I(r,L)\rangle$	Average Intensity on Receiver Plane
$\langle I(r,L)\rangle^2$	Squared Average Intensity on Receiver Plane
$\langle I^2(r,L)\rangle$	Average of the Square Intensity on Receiver Plane
$\phi(r_x,r_y)$	Spatial Phase Distribution
α_s	Source Size
(f_x,f_y)	Spatial Frequency in x and y Directions.
ε_s	Degree of Elasticity
F	Fourier transform
F^{-1}	Inverse operator of Fourier transform
∇^2	Laplace Operator

CHAPTER 1

INTRODUCTION AND MOTIVATION

1.1 Background

The Navy in America depends intensely on radio frequency (RF) correspondence systems and this dependence creates two major operational constraints: bandwidth, and absence of possibility, the ability in cases of jamming or identification by enemies [1, 2]. One conceivable corresponding answer for current RF systems is the use of free-space optical (FSO) communication systems. Free-space optical communication links have high bandwidth and are highly directional, which makes them difficult to identify or jam. Optical free-space communications have the particular important points when compared with microwave systems and conventional radio frequency in terms of security and the capacity of transmission of information [3]. Therefore, interest in optical communication channels has been on the rise for the last 45 years [4]. Additionally, there has been a considerable measure of enthusiasm throughout the years in the likelihood of utilizing optical transmitters for satellite communications. In spite of a large number of the early formative projects ending because of financing reductions, there was recharged enthusiasm in the 1990s for the utilization of optical transmitters for correspondence channels interfacing ground/airborne-to-space or space-to-ground/airborne information links

through the atmosphere [5, 6]. The atmosphere alludes to the zone surrounding the surface of the Earth to a distance of a few hundred kilometers, and it is composed of numerous elements, principally nitrogen and oxygen, and compounds including water, carbon dioxide, carbon monoxide, nitrous oxide and ozone. These particles affect the transmission of an optical wave by scattering and absorbing it and changing its refractive index. Different layers of the atmosphere show one kind of temperature, pressure, and density characteristics, which assume an essential part in the refractive index. The absorbed radiation is one of the major functions of the atmosphere, and electromagnetic radiation in the atmosphere is weakened at visible and infrared (IR) ranges due to absorption and scattering. Both absorption and scattering are deterministic impacts which can be anticipated, in light of an assortment of atmospheric conditions, for example, latitude, altitude and meteorological range.

The most injurious impacts of the atmosphere on a propagating laser beam are for the most part caused by small random temperature fluctuations which are shown as variations in the index of refraction. The cascade theory of turbulence, attributed to Kolmogorov, depicts turbulent air movement as a set of eddies, which are turbulence cells formed by pockets of air with a constant index of refraction ranging in scale and size from the inward size of turbulence (l_0) to the large size of turbulence (L_0) (Dorn 2001). In the layer at the surface up to around 100 meters, the outer scale is accepted to develop perpendicularly with the height over the ground, while the inward scale is an insignificant number of millimeters close to the surface (in spite of the fact that it can be as large as a few centimeters in the upper regions of the atmosphere). As they are affected by inertial forces, large eddies separate into

smaller eddies, shaping a series of scale sizes between (L_0) and (l_0) known as the inertial range. Vortices smaller than (l_0) are thought to be in the dispersal extent. In spite of the fact that the cascade theory alludes to changes in speed, the turbulence prompted by the speed of the wind causes a non-stop blending which brings refraction fluctuations. The index of refraction fluctuations is only caused by temperature variations resulting from this mixing. All fluctuations occur in the visible and near infrared areas of the spectrum. The execution of a laser radar (LADAR) or lasercom system can be essentially decreased by turbulence-induced scintillation coming about because of beam propagation through the atmosphere [6]. In particular, scintillation can lead to power losses at the receiver side and in the long run to a fading of the received signal [6]. Optical turbulence is caused by the arbitrarily changing refractive index along the path of propagation, and it causes a distortion in the optical wave [3]. The refractive index structure parameter, C_n^2 is adequately steady in the instance of horizontal propagation paths; however, it is a function of altitude in the case of vertical or inclined paths, and it is thought to be the most basic parameter along the propagation path in describing the impacts of atmospheric turbulence [7]. In the case of plane or spherical waves, which are limiting cases of the Gaussian beam, the Rytov variance, $\sigma_1^2 = 1.23 C_n^2 k^{7/6} L^{11/6}$, which represents the irradiance fluctuations associated with an unbounded plane wave, determines what we consider to be weak $(\sigma_1^2 \ll 1)$, moderate, or strong $(\sigma_1^2 > 1)$ fluctuation conditions. C_n^2 is the structure constant of the index of refraction, $k = 2\pi / \lambda$, is wave number, L the distance of propagation, and (λ) is the wavelength. As indicated by Huygens' Principle [8], all the subwaves at a specific distance contribute to the aggregate electric field at a greater propagation distance. In

this manner the further the wave propagates, the more distortion it endures. Additionally, these random phase velocities obtained by the electric field prompt random changes in beam direction and intensity fluctuations (scintillation). Apart from very dispersed particles, such as rain drops or snow flakes, scintillation is the most severe limitation to system performance in optical communications, such as a binary communication channel. It can represent the propagation in turbulence with a model such as the Random Phase Screen Model, for this method, two new steps are introduced: (1) Some random phase screens, say N_s, must be placed between the source and receiver planes in order to model the atmospheric turbulence. The random phase distributions on these screens are to be in proportion to the atmospheric power spectral density function. (2) A number of realizations (runs), say N_R, must be made to approach the averaged analytic result. The capacity to compensate for these impacts is of extreme significance to optical systems designers. Beforehand, plane wave, spherical wave or major Gaussian beams were dealt with in a large portion of the studies [9]. As of late, optical beams with singularity points or lines where the phase or amplitude of the field is undefined or changes or changes suddenly have drawn growing interest. In this thesis, we firstly determine the phase distribution for transmitters and receivers for different types of vortex beams that will be implemented. Secondly, we intend to make a comparison among the four types of computation of scintillation index methods, such as Rytov, Huygens-Fresnel and Random Phase Screen for the Gaussian beam. Thirdly, we build up the numerical modelling capacities to explore the higher request properties of vortex beams propagating through a turbulent atmosphere and we make comparisons with

the Gaussian beam and Gaussian vortex beams for the first time. Finally, we compute the Symbol Error Rate (SER) for Laguerre-Gaussian vortex beams.

1.2. Motivation and Objectives

The free-space optical laser communication system provides an attractive alternative to radio frequency (RF) systems because of its larger bandwidth data, higher antenna gain, higher reception apparatus, smaller component sizes and antenna, and lower component costs of optic systems [10, 11]. They have been broadly utilized as a part of numerous applications, such as space communications, impermanent system establishments, additional security items for important fiber links, flying-machine-to-air-ship interchanges, last-mile arrangements and military applications [12, 13].

FSO communication systems, in spite of their promising focal points, are extremely influenced by climatic events, such as rain, haze and so on. Consequently, a large portion of the investigation concentrates on the accessibility of FSO systems under poor weather conditions. An FSO interface is seriously influenced by the physical medium of the channel, such as the growth of trees and the construction of new buildings. Consequently, future developments through the communication interface method should be precisely considered. Receiver and transmitter alignment constraints become dependent on building movements. Scintillation: As varying the temperature of the atmosphere increments, diverse air atoms from different media (house tops, ground, etc.) are warmed in an irregular manner causing fluctuations in the refractive index of the atmosphere in a period subordinate structure, which is called scintillation. Scintillation shows up as power fluctuations on the receiver side [14]. This study has an alternative approach to reducing the effect of scintillation by

selecting different types of vortex beams, and examining the scintillation behavior for each one.

1.3. Problem Statement

Free-Space Optical Communication (FSOC) can potentially provide high data rates as well as secured and license-free transmission. However, it is very helpless in atmospheric turbulence. This study researches the impact of atmospheric conditions on FSO systems to improve its achieve ability in hard conditions, which is the main objective. The specific objective of this research is to investigate attenuation caused by scintillation effects in Free Space Optics using statistical models and to study different light beams in order to choose a suitable one.

1.4. Thesis Outline

This thesis contains eight chapters. All the necessary information about the Free Space Optic, atmosphere turbulence, scintillation, symbol error rate are introduced.

Chapter 1 is an introduction to the dissertation and its motivation and objectives. Then, the chapter presents an outline of the thesis.

Chapter 2 presents a literature survey.

Chapter 3 presents an introduction to the matrix optics approach with definitions of the Ray-Transfer Matrix and ABCD Ray-Matrix using Cartesian coordinates, including the paraxial approximation for the ABCD matrix and scintillation index using the Huygens-Fresnel Integral.

Chapter 4 presents the computation of the scintillation index equation using the Rytov method. The Wave Equation is explored to deduce the Born approximation,

which will determine the first order of the perturbation field $U_1(R)$ and higher-order perturbations. The Rytov approximation is determined by depending on the Born approximation; then the 1st-order and 2nd-order spectral representations are computed.

Chapter 5 introduces a free-space-optic approach with details related to optical turbulence, vortex beams and scintillation of laser beams.

Chapter 6 presents the theoretical background of the Gaussian and Gaussian vortex beams. They are explained, and expressions of them are defined with a formulation of source and receiver plane intensities. The methods for the SI are computed following the Huygens-Fresnel, Rytov and Random phase screen methods.

Chapter 7 includes the Results and Discussion of phase distribution behavior with multi-values of topological charge for the Gaussian vortex, Elliptical Gaussian vortex, and Laguerre-Gaussian vortex beams and other results.

The following are also presented:

- ✓ Computation of the SI of the GB following the Rytov Method, Huygens-Fresnel Method, and Random Phase Screen Methods.
- ✓ Scintillation Index (SI) for the LGVB by changing the topological charge and the polynomial degree parameters.
- ✓ Comparisons among Gaussian, Elliptical, Laguerre and Bessel vortex beams
- ✓ A comparison between the Gaussian and Gaussian vortex beams.
- ✓ Computation of the Symbol Error Rate for the Gaussian vortex beam

Chapter 8 includes the conclusion and future work.

CHAPTER 2

LITERATURE SURVEY

The free-space optical communication system is defined as an optical communication innovation which utilizes air as a medium to transmit messages wirelessly from one place to another through light propagating in free space. "Free space" implies a space such as a vacuum [15]. It is possible to define the wireless infrared communication as indoor optical wireless communication while free-space optical communication as outdoor optical wireless communication [16]. The description of attenuations of FSO links for the most part come in two types: geometric and atmospheric attenuation. Geometric attenuation occurs by changing parameters such as transmitter diameter, divergence angle, link distance, and so on. However, this depends to a great extent on weather conditions such as fog and rain [17]. On June 3, 1880 at Bell's in Washington, Alexander Graham Bell and his assistant Charles Sumner Tainted produced the world's first wireless phone and photo phone. It was an ideal and most essential invention at that time, particularly for communication lines. Nevertheless, the assistance of that photo phone signal transmission at short distances, around 213 meters (700 feet), was communicated between two places [18-19]. To enhance the signal transmission distance as well as quality and security, the German military created another optical transmitter system

called the Heliograph Telegraphy transmitter. At that point, the German military considered utilizing optical Morse transmitters called ‘Blinkered,’ which was far better than the photo phone innovation of 1880. Additionally, unique Blinkgeräts were additionally effectively utilized for communication with tanks, balloons and airplanes [20].

In 1962, Massachusetts Institute of Technology (MIT) Lincoln Labs assembled experimental Optical Wireless Communications (OWC) links which utilized a light emitting GaAs diode that could transmit TV signals over a length of 30 miles (50 kilometers).

In 1967, Harger considered the problem of estimating the unknown parameters of a signal of otherwise known form distorted by both multiplicative errors that was assumed to be due to propagation through a homogeneous, isotropic turbulent medium and an additive error that was assumed to be grain noise, etc. [21].

In 2001, the first device that transmitted data at 10 Mbps wirelessly using a beam of light the range of which was 1.4 km (0.87 miles) was invented by Reasonable Optical Near Joint Access (RONJA) FSO from the Czech Republic. However, their signal was not very secure.

In 2003, the research group “OptiKom" performed reliability and availability tests on Free Space Optics (FSO) systems at the Department of Communications and Wave Propagation, where they obtained evaluation results for commercial use as well as for self-developed optical point-to-point and point-to-multipoint FSO-systems [22].

In 2006, Baykal and Eyyuboğlu created a formula for a flat-topped Gaussian beam source in atmospheric turbulence. The variations of the on-axis scintillations at the

receiver plane were evaluated versus the link length, the size of the flat-topped Gaussian source, and the wavelength at selected flatness scales. Their results showed that single Gaussian beam scintillation was smaller than those of flat-topped Gaussian beam scintillations when the source sizes were much smaller than the Fresnel zone [23].

In 2007, Fuji TV exhibited a Light Emmitt Diode (LED) backlit, Liquid Crystal Display (LCD) TV working while a data signal was transmitted to a Personal Digital Assistant (PDA) by means of light. The most redeeming feature of the device was its secure transmission of information.

In 2008, the graphical outputs, source and receiver plane expressions, the complex degree of coherence, beam size variations and power in bucket performance for higher order partially coherent dark hollow beams propagating in a turbulent atmosphere were formulated and evaluated. The results showed that higher order partially coherent dark hollow beams would initially develop an outer ring around a central lobe, but would eventually evolve towards a Gaussian shape as the propagation distance increased. It was further observed that stronger turbulence levels and greater partial coherence had similar effects on the beam profile [24].

In 2008, MRV communication introduced an FSO based telescope TS-10GE system operating at a 10-Gbit/s data rate at a distance of 350 m (1,100 feet) [25].

In 2009, Eyyuboğlu, in his contribution, formulated the area scintillation of fundamental Gaussian and annular beams and made a comparison between them showing that under the same source power conditions, annular Gaussian beams

produced far fewer scintillations than the fundamental Gaussian beams at small source sizes [26].

In 2010, by Gurvich, Vorob'ev, and Fedorova, conducted a numerical investigation of the spectra of stellar scintillations observed through the Earth's atmosphere from spacecraft. This investigation was carried out for the atmosphere containing anisotropic large-scale and isotropic small-scale inhomogeneities of the refractive index. It was shown that the strong scintillation spectra were not equal to the sum of the spectra formed by separate, statistically independent components [27].

In 2011, Pan, Zhang, Qiao and Dan introduced the study of the analytical formulas of the on-axis average irradiance and the on-axis scintillation index for a rectangular array Gaussian-Schell model (RAGSM) beams in atmospheric turbulence that was derived according to the paraxial form of the extended Huygens-Fresnel principle, their results showed that the correlated and uncorrelated superposition RAGSM beams exhibited a different on-axis intensity distribution and a similar variation of the on-axis scintillation and the bit error rate [28].

In 2013, Gilberto, Vítor and Cruz investigated the effect of the atmospheric scintillation phenomenon in a free-space optical communication system. This evalution was performed by BER computation of the FSO system for various parameters through simulations of the link combined with the already established scintillation model as the gamma-gamma model. The results showed how an FSO connection can be affected by any turbulence regime [29].

In 2014, Yang, Gao and Slim presented a comprehensive performance analysis for the free space optic communication systems with multiuser diversity (MD) over both

weak and strong atmospheric turbulence. It was observed that with multiuser diversity, strong turbulence could yield a higher capacity [30].

In 2016, Xiumin, Jian, and Lingling focused on the properties of the Hyperbolic-Cosine-Gaussian beam, which contains a spiral optical vortex and a non-spiral optical vortex, which was researched numerically. In this study, the focal shift and focal split also appeared in the focal evolution with tunable parameters of vortex terms [31].

In 2017, Mansour, Mesleh and Abaza presented a review on new challenges in wireless communication systems and examined recent approaches to dealing with and addressing some of the lately raised issues in the wireless field. Theoretical and test results about light of a number of research projects or studies were given [32].

CHAPTER 3

MATRIX OPTICS APPROACH

3.1. Definition of Matrix Optics

Matrix optics is a technique for tracing paraxial rays; the rays are assumed to travel only within a single plane. A ray is described by its position and its angle with respect to the optical z-axis. In the paraxial approximation, position and angle at the input and output planes of an optical system are related by two linear algebra equations. As a result, the optical system is described by a 2×2 matrix called the ray transfer matrix. The convenience of using matrix methods lies in the fact that the ray-transfer matrix of a cascade of optical components (or system) is a product of ray-transfer matrices.

3.2. The Ray-Transfer Matrix

The optical system formed by a succession of refracting and reflecting surfaces all center about the Z-axis. A ray crossing the transverse plane at Z is completely characterized by the Y-coordinate (Y) of its crossing point and the angle (θ), (see Fig. 1).

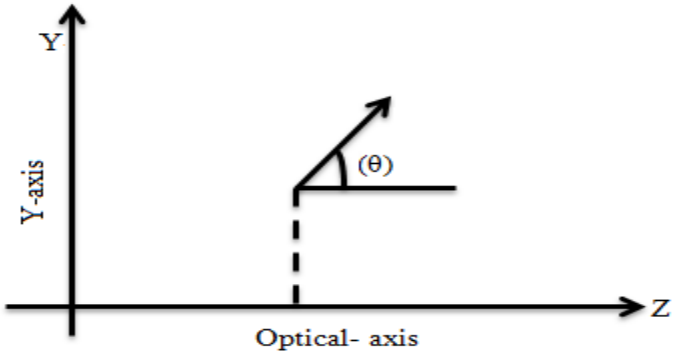

Figure 1: A ray is characterized by its coordinate (Y) and its angle (θ) [7].

An optical system is a set of optical components placed between two transverse planes (Z_1 and Z_2) referred to as the input and output planes (see Fig. 2).

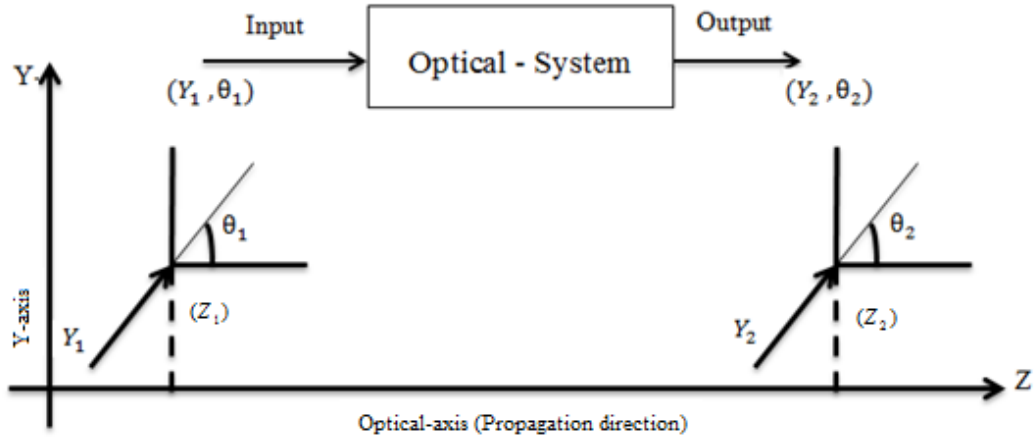

Figure 2: A ray enters an optical system at location Z_1 with position Y_1 and angle θ_1 and leaves at position Y_2 and angle θ_2 at location Z_2 [7].

where ($\sin\theta \cong \theta$ when θ value is very close to zero) , this will make the relation between (Y_2, θ_2) and (Y_1, θ_1) is linear

$$Y_2 = AY_1 + B\theta_1, \qquad (3.1\text{-A})$$

$$\theta_2 = DY_1 + C\theta_2, \tag{3.1-B}$$

where A, B, C and D are real numbers. Eqs. (3.1-A) and (3.1-B) can be written in matrix form, thus:

$$\begin{bmatrix} Y_2 \\ \theta_2 \end{bmatrix} = \begin{bmatrix} A & B \\ C & D \end{bmatrix} \begin{bmatrix} Y_1 \\ \theta_1 \end{bmatrix}, \tag{3.2}$$

Therefore, M is a matrix whose elements are A, B, C and D, and M knows the ray-transfer matrix.

3.3. ABCD Ray-Matrix in Cartesian Coordinates

Propagation of optical beams (Gaussian beams) through optical structures (lenses, apertures as 2 × 2 matrices) is known as ABCD ray matrices. Using such matrices allows us to describe the propagation of an optical beam through a series of optical elements using a cascade scheme by multiplying successive matrix representations of each optical element (lens, free space and 2 × 2 apertures) [33].

If we consider a ray of light propagating between two points denoted by r_1 and r_2 in parallel transverse planes at $z = z_1$ and $z = z_2$ separated by distance L (Fig. 3),

$$\tan\Phi = \frac{r_2 - r_1}{L} = \frac{dr_1}{dz}, \tag{3.3}$$

where Φ is the angle the light ray makes from point r_1 to point r_2.

$$r_2 = r_1 + L\frac{dr_1}{dz} = r_1 + Lr_1' \tag{3.4}$$

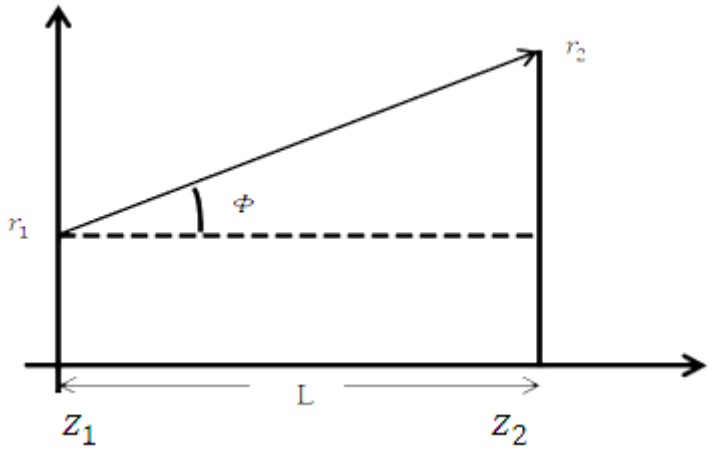

Figure 3: Line-of-sight section of length L of optical ray [7].

It can be seen that the slope of r_1 is the same as r_2

$$r_2' = r_1' \tag{3.5}$$

When combining (3.5) and (3.4), we obtain the matrix equation:

$$\begin{pmatrix} r_2 \\ r_2' \end{pmatrix} = \begin{pmatrix} 1 & L \\ 0 & 1 \end{pmatrix} \begin{pmatrix} r_1 \\ r_1' \end{pmatrix} \tag{3.6}$$

Therefore, the (2×2) matrix on the right-hand side of Eq. (3.6) $\begin{pmatrix} 1 & L \\ 0 & 1 \end{pmatrix}$ is the ABCD ray matrix of free-space propagation over a path of length L. Moreover, the ABCD matrices for a thin lens finite aperture stop with rotational symmetry are listed in Table 1.

Table 1: Ray Matrices for Various Optical Elements [7].

Structure	*Matrix*
Line-of-sight section (length L)	$\begin{pmatrix} 1 & L \\ 0 & 1 \end{pmatrix}$
Thin lens (focal length F_G)	$\begin{pmatrix} 1 & 0 \\ \frac{-1}{F_G} & 1 \end{pmatrix}$
Finite aperture stop (aperture radius W_G)	$\begin{pmatrix} 1 & 0 \\ \frac{2j}{kW_G^2} & 1 \end{pmatrix}$
Gaussian lens (thin lens and aperture stop)	$\begin{pmatrix} 1 & 0 \\ \frac{-1}{F_G + \frac{2j}{kW_G^2}} & 1 \end{pmatrix}$

where r_1 is a point at the source, $r_1' = \left(\frac{dr_1}{dz}\right)$ the slope of r_1, r_2 a point at the receiver, $r_2' = \left(\frac{dr_2}{dz}\right)$ the slope of r_2, L the propagation distance, F_G the focal length, and W_G the aperture radius.

3.3.1 Paraxial Approximation for the ABCD Matrix

When considering an optical ray propagating through a sequence of rotationally symmetric optical elements, they are aligned and arranged in cascade fashion as illustrated in Fig. 4; therefore, the overall ABCD matrix for N such matrices is obtained:

$$\begin{pmatrix} A & B \\ C & D \end{pmatrix} = \begin{pmatrix} A_N & B_N \\ C_N & D_N \end{pmatrix} \begin{pmatrix} A_{N-1} & B_{N-1} \\ C_{N-1} & D_{N-1} \end{pmatrix} \cdots\cdots\cdots \begin{pmatrix} A_1 & B_1 \\ C_1 & D_1 \end{pmatrix} \tag{3.7}$$

Input plane Output plane

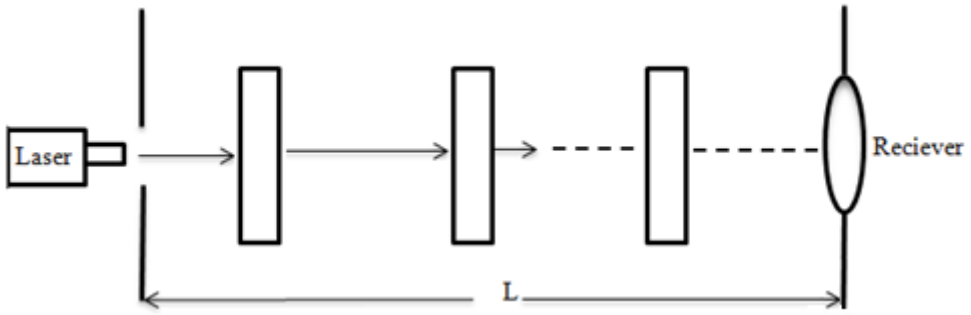

Figure 4: A ray-matrix optical system in cascade [7].

For a ray-matrix optical system in cascade for a general ABCD optical system, we have

$$\begin{pmatrix} r_2 \\ r_2' \end{pmatrix} = \begin{pmatrix} A & B \\ C & D \end{pmatrix} \begin{pmatrix} r_1 \\ r_1' \end{pmatrix} = \begin{pmatrix} Ar_1 + Br_1' \\ Cr_1 + Dr_1' \end{pmatrix}, \tag{3.8}$$

It will deduce

$$r_1' = \frac{1}{B}(r_2 - Ar_1), \tag{3.9}$$

$$r_2' = Cr_1 + Dr_1' = Cr_1 + \frac{D}{B}(r_2 - Ar_1), \tag{3.10}$$

By using an important property of all ray matrices listed in table 1, is that (AD − BC) = 1, we will find

$$r_2' = \frac{1}{B}(Dr_2 - r_1), \tag{3.11}$$

By beginning with the one-dimensional geometry associated with free space line-of-sight paraxial approximation as shown in Fig. 3 and redrawn in Fig. 5, it is assumed that an optical ray begins at point 0 in the plane $z = z_1$ at position r_1 above the optical axis (z-axis) and finishes at point T in the plane $z = z_2$ at position r_2 above the optical axis (z-axis). The paraxial approximation is then

$$R \cong L + \frac{1}{2L}(r_2 - r_1)^2 = L + \Delta L \tag{3.12}$$

where $|r_1 - r_2| \ll L$ and $R \cong |\overline{OT}|, L = |\overline{OP}| = |\overline{OS}|$

$$\Delta L = \frac{1}{2L}(r_2 - r_1)^2 \tag{3.13}$$

By using the geometry of Fig. 5, $\Delta L = |ST|$, and although not exact, $|QT| \cong 2\Delta L$.

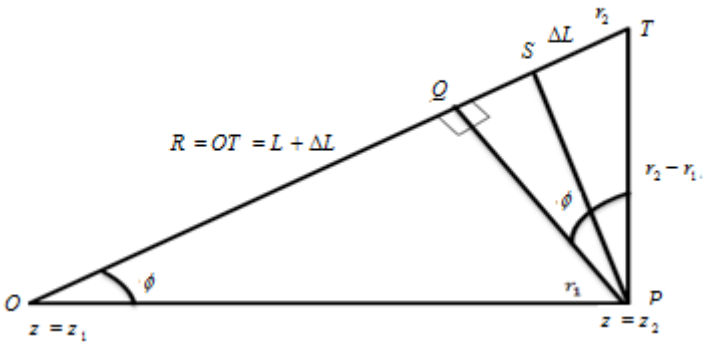

Figure 5: Geometry of propagation of the optical ray [7]

So that angle Φ in triangle ΔPQT:

$$\sin\Phi = \frac{|QT|}{r_2 - r_1} \cong \frac{2\Delta L}{r_2 - r_1} \tag{3.14}$$

Using small angle approximation, sin Φ = tan Φ. This leads to

$$\Delta L \cong \frac{1}{2}(r_2 - r_1)\tan\phi \cong \frac{1}{2}(r_2 r_2' - r_1 r_1') \tag{3.15}$$

where $r_1' = \frac{dr_1}{dz}$ is the slope of r_1, $r_1 = s$, $r_2' = \frac{dr_2}{dz}$ is the slope of r_2, $r_2 = s$, and by using (3.3) and (3.5).

Recognizing that Φ in ΔPOT in Fig. 5 is the same as ΔQPT, we substitute r_1 and r_2 from (3.9) and (3.10) into (3.15) and find that

$$\Delta L \cong \frac{1}{2}(r_2 r_2' - r_1 r_1') \cong \frac{1}{2}(r_2 \frac{1}{B}(Dr_2 - r_1) - r_1 \frac{1}{B}(r_2 - Ar_1)) \cong \frac{1}{2B}(r_2(Dr_2 - r_1) - r_1((r_2 - Ar_1)), \tag{3.16}$$

Now the overall path length or (eikonal function) $\rho(r_1, r_2)$ of optical ray passing through the ABCD system from r_1 to r_2.

where

$$\rho(r_1, r_2) = \rho(s, r) \tag{3.17}$$

In the plane at $z = z_1$ to position r_2 in the plane at $z = z_2$ leads to a general form of the paraxial a proximal

$$\rho(r_1, r_2) \cong L + \Delta L \cong L + \frac{1}{2B}(Ar_1^2 - 2r_1 r_2 + Dr_2^2) \tag{3.18}$$

3.3.2 Scintillation Index using the Huygens-Fresnel Integral

Using the ABCD ray-matrix for the propagation media between the input and output planes with the length of propagation distance (Green's Function) in the Huygens-Fresnel Integral Eq. (3.19) assumes in more general form [33]:

$$U_0(r,z) = -2ik\int_{-\infty}^{\infty} G(s,r;z)U_0(s,0)d^2s \tag{3.19}$$

$$G(s;r;L) = \frac{1}{4\pi B}\exp[ik\rho(s,r)] = \frac{1}{4\pi B}\exp\left[ikL + \frac{ik}{2B}(As^2 - 2s\cdot r + Dr^2)\right] \tag{3.20}$$

The factor $\frac{1}{4\pi B}$ is necessary for power conservation. In terms of a more general Green's Function, the Generalized Huygens-Fresnel integer can be deduced:

$$U_0(r,L) = -\frac{ik}{4\pi B}\exp(ikL)\int_{-\infty}^{\infty} d^2sU_0(s,0)\exp\left[\frac{ik}{2B}(As^2 - 2s\cdot r + Dr^2)\right] \tag{3.21}$$

where A = D = 1 and B = L. Eq. (3.21) can be reduced to the standard form of the Huygens-Fresnel Integral Eq. (3.19), and when the optical field of a lowest order Gaussian-beam wave at the emitting aperture of a transmitter in the plane $z = 0$ can be characterized by (assuming unit amplitude; $A_c = 1$).

$$U_0(s,0) = \exp\left[-\frac{1}{2}\alpha_0 ks^2\right], \tag{3.22}$$

Now the field of the wave at the output plane $z = L$ can be described by Eq. (3.19), which leads to

$$U_0(r,L) = -\frac{ik}{2\pi B}\exp(ikL)\iint_{-\infty}^{\infty} d^2s \exp\left[-\frac{1}{2}\alpha_0 k s^2\right]\exp\left[\frac{ik}{2\pi B}\left(As^2 - 2s\cdot r + Dr^2\right)\right], \tag{3.23}$$

$$U_0(r,L) = \frac{1}{\rho(L)}\exp(ikL)\exp\left[-\frac{1}{2}\alpha(L)kr^2\right] \tag{3.24}$$

where

$$\rho(L) = A + i\,\alpha_0 B, \tag{3.25}$$

$$\alpha(L) = \frac{\alpha_0 D - iC}{A + i\,\alpha_0 B} = \frac{2}{kW^2} + i\,\frac{1}{F}, \tag{3.26}$$

where $W = \sqrt{2/\mathrm{Re}[k\,\alpha(L)]}$ and $F = 1/\mathrm{Im}[\alpha(L)]$ are, respectively [7].

The ABCD is defined in a matrix fashion and the combined transfer function of a propagating medium including optical elements on the way. In Fig. 6, the optical path does not contain optical elements [34].

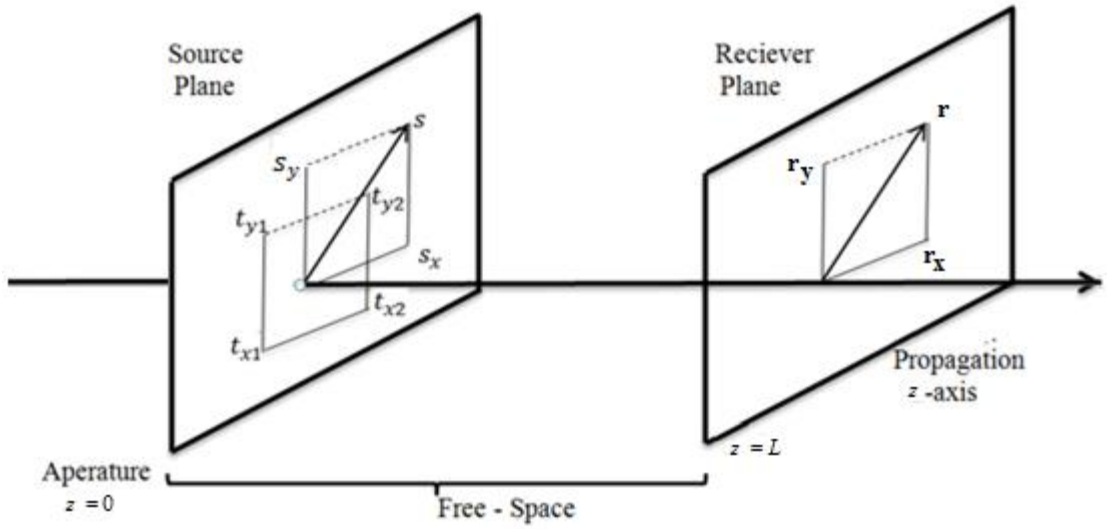

Figure 6: Propagation path without optical elements [34].

$$\begin{bmatrix} A & B \\ C & D \end{bmatrix} = \begin{bmatrix} 1 & L \\ 0 & 1 \end{bmatrix} \tag{3.27}$$

The general form of the ABCD matrix is the Huygens-Fresnel Integral (also known as the Collins Integral). The Huygens-Fresnel Integral will be in Cartesian coordinates with a rectangular aperture placed on the source plane with the dimensions in Figure 6 [34].

$$U_r(r, z = L) = \frac{-ik \exp(ikz)}{2\pi B} \int_{t_{y1}}^{t_{y2}} \int_{t_{x1}}^{t_{x2}} d^2 s$$
$$U_s(s) \exp\left\{ \frac{ik}{2B} [A(s_x^2 + s_y^2) - 2(s_x r_x + s_y r_y) + D(r_x^2 + r_y^2)] \right\}, \tag{3.28}$$

where A = D = 1, B represents L. C is not used, $t_{x1}, t_{y1} \to -\infty, t_{x2}, t_{y2} \to \infty$. Eq. (3.28) became identical to Eq. (3.23).

$$\left\langle I(r, z=L)\right\rangle = \left\langle U_r(r, z=L) U_r^*(r, z=L)\right\rangle \tag{3.29}$$

where $\langle\ \rangle$ and * refer to the mean value and conjugate operator, respectively.

$$\left\langle I(r_x, r_y, L)\right\rangle = \left(\frac{k}{2\pi L}\right)^2 \int_{-\infty}^{\infty}\int_{-\infty}^{\infty}\int_{-\infty}^{\infty}\int_{-\infty}^{\infty} ds_{1x} ds_{1y} ds_{2x} ds_{2y} U_S\left(s_{1x}, s_{1y}\right) U_S^*\left(s_{2x}, s_{2y}\right)$$
$$\exp\left[\frac{jk}{2L}\left(s_{1x}^2 - 2r_x s_{1x} + s_{1y}^2 - 2r_y s_{1y} - s_{2x}^2 + 2r_x s_{2x} - s_{2y}^2 + 2r_y s_{2y}\right)\right]$$
$$\left\langle \exp\left[\Psi\left(s_{1x}, s_{1y}\right) + \Psi^*\left(s_{2x}, s_{2y}\right)\right]\right\rangle \tag{3.30}$$

Therefore, $\left\langle I(r, L)\right\rangle$ in Eq. (3.30) is given by Eq. (3.29) and this way, a source beam of $U_S\left(s\right)$ propagates in the turbulent atmosphere will become the average intensity on the receiver plane , and $\Psi\left(s_{1x}, s_{1y}\right) + \Psi^*\left(s_{2x}, s_{2y}\right)$ is known as the wave structure function [35].

However, when the scintillation index (SI) is required, it is computed thus:

$$b^2(r, L) = \frac{\left\langle I^2(r, L)\right\rangle}{\left\langle I(r, L)\right\rangle^2} - 1, \tag{3.31}$$

CHAPTER 4

SCINTILLATION INDEX EQUATION BY USING THE RYTOV APPROACH

4.1 Introduction

There are several different theoretical approaches that have been developed to describe random variations in amplitude and the phases of optical-electrical fields are based upon solving the wave equation. However, the remaining ABCD method greatly simplifies the analysis as compared with other techniques [36].

4.2 Wave Equation

The problem of the propagation of optical waves through infinite continuous media with smooth variations of the refractive index has a controlling differential equation with random coefficients [37-39].

Therefore, it is assumed that a sinusoidal time variation (a monochromatic wave) in the electric field has shown that (Maxwell's equation) for the vector amplitude E(R) of a propagating electromagnetic wave leads directly to [40, 41]:

$$\nabla^2 E + k^2 n^2(R)E + 2\nabla[E.\nabla \log n(R)] = 0, \tag{4.1}$$

where, $R=(x,y,z)$ indicates a point in space and $n(R)$ is the refraction index whose time variations have been suppressed.

$$\nabla^2=\frac{\partial^2}{\partial x^2}+\frac{\partial^2}{\partial y^2}+\frac{\partial^2}{\partial z^2}, \tag{4.2}$$

where ∇^2 is the Laplace operator.

Because the variations of the refractive index are slow, a quasi-steady-state approach can be used. As a result, $n(R)$ becomes a function of position only.

Eq. (4.1) can be reduced to Eq. (4.3) by imposing the following assumptions:

1- Backscattering and the efforts of depolarization are neglected.

2- The refractive index is data correlated in the direction of propagation [42].

Assumptions (1) and (2) follow the same idea. Because λ for the optical is much smaller than the smallest scale of turbulence (i.e., the inner scale l_0), the maximum scattering angle (λ / l_0) is nearly 10^{-4} rad.

The final term on the left-hand side of Eq. (4.1) is negligible and Eq. (4.1) simplifies to Eq. (4.3) , thus:

$$\nabla^2 E+k^2 n^2(R)E=0, \tag{4.3}$$

If we let $U(R)$ denote a scalar component that is transverse to the direction of propagation along the positive z-axis, then Eq. (4.3) can be replaced with the scalar stochastic Helmholtz Equation:

$$\nabla^2 U + k^2 n^2(R) U = 0, \tag{4.4}$$

Under Assumption (3), the refractive index can be expressed as:

$$n(R) = n_0 + n_1(R) \tag{4.5}$$

For the free space:

$$n_0 = \langle n(R) \rangle \cong 1, so \langle n_1(R) \rangle = 0, \tag{4.6}$$

$$R = (r_x, r_y, z) or R = (r, \phi, z), \tag{4.7}$$

The first approach to solving Eq. (4.4) depended on the Method of Green's function, reducing Eq. (4.4) to an equivalent integral equation. However, exact solutions to Eq. (4.4) using Green's function or any other method have never been found. Further attempts to solve Eq. (4.4) depended on the geometric optic method (GOM) and on two famous perturbation theories, namely the Born approximation and the Rytov approximation.

4.3 The Born Approximation

The Born approximation was first applied to the integral equation for scattering that can be derived directly from Schrödinger's equation. It is intended to solve Eq. (4.4), which is called the stochastic Helmholtz Equation.

$U(R)$ and U are used synonymously. The Born and Rytov methods are the most well-known classical approaches to solving Eq. (4.4). The difference between the two methods is that the Born approximation depends on the addition of the

perturbation terms to the unperturbed field in contrast to the Rytov approximation involving the multiplication of perturbation terms. To solve Eq. (4.4) using the Born approximation, firstly it is written as the square of the index of refraction terms, thus:

$$n^2(R) = [n_0 + n_1(R)]^2 \cong 1 + 2n_1(R), \tag{4.8}$$

If the light beam propagates along the positive z-axis, it can expand U(R), thus:

$$U(R) = U_0(R) + U_1(R) + U_2(R) + ..., \tag{4.9}$$

where $U_0(R)$ is the unperturbed (unscattered) portion of the field in free space (without turbulence), $U_1(R)$ is the perturbed field due to first-order scattering (due to turbulence), $U_2(R)$ is the perturbed field due to second-order scattering, $U_3(R)$ is the perturbed field due to third-order scattering, and so on.

In general, it is assumed that

$$|U_3(r,L)| << |U_2(r,L)| << |U_1(r,L)| << |U_0(r,L)|, \tag{4.10}$$

By substituting Eq. (4.8) and Eq. (4.9) into Eq. (4.11), this work reduces Eq. (4.11) to a system of equations:

$$\nabla^2 U_0 + k^2 U_0 = 0, \tag{4.11}$$

$$\nabla^2 U_1 + k^2 U_1 = -2k^2 n_1(R) U_0(R), \tag{4.12}$$

$$\nabla^2 U_2 + k^2 U_2 = -2k^2 n_1(R) U_1(R), \tag{4.13}$$

The system of equations above means that once U_0 is known, it is possible to determine higher order $U_1(R)$, $U_2(R)$, $U_3(R)$.

4.3.1 Computation of First-Order Field Perturbations $U_1(R)$

The solution to Eq. (4.12), by giving the unperturbed field $U_0(R)$ and (Green's Function, can be expressed in the integral form:

$$U_1(R) = \iiint_v G(S,R)[2k^2 n_1(S)U_0(S)]d^3s = 2k^2 \iiint_v G(S,R)n_1(s)U_0(S)d^3s \tag{4.14}$$

where $G(S,R) \equiv G(R,S)$ is the free space; it can define Green's function by depending on the GOM.

Eq. (4.14) represents the first Born approximation and has the physical interpretation that the field $U_1(R)$ is a sum of spherical waves generated at various points (S) through volume (v).

$$G(S,R) = \frac{1}{4\pi|R-S|}\exp(ik|R-S|) \tag{4.15}$$

It can be observed that the maximum extent of the atmospheric effects in the transverse distance is far lower than the longitudinal distance from the transmitter to the receiver, so it is useful to use cylindrical coordinate representations:

$$R = (r,L),\ S = (s,z) \tag{4.16}$$

where (s) is used as a dummy to receive the coordinate and should not be confused with source coordinate S. The variables r and s in $R=(r,L)$ and $S=(s,z)$ transverse to the axis of propagation. Moreover, it is useful to use the paraxial approximation to rewrite Green's Function (4.15) and to simplify the calculation.

By giving two points in space $R=(r,L)$ and $S=(s,z)$. The distance between the points $|R-S|$ is

$$|R-S|=\left|(L-z)^2+(r-s)^2\right|^{\frac{1}{2}}=|L-z|\left[1+\frac{(r-s)^2}{(L-z)^2}\right]^{\frac{1}{2}}, \tag{4.17}$$

In Fig. 7, when the transverse distance $|r-s|$ is far less than the longitudinal distance $|L-z|$, the distance $|R-S|$ can be $\left[1+\frac{(r-s)^2}{(L-z)^2}\right]^{\frac{1}{2}}$ approximated by the next factor.

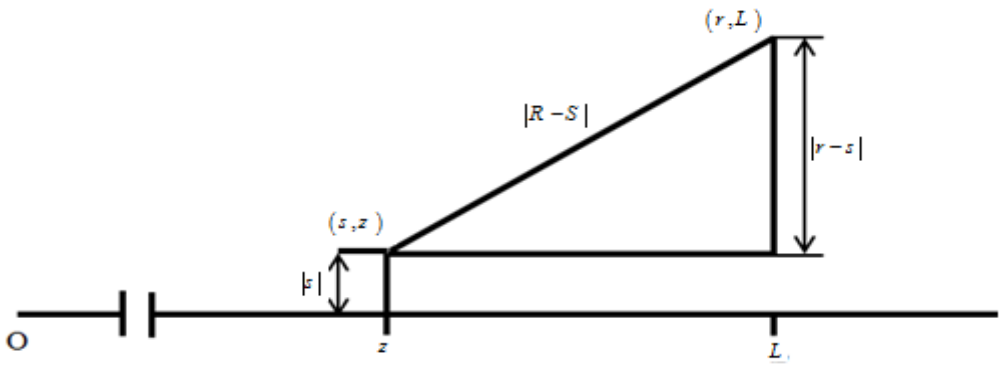

Figure 7: Two points of the optical path transverse to the axis of propagation

Finally,

$$|R-S| \approx |L-z| + \frac{|r-s|^2}{2|L-z|}, \qquad |r-s| << |L-z| \tag{4.18}$$

Then we can have Eq. (4.19) when substituting Eq. (4.18) into Eq. (4.15).

$$G(S,R) \cong G(s,r;L,z) = \frac{1}{4\pi(L-z)} \exp\left[ik(L-z) + \frac{ik|s-r|^2}{2(L-z)} \right], \tag{4.19}$$

By inserting Eq. (4.19) into Eq. (4.14), we have Eq. (4.20):

$$U_1(r,L) = \frac{k^2}{2\pi} \int_0^L dz \iint_{-\infty}^{\infty} ds^2 \exp\left[ik(L-z) + \frac{ik|s-r|^2}{2(L-z)} \right] U_0(s,z) \frac{n_1(s,z)}{L-z}, \tag{4.20}$$

Since $\langle n_1(s,z) \rangle = 0$ by definition,

$$\langle U_1(r,L) \rangle = 0 \tag{4.21}$$

4.3.2 Computation of Higher-Order Field Perturbations Um(r,L)

To solve the second-order perturbation in Born approximation, the term on the right-hand side of Eq. (4.13) is similar to Eq. (4.12). Using Green's Function, similarly to the first-order perturbation, we have

$$U_2(r,L) = \frac{k^2}{2\pi} \int_0^L dz \iint_{-\infty}^{\infty} ds^2 \exp\left[ik(L-z) + \frac{ik(s-r)^2}{2L-z)} \right] U_1(s,z) \frac{n_1(s,z)}{L-z}, \tag{4.22}$$

where $U_1(s,z)$ is computed from Eq. (4.20). Here, $\langle U_2(r,L)\rangle \neq 0$ and it is unlike $\langle U_1(r,L)\rangle = 0$.

Then, generally the mth-order perturbation term can be expressed in the following form:

$$U_m(r,L) = \frac{k^2}{2\pi}\int_0^L dz \iint_{-\infty}^{\infty} d^2 s \exp\left[ik(L-z) + \frac{ik|s-r|^2}{2(L-z)} \right] U_{m-1}(s,z)\frac{n_1(s,z)}{L-z} \quad (4.23)$$

$m = 1,2,3.....$

The Born approximation is valid only over short propagation distances based on experimental data obtained from [43].

4.4 The Rytov Approximation

The Rytov approximation is a different approach to solving Eq. (4.4) (the stochastic Helmholtz equation). However, the most well-known classical approaches to solving this equation are approximation methods [44]. The main difference between these two approaches is that the Born method is based on the addition of perturbation fields to the unperturbed field $U_0(R)$, whereas the Rytov method contains many perturbation terms of the field.

$$U_1(R), U_2(R).....U_m(R), \quad (4.24)$$

The Rytov approximation was first applied to a problem of the wave equation in random media by Obukhov [45], after which the Rytov approximation was used in the well-known works of Tatarskii [46].

In the Rytov method, the primary distinction is that perturbations due to the randomness of the propagation medium are represented by an exponential complex phase, thus:

$$U(R) \equiv U(r,L) = U_0(r,L)\exp\left[\Psi(r,L)\right], \tag{4.25}$$

Here, Ψ (the complex phase perturbation) was produced by the turbulence.

Now it can take $\Psi(r,L)$ is the (random part of the complex phase) in the form

$$\Psi(r,L) = \Psi_1(r,L) + \Psi_2(r,L) + \Psi_3(r,L) + ..., \tag{4.26}$$

where $\Psi_1(r,L)$ is the first-order of complex phase perturbation, $\Psi_2(r,L)$ the second-order of complex phase perturbation, and so on.

It is possible to apply Eq. (4.25) to Eq. (4.4) to obtain the Rytov solutions.

However, this is not necessary because we can relate these perturbations that are already developed Born approximation.

It is introduced the normalized Born perturbation:

$$\Phi_m(r,L) = \frac{U_m(r,L)}{U_0(r,L)}, \quad m = 1,2,3,..... \tag{4.27}$$

By equating the (first-order) of the Rytov and Born perturbations,

$$U_0(r,L)\exp[\Psi_1(r,L)] = U_0(r,L) + U_1(r,L), \tag{4.28}$$

When applying Eq. (4.27) to $U_1(r,L)$,

$$U_1(r,L) = U_0(r,L)\Phi_1(r,L) \tag{4.29}$$

Substituting (4.29) into (4.28), and dividing by $U_0(r,L)$, it can obtain:

$$\begin{aligned} &\exp[\Psi_1(r,L)] = 1+\Phi_1(r,L) \\ &\therefore \Psi_1(r,L) = \ln[1+\Phi_1(r,L)] \\ &\Psi_1(r,L) \cong \Phi_1(r,L), when \rightarrow \Phi_1(r,L) << 1, \end{aligned} \tag{4.30}$$

Then $\Psi_1(r,L)$ will become

$$\Psi_1(r,L) \cong \Phi_1(r,L) = \frac{U_1(r,L)}{U_0(r,L)} \tag{4.31}$$

Recalling Eq. (4.23) to get $U_1(r,L)$:

$$\Phi_1(r,L) = \frac{k^2}{2\pi}\int_0^L dz \iint_{-\infty}^{\infty} d^2 s \exp\left[ik(L-z) + \frac{ik|s-r|^2}{2(L-z)}\right]\frac{U_0(s,z)n_1(s,z)}{U_0(r,L)(L-z)}, \tag{4.32}$$

where $U_0(r,L)$ is the optical field in the receiver at $(z=L)$ and $U_0(s,z)$ is the optical field in the receiver at an arbitrary plane along the propagation path.

Similarly, it can compute $\Phi_2(r,L)$:

$$\Phi_2(r,L)=\frac{U_2(r,L)}{U_0(r,L)}$$
$$=\frac{k^2}{2\pi}\int_0^L dz\iint_{-\infty}^{\infty}d^2s\ \exp\left[ik(L-z)+\frac{ik|s-r|^2}{2(L-z)}\right]\frac{U_0(s,z)\Phi_1(s,z)n_1(s,z)}{U_0(r,L)(L-z)}, \quad (4.33)$$

Most works based on the Rytov theory have made use of Ψ_1 (first-order perturbation). The Rytov approximation is called a Single Scattering proximal because it is directly related to the first of the Born approximations.

The first order perturbation $\Psi_1(r,L)$ is sufficient for the calculation of a number of statistical quantites of interest, such as the log-amplitude variance, phase variance, intensity and phase correlation functions and the wave structure function. Using the Rytov theory to obtain any of the statistical moments of the optical field, including the mean value $\langle U(r,L)\rangle$, it becomes necessary to require $\Psi_2(r,L)$ in addition to first-order $\Psi_1(r,L)$ [47].

4.4.1 Computation of First-Order Spectral Representation.

For the purpose of computing the static moment of the field, it is very important to develop a spectral representation of Born and Rytov. To compute it, it is necessary to know the refractive index $n_1(s,z)$ in 2D [48].

$$n_1(s,z)=\int_{-\infty}^{\infty}\exp(i\,\mathrm{K}.s)dv(\mathrm{K},z), \quad (4.34)$$

where $dv(\mathrm{K}, z)$ is the random amplitude of the fluctuation of the refractive index, K $\mathrm{K} = \left(\kappa_x, \kappa_y, 0\right)$ the wave vector practically with $\kappa_x = 0$.

$U_0\left(r, L\right)$ at distance L is

$$U_0(r,L) = \frac{1}{\rho(L)} \exp\left[ikL - \frac{\alpha_0 k r^2}{2\rho(L)}\right], \tag{4.35}$$

$$\rho(L) = 1 + i\alpha_0 L \tag{4.36}$$

$$\alpha_0 = \frac{2}{kW_0^2} + i\frac{1}{F_0} \tag{4.37}$$

where, W_0 is the beam radius and F_0 is the phase of the radius of curvature.

$$\frac{U_0(s,z)}{U_0(r,L)} = \frac{\rho(L)}{\rho(z)} \exp\left[ik\left(z - L\right)\right] \exp\left[-\frac{\alpha_0 k s^2}{2\rho(z)}\right] \exp\left[-\frac{\alpha_0 k r^2}{2\rho(L)}\right], \tag{4.38}$$

By substituting Eq. (4.33) and Eq. (4.38) into Eq. (4.32), and after some modifications and re-arranging, we have a first-order Spectral Representation $\Phi_1\left(r, L\right)$, thus:

$$\Phi_1(r,L) = \frac{k^2}{2\pi} \int_0^L dz \int\int_{-\infty}^{\infty} \frac{dv(\mathrm{K}, z)}{\gamma(L-z)} \exp\left[\frac{i\gamma k r^2}{2(L-z)}\right]$$
$$\times \int\int_{-\infty}^{\infty} d^2 s \exp\left[i\left(\mathrm{K} - \frac{kr}{L-z}\right)\cdot s\right] \exp\left[\frac{iks^2}{2\gamma(L-z)}\right], \tag{4.39}$$

where

$$\gamma = \frac{\rho(z)}{\rho(L)} = \frac{1+i\,\alpha_0 z}{1+i\,\alpha_0 L} \Rightarrow \frac{1}{\gamma} = \frac{\rho(L)}{\rho(z)} \tag{4.40}$$

By recalling (4.30) and $\kappa = |\mathrm{K}|$, we get the first-order spectral representation [7].

$$\Psi_1(r,L) = \Phi_1(r,L) = ik\int_0^L dz \iint_{-\infty}^{\infty} d\nu(\mathrm{K},z)\exp\left[i\gamma \mathrm{K}.r - \frac{i\kappa^2\gamma}{2k}(L-z)\right], \tag{4.41}$$

4.4.2 Computation of Second-Order Spectral Representation.

The second-order spectral representation may be obtained using Eq. (4.33) by inserting Eqs. (4.34), (4.38) and (4.41) into Eq. (4.33) to get

$$\begin{aligned}\Phi_2(r,L) &= \frac{ik^3}{2\pi}\int_0^L dz \int_0^z dz' \iint_{-\infty}^{\infty} \frac{d\nu(\mathrm{K},z)d\nu(\mathrm{K}',z')}{\gamma(L-z)} \\ &\times \exp\left[\frac{i\gamma k r^2}{2(L-z)} - \frac{i\gamma'\kappa'^2}{2k}(z-z')\right] \\ &\times \iint_{-\infty}^{\infty} d^2 s \exp\left[is.\left(\mathrm{K}+\gamma\mathrm{K}' - \frac{kr}{L-z}\right)\right]\exp\left[\frac{iks^2}{2\gamma(L-z)}\right],\end{aligned} \tag{4.42}$$

where

$$\gamma' = \frac{1+i\,\alpha_0 z'}{1+i\,\alpha_0 z}, \tag{4.43}$$

This leads to the second-order spectral representation for the normalized second-order Born perturbation given by

$$\Phi_2(r,L) == -k^2 \int_0^L dz \int_0^z dz' \int_{-\infty}^{\infty}\int_{-\infty}^{\infty}\int_{-\infty}^{\infty} d\nu(\mathrm{K},z)d\nu'(\mathrm{K}',z') \times \exp\left[i.\gamma(\mathrm{K}+\gamma'\mathrm{K}').r - \frac{i\gamma\left|\mathrm{K}+\gamma'\mathrm{K}'\right|^2}{2k}(L-z) - \frac{i\gamma'\kappa'^2}{2k}(z-z') \right] \tag{4.44}$$

$$\Phi_2(r,L) = \Psi_2(r,L) + \frac{1}{2}\Psi_1^2(r,L) \tag{4.45}$$

From the expression above, we can obtain the second-order spectral representation. Despite the result of Eq. (4.45), it actually needs to compute the SI.

Although direct use of the Born approximation in the optical wave propagation problem is not applicable, it is interesting that the Born approximation can play a central role in Rytov methods. There are three important integrals that define second-order statistics for both the Born and Rytov approximations.

$$E_1(0,0) = \left\langle \Psi_2(r,L) \right\rangle + \frac{1}{2}\left\langle \Psi_1^2(r,L) \right\rangle = -2\pi^2 k^2 \int_0^L dz \int_0^\infty d\kappa\, \kappa\, \Phi_n(\kappa,z) \tag{4.46}$$

$$E_2(r_1,r_2) = \left\langle \Psi_1(r_1,L)\Psi_1^*(r_2,L) \right\rangle = 4\pi^2 k^2 \int_0^L dz \int_0^\infty d\kappa\, \kappa \Phi_n(\kappa,z) J_0\left(\kappa\left|\gamma r_1 - \gamma^* r_2\right|\right) \times \exp\left[-\frac{i\kappa^2}{2k}\left(\gamma-\gamma^*\right)(L-z) \right] \tag{4.47}$$

$$E_3(r_1,r_2)=\left\langle \Psi_1(r_1,L)\Psi_1(r_2,L)\right\rangle =-4\pi^2k^2\int_0^L dz\int_0^\infty d\kappa\,\kappa\Phi_n(\kappa,z)J_0\left(\gamma\kappa|r_1-r_2|\right)$$
$$\times\exp\left[-\frac{i\kappa^2\gamma}{2k}(L-z)\right] \tag{4.48}$$

where $J_0(x)$ is a Bessel function of the first kind and order zero. This will explore the steps of deriving the scintillation index formula by depending on the previous integral. As can be seen below, for the scintillation the use of $\left\langle \Psi_1(r,L)\right\rangle$ will be sufficient, whereas the calculation of $\left\langle U(r,L)\right\rangle$ will require second-order perturbation. Now covering the first and second order perturbations $\Psi_1(r,s)$ **&** $\Psi_2(r,s)$, we need the following ensemble of averages for the field, intensity and intensity square.

1- $\left\langle U(r,L)\right\rangle$ requires the calculation of

$$\left\langle \exp[\Psi(r,L)\right\rangle =\left\langle \exp\left[\Psi_1(r,L)+\Psi_2(r,L)\right]\right\rangle, \tag{4.49}$$

2- $\left\langle I(r,L)\right\rangle$ requires the calculation of

$$\begin{aligned}&\left\langle \exp\left[\Psi(r_1,L)+\Psi^*(r_2,L)\right]\right\rangle\\&=\left\langle \exp[\Psi_1(r_1,L)+\Psi_2(r_1,L)+\Psi_1^*(r_2,L)+\Psi_2^*(r_2,L)]\right\rangle,\end{aligned} \tag{4.50}$$

3- $\left\langle I^2(r,L)\right\rangle$ requires the calculation of

$$\left\langle \exp\begin{bmatrix}\Psi_1(r_1,L)+\Psi_2(r_1,L)+\Psi_1^*(r_2,L)+\Psi_2^*(r_2,L)\\+\Psi_1(r_3,L)+\Psi_2(r_3,L)+\Psi_1^*(r_4,L)+\Psi_2^*(r_4,L)\end{bmatrix}\right\rangle \tag{4.51}$$

By using the following order approximation Eq. (4.52) from (14) of Andrews (2005) on p. 184 and $\left\langle n_1(R)\right\rangle=0$, thus $\left\langle \Psi_1(r,L)\right\rangle=0$, we can find for the ensemble

averages of the exp expressions in Eqs. (4.49), (4.50), (4.51), in another forms, Eqs. (4.53), (4.54), (4.55), ref. [35].

$$\left\langle \exp(\Psi)\right\rangle = \exp\left[\left\langle\Psi\right\rangle + \frac{1}{2}\left(\left\langle\Psi^2\right\rangle - \left\langle\Psi\right\rangle^2\right)\right] \tag{4.52}$$

$$\left\langle U\left(r,L\right)\right\rangle = \exp\left[E_1(0,0)\right], \tag{4.53}$$

$$\left\langle I\left(r,L\right)\right\rangle = \exp\left[2E_1(0,0) + E_2(r_1,r_2)\right], \tag{4.54}$$

$$\left\langle I^2\left(r,L\right)\right\rangle = \exp\begin{bmatrix} 4E_1(0,0) + E_2(r_1,r_2) + E_2(r_1,r_4) \\ +E_2(r_2,r_3) + E_2(r_3,r_4) + E_3(r_1,r_3) + E_3^*(r_2,r_4) \end{bmatrix} \tag{4.55}$$

Now, it possible to get quantities $\left\langle I^2\left(r,L\right)\right\rangle$ average intensity square and $\left\langle I\left(r,L\right)\right\rangle^2$ squared average intensity by defining mutual coherence function Γ [35].

$$\begin{aligned} &\Gamma\left(r_1,r_2,L\right) = U\left(r_1,L\right)U^*\left(r_2,L\right) \\ &= U_0\left(r_1,L\right)U_0^*\left(r_2,L\right)\exp\left[2E_1(0,0) + E_2(r_1,r_2)\right], \end{aligned} \tag{4.56}$$

$$\begin{aligned} &\left\langle I\left(r,L\right)\right\rangle^2 = \Gamma^2\left(r_1 = r, r_2 = r, L\right) \\ &= U_0^2(r,L)\left[U_0^*(r,L)\right]^2 \exp\left[4E_1(0,0) + 2E_2(r,r)\right] \end{aligned} \tag{4.57}$$

4- $\left\langle I^2(r,L)\right\rangle$ requires the calculation of

$$\begin{aligned} &\left\langle I^2(r,L)\right\rangle = \Gamma\left(r_1 = r, r_2 = r, r_3 = r, r_4 = r, L\right) \\ &= U_0\left(r_1 = r, L\right)U_0^*\left(r_2 = r, L\right)U_0\left(r_3 = r, L\right)U_0^*\left(r_4 = r, L\right) \\ &\times \exp\left[4E_1(0,0) + E_2(r_1,r_2) + E_2(r_1,r_4) + E_2(r_2,r_3) + E_2(r_3,r_4) + E_3(r_1,r_3) + E_3^*(r_2,r_4)\right] \\ &= U_0^2(r,L)\left[U_0^*(r,L)\right]^2 \\ &\times \exp\left[4E_1(0,0) + E_2(r,r) + E_2(r,r) + E_2(r,r) + E_2(r,r) + E_3(r,r) + E_3^*(r,r)\right], \end{aligned} \tag{4.58}$$

According to the Rytov method, without optical elements between the transmitter (input) and receiver (output), the propagation channel is characterized as line-of-sight propagation, the receiver can "see" from the transmitter.

By using the classical Rytov method, the propagation of beam under weak fluctuation can be analyzed [9, 40, 41,46], which is explained by Eq. (4.59).

$$U(r,L)=U_O(r,L)\exp[(\Psi(r,L)]=U_O(r,L)\exp\left[\Psi_1(r,L)+\Psi_2(r,L)+..\right], \tag{4.59}$$

where $U(r,L)$ is the wave of the Gaussian beam at the receiver, $\Psi(r,L)$ is the total complex phase perturbation of the field due to random inhomogeneity along the propagation path. $\Psi_1(r,L)$ is the 1st-order perturbation and $\Psi_2(r,L)$ is the 2nd-order perturbation.

Finally, the scintillation index can be deduced as a measure of normalized variance of amplitude fluctuations in the beam that propagates in a turbulent medium. Therefore, the scintillation index can be represented as $SI=b^2(r,L)$. Recalling Eq. (3.31) to compute the SI in another way:

where

$$\begin{aligned} b^2(r,L) &= \frac{\langle I(r,L)\rangle^2 \exp\left\{2E_2(r,r)+2\mathrm{Re}\left[E_3(r,r)\right]\right\}}{\langle I(r,L)\rangle^2}-1 \\ &=\exp\left\{2E_2(r,r)+2\mathrm{Re}\left[E_3(r,r)\right]\right\}-1\cong 2E_2(r,r)+2\mathrm{Re}\left[E_3(r,r)\right] \\ &=2\left\langle\Psi_1(r_1,L)\Psi_1^*(r_2,L)\right\rangle+2\mathrm{Re}\left[\left\langle\Psi_1(r_1,L)\Psi_1(r_2,L)\right\rangle\right], \end{aligned} \tag{4.60}$$

CHAPTER 5

VORTEX BEAMS IN FREE-SPACE-OPTICS WITH TURBULENCE ATMOSPHERE

5.1 Introduction

The first working laser, an acronym for light amplification by stimulated emission of radiation, was introduced in 1960. Since then, the scientific community has focused a great deal of attention on the possible applications of the LASER, mainly suggesting that lasers can be used to extend radio-frequency atmospheric communication and radar techniques to the optical-frequency band. There are other places where laser technology is applied, such as weaponry, ranging, remote sensing, target designation, adaptive optics, and medical uses, among others. Though, regardless of the system using optical (visible) or infrared (IR) waves, what is to be considered is the general propagation effects associated with the medium as well as the impacts related with the wave itself.

Most of the time, the propagation medium is the turbulent atmosphere for which small index-of-refraction fluctuations along the propagation path bring about a series of deleterious effects on the wave. Moreover, random fluctuations in the refractive index of the atmosphere are closely linked with minute changes in temperature as a result of the wind and convection turbulent movements. Despite such refractive-

index fluctuations being only a few parts in 106, a propagating optical wave passes through a large number of refractive-index in homogeneities. As a consequence, the cumulative effect on the optical wave is rather significant; to illustrate, refractive-index fluctuations are behind the twinkling of stars and limit the "seeing" ability of astronomers to resolve small objects to within a few seconds of arc. Such an atmospheric effect inspires the use of adaptive optics techniques and the placement of large telescopes in space, such as the famous Hubble Telescope.

Earlier studies on the propagation of electromagnetic radiation and other waves through random media included starlight and sound waves propagation through the atmosphere and ocean, of microwaves through planetary atmospheres, and of radio waves through the ionosphere and interplanetary space. Thus, some of the theoretical work concerning this concept was already completed before the laser came to the fore. The propagation of laser light, being merely another form of electromagnetic radiation, is yet another topic of much of this early research. Both Chernov and Tatarskii published monographs before 1960 on the propagation of optical plane waves and spherical waves through turbulence; later, these monographs were translated into English in 1960 and 1961, respectively [40, 48]. Other preliminary studies on optical wave propagation in random media, along with many early references, include Lawrence and Strohbehn [50], Prokhorov et al. [51], Fante [52, 53], Uscinski [54], Strohbehn [38], Ishimaru [41], Zuev [55], Rytov et al. [42], Tatarskii et al. [56], Sasiela [57], Andrews et al. [58], and Wheelon [59, 60].

There are many important applications for laser beam propagation through turbulent atmospheres in numerous fields including free space optical communications, Light Detection and Ranging (LIDAR), Laser Radar (LADAR), remote detecting and

imaging. The turbulence severely influences laser beam properties, thereby limiting FSOC efficiency. For this reason, one has to gain a better understanding of these properties for the sake of system optimization. In this respect, most previous studies have already addressed plane wave, spherical wave or fundamental Gaussian beams [9], while others have lately dealt with modified Gaussian beams or higher order Gaussian [61-68], all leading to the finding that initial beam properties (shape, phase, coherence, etc) strongly affect propagation results. More recently, there has been growing interest in applying optical vortex beams for free space optical communications as well as remote sensing [69-72].

5.2 Free space optics

Today, optical wireless communications (OWC), better known as Free Space Optics, have many important applications due to the increasing demand for larger bandwidths and high-data-rate transfer of information required at optical wavelengths although earlier attention was paid rather to ever-increasing data rates afforded by optical systems over radio frequency (RF) systems. In general, we agree that laser communication has the following benefits: (i) It uses lower power, mass and volume as compared with Radio Frequency systems. (ii) It has an intrinsic narrow beam. (iii) It exploits the high-gain nature of laser beams. (iv) There are *n*o limitations on frequency and bandwidth.

Free space optics communication is a line-of-sight technology using a laser technique to supply optical bandwidth connections between locations. These days, FSOP can transmit up to 2.5 Gbps of voice, data and multimedia through free space by allowing optical connectivity without the use of fibre-optic technology. In the USA, only 5% of companies are connected to fibre-optic infrastructure, yet 75% are

placed within one mile of cables, known as the “Last Mile Problem”. With increasing the demand on bandwidth and with more businesses shifting to high-speed local area network (LANs), it is becoming increasingly spiritless to be connected to the outside world through lower-speed connections (wire- and copper-based technologies) such as cable modems, digital subscriber line (DSL), or T1s (transmission system 1). Therefore, in order to solve these problems, small FSOC networks were set up in Dallas, Denver, Seattle and Los Angeles [7].

In Europe, regional fibre-optic carriers are supplying companies that wish to acquire high-speed connections. Commercial FSO companies have offered equipment with transfer rates at a far higher level than coaxial cables or digital subscriber lines from 10 Mbps to 1.25 Gbps, rates that are far above the level required by most high-end broadband services and applications. In addition, state-of-the-art laser diodes already on the market can be switched on and off at speeds that could transmit information at even higher rates—as much as 9.6 Gbps. Although this technology is still not adjusted for use by FSOs, it would be able to generate optical pulses lasting a mere 100 picoseconds (100 trillionths of a second) each [7].

Ordinarily, laser wavelengths designed for FSO systems are 850 and 1550 nm. Low-power infrared lasers functioning in an unlicensed electromagnetic frequency band are designed, or can be potentially arranged, to be active in an eye-safe fashion. Nevertheless, the restricted capacity of lasers’ in turn can limit the scope of its applicability. Given weather conditions, FSO links along horizontal near-ground paths may cover anywhere between a few hundred meters to one or more kilometers – a distance which is large enough to receive broadband traffic from a backbone to many end-users and all the way back. As unfavorable weather conditions, thick fog

in particular is capable of interfering with the reach of these line-of-sight equipment, each optical transceiver node or link head may be arranged so as to communicate with numerous other nodes closely in a network environment.

This so-called “mesh topology” is in place to guarantee large amounts of data relayed without limitations from sensor sites to central control centers and users alike. The fog impact slows commercial deployment of near-ground FSO systems. Together with rain and snow to a lesser extent, fog can considerably limit the maximum range of an FSO link. As this phenomenon creates a major loss of optical power, a practical FSO link must then be designed with some specified “link margin,” i.e., extra optical power to overcome foggy conditions when required. On the other hand, in ideal weather conditions, the absolute reliability of a laser communication link through the atmosphere can yet be subject to absorption by atmospheric constituents and the ever-present turbulence [7].

In case of any given link margin, one has to address another important factor, link availability, which is the fraction of the total operating time that the link fails due to fog or any other physical hindering element. Link-availability objectives depend on the application; once used for private enterprise networking (for instance, to connect two offices located in separate buildings); FSO technology with 99.9-percent uptime can be regarded as satisfactory. Values like these are in line with a downtime of about nine hours per annum. On the contrary, public carrier-class service is provided to a carrier’s prime business customers, requiring link availability at 99.999 percent, (commonly referred to as “five-nine benchmark” in the telecommunications industry). This means only five minutes of allotted downtime each year. It should not

be forgotten that fiber optic systems regularly operate at the five-nines-service level [7].

The FSO technology was initiated in the 1960s; yet in the early 1970s, deleterious atmospheric effects on optical waves alongside the introduction of optical fibers brought about a major drop in the use of FSO. Nevertheless, these systems are capable of offering high-speed connections between buildings, between a building and the optical fiber network, aircraft to aircraft, or ground and satellite. Furthermore, given the circumstances, an FSO system is often installable within a few days or even hours; this is while weeks or months may be required to set up an optical fiber connection. Today, due to the need for high-data-rate connections across the globe as well as the inevitable hindrances associated with optical fiber networks in specific settings, FSO use is once again popular and on the rise [7].

5.3 Optical turbulence

Atmospheric turbulence, generated by a temperature differential between the Earth's surface and the atmosphere, can impact optical waves and, hence, has been subject to much effort and study by specialists for a very long time now. Throughout the day, the ground is warmer than the air, making the air nearest to the surface become hotter than the above layers. This negative temperature gradient generates rays of light parallel to the Earth to bend upward. If the negative temperature gradient is high enough, it can bring about an inverted image known as a "mirage" (another meteorological phenomenon). On the other hand, temperature gradients are positive at night, causing light rays to bend downward through refraction and allowing us to see objects, such as stars, somehow below the horizon. This is commonly referred to as "looming" [7].

In essence, immediately prior to the sun sinking in the horizon at sunset; its position is in fact about a diameter already below the horizon. In line with this phenomenon, wave front distortions in the optical wave caused by atmospheric turbulence spread the beam beyond due to pure diffraction. A random variation of the beam centroid position is called “beam wander” and a random redistribution of the beam energy within a cross section of the beam leads to irradiance fluctuations. Perhaps, one of the most well-known effects of atmospheric turbulence is the twinkling of stars, a random fluctuation in the degree of image brightness. Moreover, the turbulence restricting astronomical seeing can slowly deteriorate the spatial coherence of a laser beam as it travels through the atmosphere, thus limiting beam collimation and concentration and resulting in major power reductions in optical communication and radar systems. Additionally, heterodyne detection optical receivers are quite susceptible to the loss of spatial coherence as it limits the effective aperture size of such detection systems [7].

Wave front distortions in the optical wave caused by atmospheric turbulence can result in beam scattering as a result of pure diffraction, irregularities in beam centroid position called beam wander, and a random redistribution of the beam energy within a cross section of the beam leading to irradiance fluctuations. Perhaps the most well-known effect of atmospheric turbulence is the twinkling of stars, which is an irregular change in brightness of the image. In addition, the atmospheric turbulence that limits astronomical seeing gradually destroys the spatial coherence of a laser beam as it propagates through the atmosphere. This loss of spatial coherence limits the extent to which laser beams may be collimated or focused, resulting in significant power level reductions in optical communication and radar systems.

Heterodyne detection optical receivers are very sensitive to the loss of spatial coherence because this limits the effective aperture size of such a detection system. Wind blowing over an aerodynamically uneven area of the Earth's surface when there is a temperature gradient causes changes in the atmosphere's refractive index, otherwise known as "optical turbulence".

One can define statistically the behavior of a sub portion of optical turbulence to set up the basis for most propagation theories. By the same token, the propagation of an optical/IR wave through optical turbulence can be defined in statistical terms. Generally speaking, theoretical approaches visible in analyses concerning optical IR wave propagation through optical turbulence are grouped as either in weak fluctuation terms or strong fluctuation terms [7].

5.4 Vortex Beams

Today, vortex beams are quite popular following a great deal of research on the impact of turbulence on beam propagation [69, 73-81].The generation and propagation of vortex beams are two other important issues under the spotlight in the literature [82-87]. For a vortex beam, each photon carries a quantized intrinsic orbital angular momentum expected to use a beam's topological charge l as the alphabet for the optical message. The propagation property of such a beam in a turbulent atmosphere plays an important role; yet to the best of our knowledge, the experimental study of the vortex beam propagating in a turbulent atmosphere has not been reported.

5.4.1 Phase Distribution of Vortex Beams

Lately, much focus has been on the propagation of light beams carrying optical vortices [88-91]. These beams may be created using either static optical elements (such as spiral phase plates or computer-synthesized diffraction grating with “forks” and dynamic spatial light modulators [69-88]. Light beams with optical vortices possess orbital angular momentum (OAM) [88-90]. The main focus of this part of the thesis is Light beams with optical vortices possess OAM [2-5, 89, 91], this is the first part of our research.

5.4.2 Scintillation of Laser Beams

In recent years, optical wave propagation processing through random media has been studied. The turbulent medium is meaning the refraction index of it exhibits random spatial variations that are large with respect to the optical wavelength. No solution to the irradiance fluctuations problem by depending on principles of electromagnetic wave propagation applies to all conditions of optical turbulence. Early investigations concerning the propagation of unbounded plane waves and spherical waves through random media led to the classical monographs published in the early 1960s by Chernov [40] and Tatarskii [48], but their scintillation results were limited to weak fluctuations. Experimentally work was done by Gracheva and Gurvich [92]. This work attracted much attention and stimulated a number of theoretical and experimental studies devoted to irradiance fluctuations under conditions of strong turbulence.

CHAPTER 6

THEORETICAL BACKGROUND OF GAUSSIAN BEAM AND GAUSSIAN VORTEX BEAMS

6.1. Introduction

In this section, we explain the Gaussian vortex beams alongside and different types of vortex source beams in radial and Cartesian coordinates. Later, then these beams will be applied to estimate scintillation index in the strong beam, phase distribution for source and receiver planes and the symbol error rate.

6.2. Expression of Gaussian Beam (GB)

For the receiver coordinate representation, we choose r , at $z > 0$. Therefore, s is the coordinate for the source plane. The source beams are defined either in radial, i.e. (s, ϕ) or Cartesian, i.e. (s_x, s_y) coordinates. Hence, in what follows $U_s(s, \phi)$ is the field on source plane [34].

In cylindrical coordinates,

$$U_s(\mathrm{s}, \phi_s) = \mathrm{A}_c \exp(-k \ \alpha \ \mathrm{s}^2), \tag{6.1}$$

where A_c refers to amplitude coefficient.

$$\alpha = 1/(k\ \alpha_s^2) + 0.5j/F_s \tag{6.2}$$

where α_s and F_s refer to radial Gaussian source size and the focusing parameter, respectively [34].

6.3. Formulation of Source and Receiver Plane Intensities for Gaussian Beam

The propagation geometry is depicted in Figure 6, where transversal planes, $(i.e. s_x = s_y, z = 0)$, $s = (s_x, s_y)$ are the coordinates of the transverse source plane, $r = (r_x, r_y)$ represents the Cartesian coordinates of the transverse receiver plane, and the transverse source and receiver planes confront the axis of propagations z, at positions $z = 0$ and $z = L$, independently. Hence, L link length estimation. Eq. (6.1) reveals the distribution field of the Gaussian beam around the point of origin $(i.e. s_x = s_y, z = 0)$.

Numerous theoretical approaches have been created in order to describe random variation in the amplitude and phase of the electrical field of the optical wave propagating in the form of random medium-like atmospheric and phase fluctuations and through solving the related wave equation. In the following, we will introduce the methods used to compute the SI.

6.4. The Methods for Computing Scintillation Index.

At this stage, the ultimate goal is to achieve the best excitation level to decrease the degrading effects of turbulence in atmospheric optical links [93]. Scintillations as a result of turbulence in the atmosphere can bring about fluctuations in the intensity of the received beam. This, at the same time, is one of the major limiting factors in

atmospheric communication and imaging systems operating at optical frequencies; for this reason, the field has been under research for quite some time, both theoretically and experimentally, by many experts [94-100]. A comprehensive review of all contributions can be found in the works carried out by Tatarskii [47], Ishimaru [101], Andrews and Phillips [7], and Andrews et al [57]. First, one has to determine the received intensity profile that might influence the receiver design. Another issue under investigation in this work is the scintillation index, for which source plane excitation is described by a Gaussian laser beam. The average intensity profile of this beam is obtained at the receiver plane after passing through a turbulent atmosphere. The limiting cases of our formulation are compared with both the known Gaussian beam wave solution in the turbulent atmosphere and the Gaussian beam solution in free space (i.e., in the absence of turbulence). This yields exact conformity to these limiting cases. Numerical evaluations are made at various link lengths and turbulence levels. In the results, a Random Phase Screen (RPS) exhibits lower scintillations and, accordingly, has a likelihood of being better than a pure Gaussian beam, especially at long propagation lengths. Finally, we introduce a scintillation index analysis on the Gaussian beam and examine it using three methods. Here, our motivation is to determine different ways of computing the SI for the Gaussian beam in optical links as there exist different types of SI computation for beams to evaluate the performance of laser communication systems.

The scintillation index can be deduced as a measure of normalized variance of amplitude fluctuations in the beam, which propagates in the turbulent medium. Consequently, the SI is represented as $SI = b^2(r, L)$; recall Eq. (3.31) to compute the SI.

Finally, the next sections will introduce the methods, those used to compute the SI in turbulence atmospheres.

6.4.1 Huygens-Fresnel Method

By depending on Section 4.3.2, integrations are made in a semi-analytic manner by the associated Matlab function, thereby preventing lengthy, time-consuming and error-prone hand derivations. The results are obtained for the Gaussian beam. By plotting the SI against the propagation distance, we illustrate the on-axis scintillation behaviors of this beam.

6.4.2 Rytov Method

In the Rytov method, the underlying difference is that perturbations due to the randomness of the propagation medium are introduced in the form of an exponential complex phase, as shown in Chapter 4. Then, we can apply Eq. (4.27) to arrive at the Rytov solutions; though this will very much resemble the already developed Born approximation. Finally, the SI is obtained with the Rytov method for Eq. (3.31).

6.4.3 Random Phase Screen Method

Herman and Strugala first investigated the subharmonics. While using an exceptional form of the subharmonic method, they proposed that the method produces phase screens that create a structure work agreeable to the actual theory. Moreover, they examined the normal Strehl proportion from their subharmonic screens, obtaining a close match with the hypothesis [102]. Later, Lane et al. formed the specific subharmonic technique, also in use in our research, showing that their screens also matched the theoretical structure function to a very great extent. Shortly after that,

Johansson and Gavel [103] examined the methodologies of Herman and Strugala and Lane et al., later to introduce their own subharmonic procedure with screens that form a structure work matching the hypothesis even more [103]. Later, while researching on the precision of no square subharmonic phase screens, Sedmak demonstrated a high level of concurrence with the stage structure capacity and the aperture-averaged phase [104].

In the case of the present thesis number of grid points (N_g), tests revealed that N_g = 512 is an ideal option as it is also in concurrence with the qualities cited in the literature [105-107]. Here, the numerical computations of propagation of the beam in turbulence are represented by a Random Phase Screen (RPS), developed by Halil T. Eyyuboğlu [108].

The numeric is acquired by settling (α_s = 1 cm) and considering the source. Furthermore, the propagation conditions are implemented using a suitable random phase screen numbers (N_s) model and a wide range of intermediate planes is represented between the source and the receiver is taken to be 21. To ensure reliability, precautions are taken so that the RPS setup can withstand extreme turbulence conditions. This is achieved by opting for a wide range of grid points on supply and receiver planes, mainly N_g = 1024 grids, where L_s is source aperture length and L_r is the side length of square aperature opening of the receiver plane, so the source $(L_s \times L_s)$ and the receiver $(L_r \times L_r)$ plane dimensions are set at 10 cm × 10 cm and 40 cm × 40cm, respectively. The receiver aperture has a square opening of 14 cm × 14 cm. The grid spacing of the source plane is d_1, as in the following:

$$d_1 = \frac{L_s}{N_g} \tag{6.3}$$

The grid spacing of the receiver plane is d_2, thus:

$$d_2 = 1.227\times10^{-6}\times L - 1.953\times10^{-6} \tag{6.4}$$

The number of realization N_R must be made to approach the averaged analytic result, and it was adjusted to 500. All numerical computations with all of the numerical computations are carried out within a range of wavelengths (1350 μm to 1550 μm).

The vortex beams are explained in the next section and they are established in order to evaluate SI performance in strong turbulence. To define these beams, radial and Cartesian coordinates are used, i.e., (s, ϕ_s) and (s_x, s_y).

For cylindrical coordinates:

$$s = (s, \phi_s), \tag{6.5}$$

For Cartesian coordinates:

$$s = \sqrt{s_x^2 + s_y^2}, \tag{6.6}$$

The mathematical model is explained in Eq. (6.7):

$$U_r(r_x, r_y, L) = F^{-1}\left\{F\left[U_s(s_x, s_y)\right]F\left[h(r_x, r_y)\right]\right\} = F^{-1}\left[\left[U_s(f_x, f_y)\right]F\left[H(f_x, f_y)\right]\right], \tag{6.7}$$

where $U_r(r_x, r_y, L)$ is the receiver field, $U_s(s_x, s_y)$ is the source field, $h(r_x, r_y)$ is the spatial response of the propagation medium, (r_x, r_y) are the transverse coordinates in the receiver plane., F indicates the Fourier Transform, F^{-1} denotes the inverse Fourier Transform and the arguments (f_x, f_y) are the spatial frequencies. It is important to note that $U_s(s_x, s_y)$ and $H(f_x, f_y)$ has the inclusion that the source and receiver coordinates are of the same scale or of the same increments.

$$H(f_x, f_y) = F\left[h(r_x, r_y)\right] = \exp\left(j\frac{2\pi}{\lambda}L\right)\exp\left[-j\pi\lambda L(f_x^2 + f_y^2\right], \tag{6.8}$$

By setting and the number of realizations (runs) is denoted by N_R and equal to 500, and the total numbers of random phase screens to N_S = 21, which goes from (n − 1) to the nth one [108].

$$U_r(r_x, r_y, n\Delta L) = F^{-1}\left(F\left\{U_r\left[r_x, r_y, (n-1)\Delta L\right]\exp\left[j\phi(r_x, r_y)\right]\right\}H\left(f_x, f_y\right)\right), \tag{6.9}$$

where $\phi(r_x, r_y)$ signifies spatial phase distribution derived from the power spectral density function and ΔL is the distance between the two screens. Fig. 8 illustrates a picturesque view of modeling propagation in turbulence via random phase screens.

$$\left\langle I(r, L)\right\rangle = \left\langle U(r, L)U(r, L)^*\right\rangle, \tag{6.10}$$

$$r = \sqrt{r_x^2 + r_y^2}, \tag{6.11}$$

This can classify the scintillation index into the point like scintillation and aperture average scintillation, otherwise known as power scintillations [108].

r refers to a certain coordinate location, whereas the results are over a certain aperture opening with radius R_a, $\langle\ \rangle$ denotes the mean value and $I(r,L)$ is the receiver intensity. Eq. (3.31) is the scintillation index (SI) at a specific location on the receiver plane, and this equation is valid so long as $R_a \langle \sqrt{0.5\lambda L/\pi}$; otherwise, the aperture averaged scintillation or power scintillation will occur, defined as:

$$P(L) = \int_{-0.5\sqrt{\pi R_a}}^{0.5\sqrt{\pi R_a}} \int_{-0.5\sqrt{\pi R_a}}^{0.5\sqrt{\pi R_a}} I(r_x, r_y, L) dr_x dr_y, \tag{6.12}$$

$$b^2(L) = \frac{\langle P^2(L)\rangle}{\langle P(L)\rangle^2} - 1, \tag{6.13}$$

where $P(L)$ denotes the power of the beam at L, and this power can be collected by a circular aperture of radius R_a. In case the aperture is square-shaped, the $0.5\sqrt{\pi R_a}$ is equivalent to the side length L_r [108].

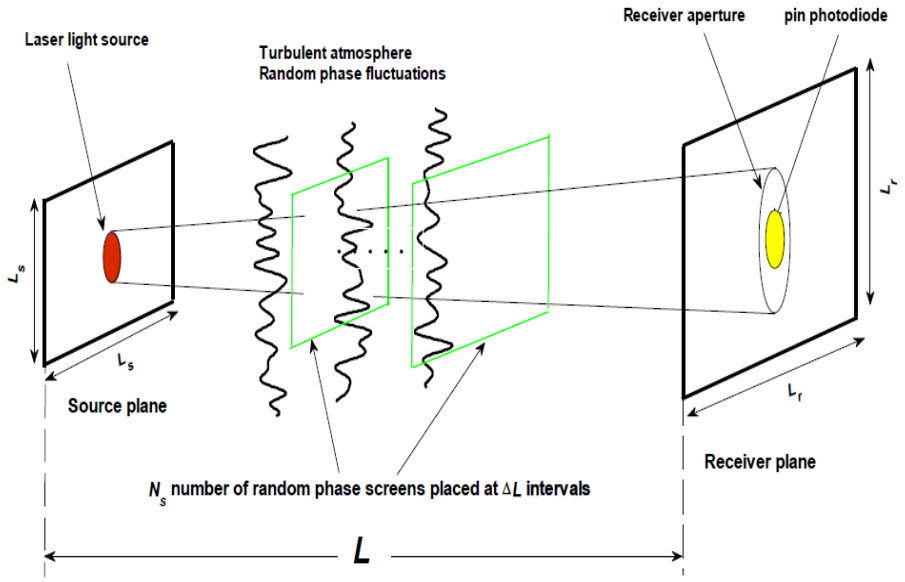

Figure 8: Random Phase Screen Model of the propagation of the beam in turbulence [108]

6.5 Expression of Gaussian Vortex Source Beams

A list of selected vortex source beams is provided whose phase distribution of the source and receiver are (Φ_s & Φ_r) to be assessed $(U_1, U_2, U_3, U_4, U_5)$.

As stated previously, these source beams are defined either in radial, i.e., (s,∅), or Cartesian coordinates, i.e., (s_x, s_y).

Firstly, a simple form of the Gaussian vortex beam (GVB) has been utilized in many studies; for instance, in [109-111], with the source field expression as in the following:

$$U_1(s,\phi) = \left(\frac{s}{\alpha_s}\right)^m \exp\left(-\frac{s^2}{\alpha_s^2}\right)\exp(jm\phi), \tag{6.14}$$

where m is known as the topological charge, while α_s refers to the source size. Secondly, the field of the elliptical Gaussian vortex beam can be written as follows [112].

$$U_2(s_x, s_y) = \left(\frac{s_x + j\,\varepsilon_s s_y}{\alpha_s} \right)^m \exp\left(-\frac{s_x^2 + \varepsilon_s s_y^2}{\alpha_s^2} \right) \exp(jm \tan \frac{\varepsilon_s s_y}{s_x}), \tag{6.15}$$

where ε_s stands for the degree of elasticity.

Thirdly, the Laguerre-Gaussian beam is most commonly known in vortex beam [113-115].

$$U_3(s, \phi) = \left(\frac{s}{\alpha_s} \right)^m \exp\left(-\frac{s^2}{\alpha_s^2} \right) L_n^m \exp(jm\phi), \tag{6.16}$$

Fourthly, the Bessel-Gaussian type vortex beam can be written as follows:

$$U_4(s, \phi) = \exp\left(-\frac{s^2}{\alpha_s^2} \right) J_m \exp\left(\frac{s}{\alpha_s} \right) \exp(jm\phi) \tag{6.17}$$

Recently, flat-topped Gaussian vortex beams have been introduced with the related source field expression being [116].

$$U_5(s_x, s_y) = \frac{1}{N} \left(\frac{s_x + j s_y}{\alpha_s} \right)^m \sum_{n=1}^{N} (-1)^{n-1} (Nn) \exp\left(-n \frac{s_x^2 + s_y^2}{2} \right) \tag{6.18}$$

CHAPTER 7

RESULTS AND DISCUSSION

7.1 Introduction

Vortex beams have become popular nowadays. In this section, it is possible to encounter extensive investigations of radiation, the OAM and the phase distribution of source and receiver fields. Moreover, a scintillation index formulation is carried out for the Gaussian beam on the propagation length in turbulent atmospheres, and depending on the generalized beam formulation of the field, the computation of scintillation index methods is compared in order to select the best way to describe the phenomenon.

Three types of scintillation index methods are examined: the Rytov, Huygens-Fresnel and Random Phase Screen methods. In addition, the variation of polynomial parameters (the *m*-radial number or topological charge number, *n*-orbital angular momentum quantum number or degree of the polynomial) of the Laguerre function is applied to the Laguerre-Gaussian vortex beam (LGVB) which is propagated into random media of an atmosphere modeled by the phase screen technique. This investigation is implemented by using the 7-Mary symbols of Laguerre Beams with different values of polynomial parameters that are transmitted in strong turbulence.

The Gaussian, Elliptical, Laguerre and Bessel vortex beams were selected and measurements of the SI were taken for different values of the *n* and *m* parameters for their respective beams. The Gaussian (GB) and Gaussian vortex beams (GVB) were selected and measurements of the SI were taken for different values of the *n* and *m* parameters of the GVB.

7.2. Phase Distribution Behavior with Multi-values of Topological Charge of Vortex Beams

In this section, we present the numeric results obtained for plane phase distribution source and receiver (Φ_s , Φ_r) with multi-values of topological charge for Gaussian vortex, Elliptical Gaussian vortex and Laguerre-Gaussian vortex beams, respectively. Their sources plane fields are given by Eqs. (6.14), (6.15) and (6.16)

7.2.1. Gaussian Vortex Beam

The source field expression of it is explained in Eq. (6.14) with the topological charges are −3, 3, −5, 5, −7 and 7 and α_s = 1 cm. The phase distribution source and receiver with multi-values of topological charge are explored in Figure 9.

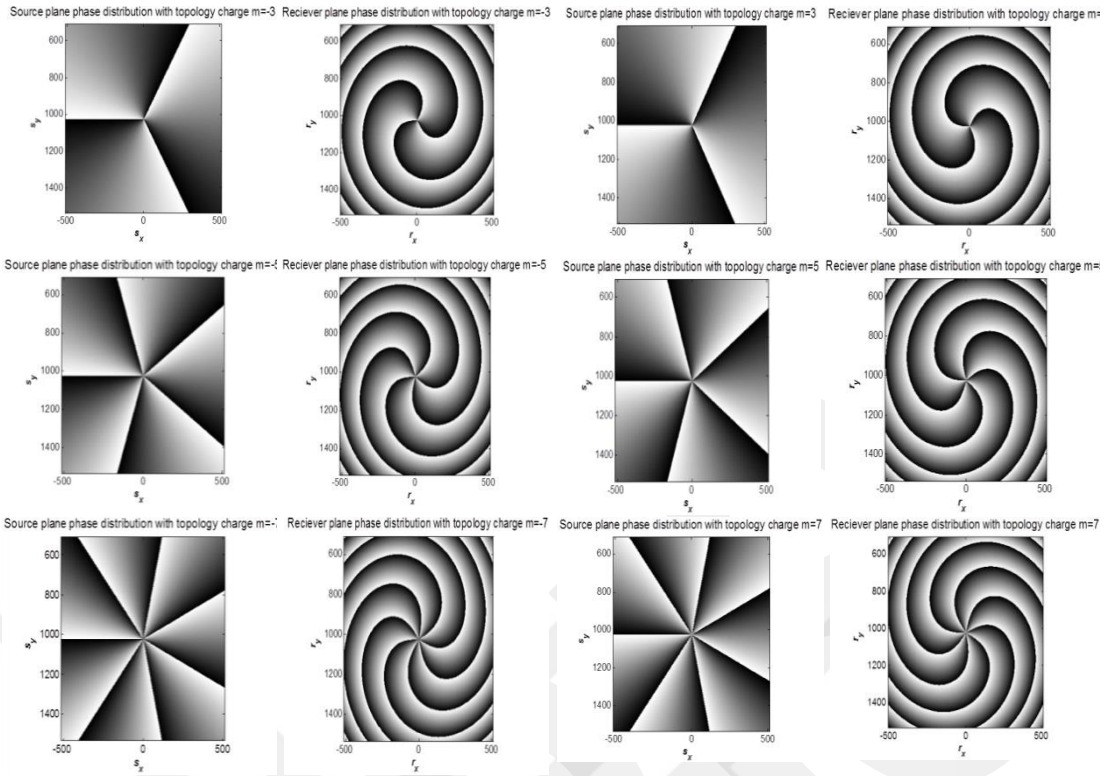

Figure 9: Source and receiver planes phase distribution of Gaussian vortex beam with the topological charge of $m = m_{-3} = -3$, $m = m_3 = 3$, $m = m_{-5} = -5$, $m = m_5 = 5$, $m = m_{-7} = -7$ and $m = m_7 = 7$

7.2.2. Elliptical Gaussian Vortex Beam

The source field expression of the Elliptical Gaussian vortex beam is explained in Eq. (6.15) with topological charges of −3, 3, −5, 5, −7 and 7, while $\alpha_s = 1$ cm and the ε_s degree of elasticity is equal to 0.8. We explore the phase distribution source and receiver with multi-values of the topological charges in Figure 10.

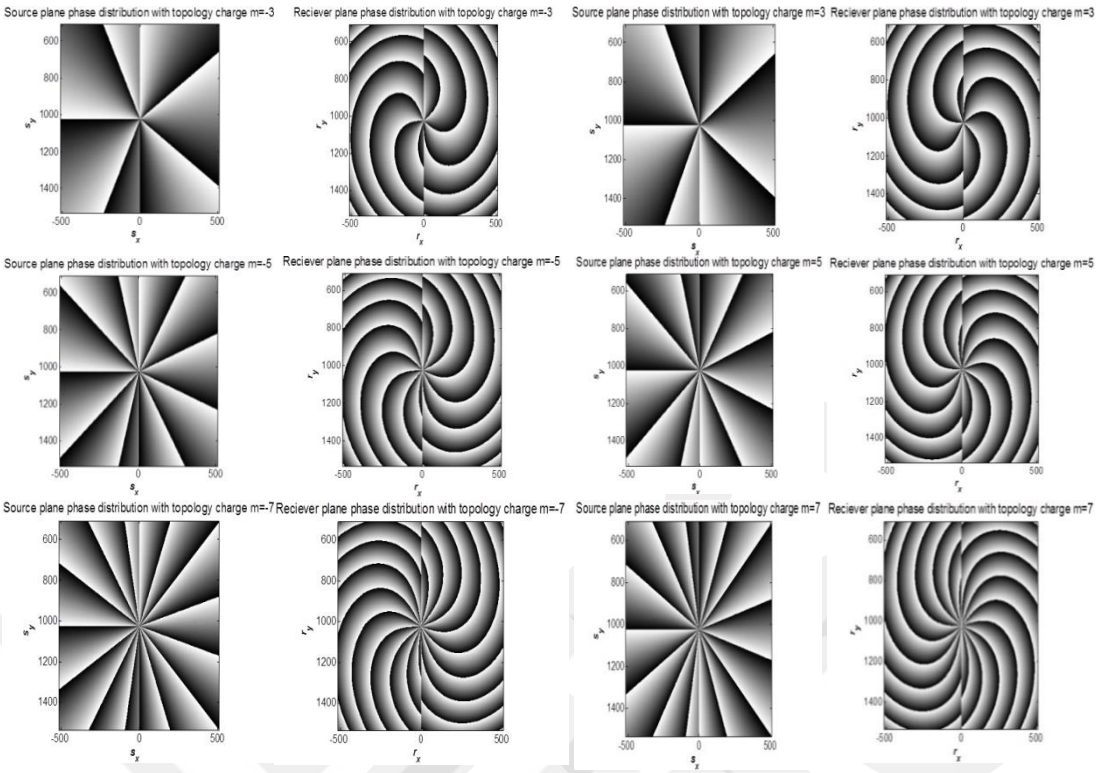

Figure 10: Source and receiver planes phase distribution of Elliptical Gaussian vortex beam with the topological charge of $m = m_{-3} = -3$, $m = m_3 = 3$, $m = m_{-5} = -5$, $m = m_5 = 5$, $m = m_{-7} = -7$ and $m = m_7 = 7$

7.2.3 Laguerre-Gaussian Vortex Beam

The source field expression of the Laguerre-Gaussian vortex beam is explained in Eq. (6.16) with the topological charges being −3, 3, −5, 5, −7 and 7, α_s = 1 cm, and n is the degree of the polynomial. We explore the phase distribution of the source and receiver with multi-values of topological charge in Figure 11.

Finally, it is expected that the results in Section 7.2 will be beneficial to optical links, and this work is assisted to know the phase distribution receiver. Therefore, we collected the results into an article that had been acceepted for publication in a science journal [117].

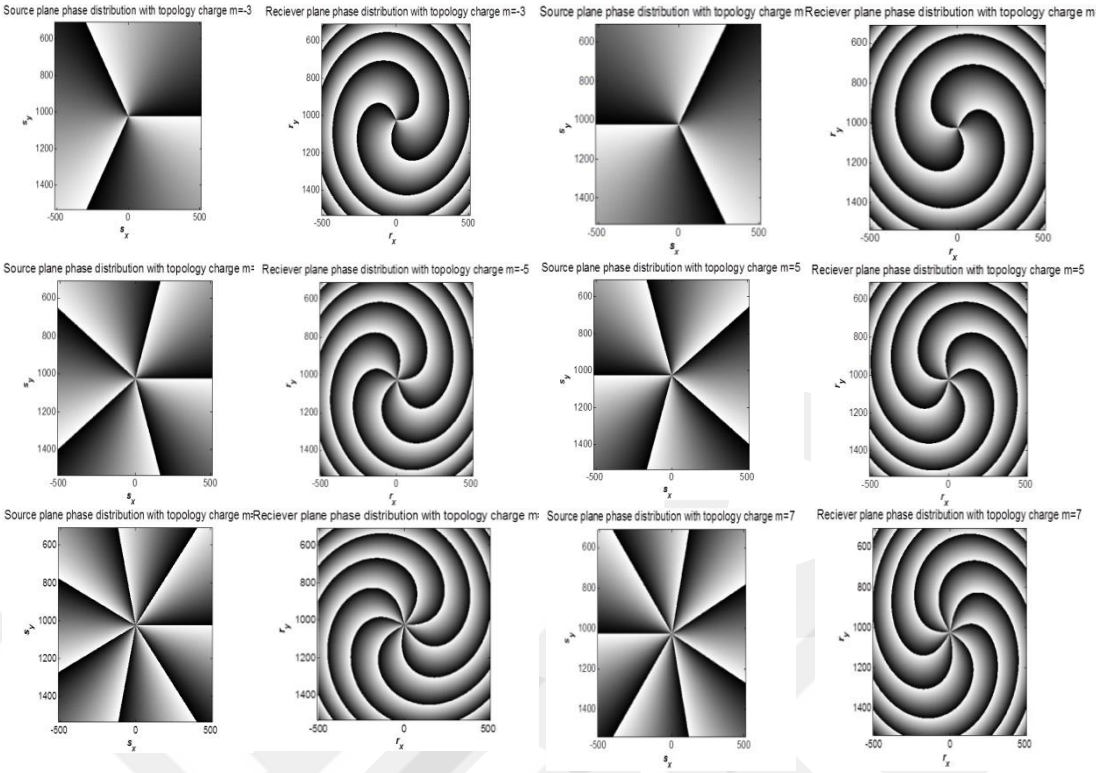

Figure 11: Source and receiver planes phase distribution of Laguerre-Gaussian vortex with the topological charge of $m = m_{-3} = -3$, $m = m_3 = 3$, $m = m_{-5} = -5$, $m = m_5 = 5$, $m = m_{-7} = -7$ and $m = m_7 = 7$

7.3 Computing the Scintillation Index of a Gaussian Beam Using Different Methods

In this section, we present the numeric results obtained for scintillation characteristics in strong atmospheric turbulence for Gaussian beams at various propagation distances using Rytov, Huygens–Fresnel and Random Phase Screen methods. Their source plane field and the equations of the SI are given by: Equations (6.1) and (3.31).

7.3.1. SI Results with the Rytov Method

The source field expression was explained in Eq. (6.1), which is able to generate a Gaussian beam. We concentrate on the Rytov method to compute the SI of the Gaussian beam. For this, in Figures 12 and 13, we explore the scintillation index of

the Gaussian beam with a wavelength operation of λ = 1.35 μm, $\lambda = 1.55\mu\text{m}, C_n^2 = 10^{-15}\,\text{m}^{-2/3}$, and a source size $\alpha_s = 1\,\text{cm}$. In this section, graphic illustrations were provided based on the numerical evaluation of Eq. (9) of Ref. [118]. Although the scintillation index expression of Eq. (9) is able to generate results for any type of beam composed of the summation of different fundamental Gaussian beams, in the current study, we concentrate only on the Gaussian beam. A comparison was made between the data available in Figure 13 and those of the mentioned Figure 1 in Ref. [118], a good agreement was found between the two cases. Figure 14 shows the SI of the GB with wavelengths of operation of λ = 1.35 μm and λ = 1.55 μm together. It is clear that an SI with λ = 1.55 μm is better than an SI with λ = 1.35 μm.

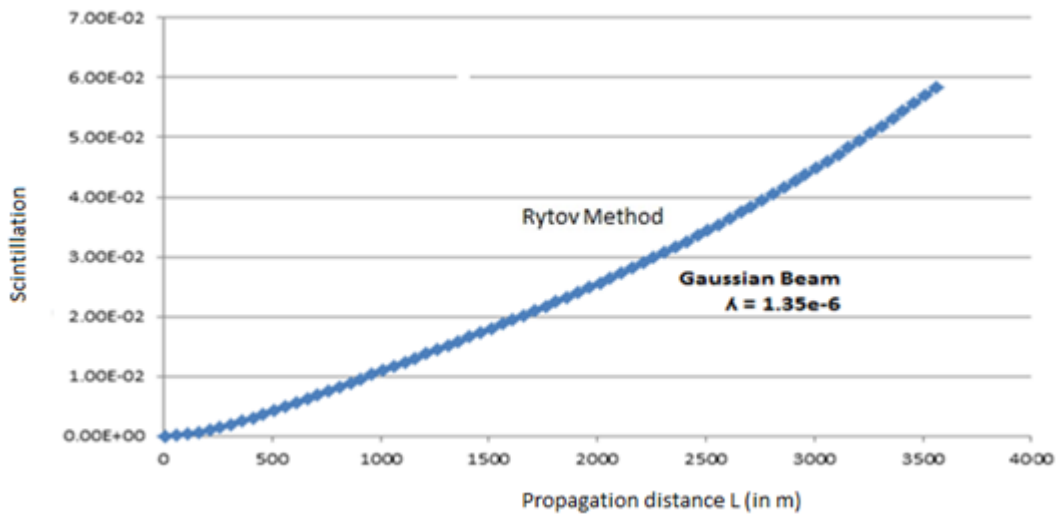

Figure 12: Scintillation behavior of the Gaussian beam against the propagation distance using the Rytov method for λ = 1.35 μm

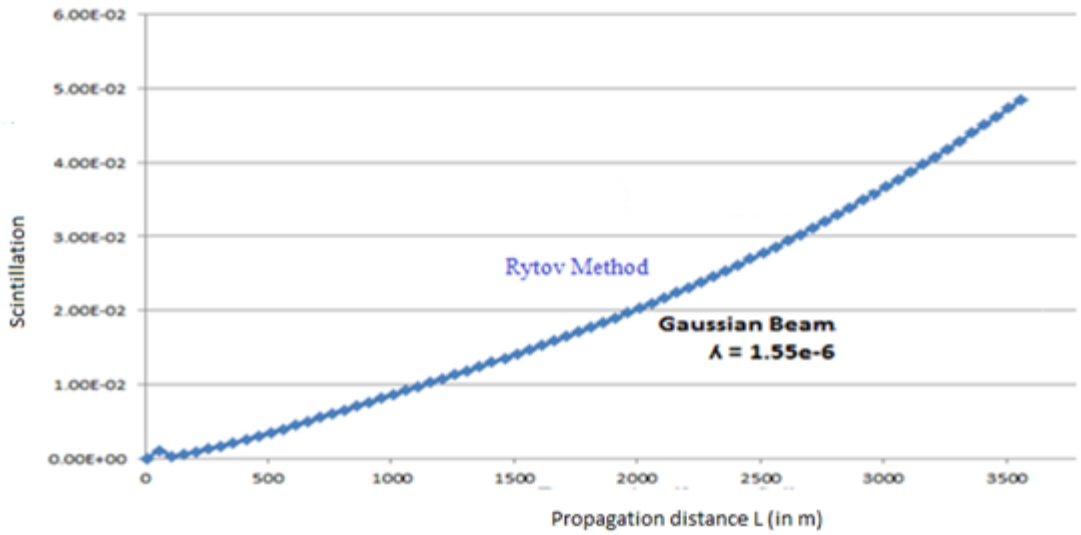

Figure 13: Scintillation behavior of the Gaussian beam against the propagation distance using the Rytov method for λ = 1.55 µm

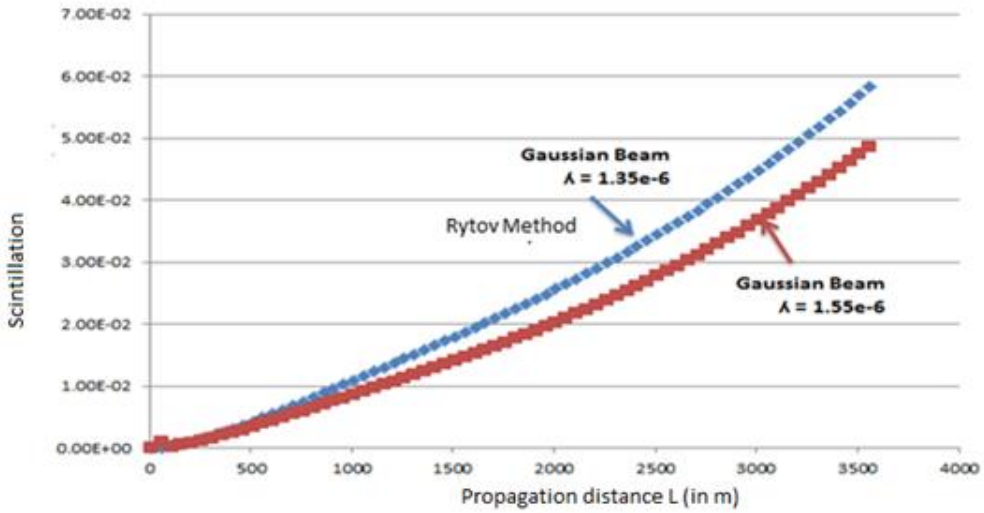

Figure 14: Scintillation behavior of the Gaussian beam against the propagation distance using the Rytov method for λ = 1.35 µm and λ = 1.55 µm

7.3.2. SI Results with the Huygens-Fresnel Method

The source field expression was explained in Eq. (6.1), which can be used to generate a Gaussian beam. In the current study, we concentrate on the Huygens-

Fresnel method to compute the SI for the beam, it was presented these scintillation calculations in weak atmospheric turbulence for he Gaussian beam based on the extended Huygens–Fresnel integral and a mathematical function designed by [119]. As demonstrated in Figures 15 and 16, we explore the scintillation index of the Gaussian beam with wavelengths of operation of $\lambda = 1.35\mu$m and $\lambda = 1.55\mu$m, $C_n^2 = 10^{-15}\,\mathrm{m}^{-2/3}$, and source size $\alpha_s = 1$cm. Adjusting of parameters in our study with those of Ref. [119], and based on the numerical computations of Eqs. (3), (6) and (9) of Ref. [119]. A comparison was made between the data available in Fig. 16 and those of the mentioned Fig. 1 in Ref. [119], good agreement was found between the two cases. Finally, Fig. 17 shows the SI of the GB with wavelengths of operation of $\lambda = 1.35\mu$m and $\lambda = 1.55\mu$m together, and it is clear that the SI with $\lambda = 1.55\mu$m is better than the SI with $\lambda = 1.35\mu$m.

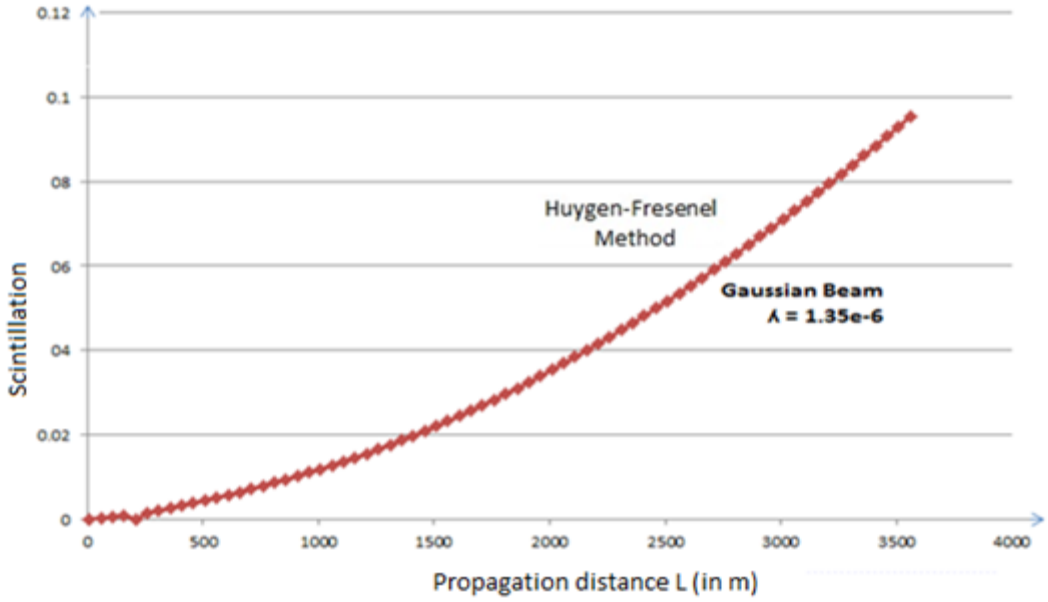

Figure 15: Scintillation behavior of the Gaussian beam against the propagation distance using the Huygens-Fresnel method for λ = 1.35 μm

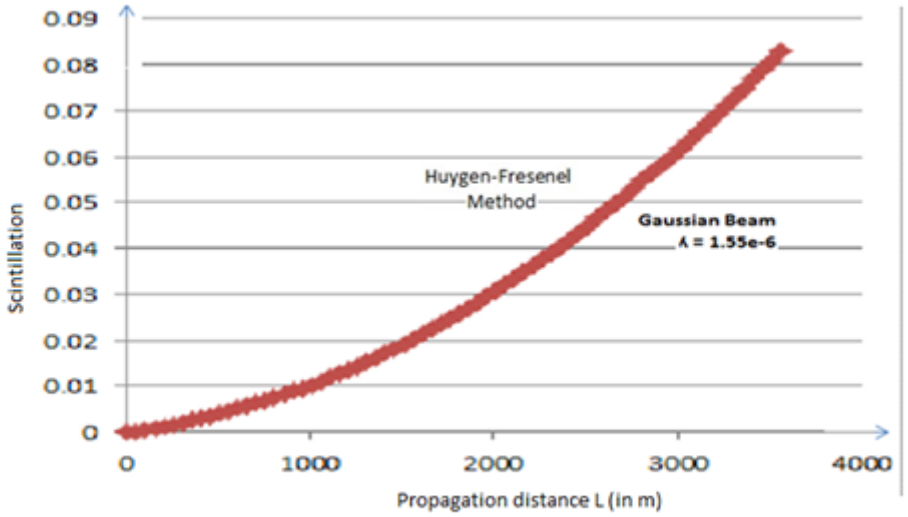

Figure 16: Scintillation behavior of the Gaussian beam against the propagation distance using the Huygens-Fresnel method for λ = 1.55 µm

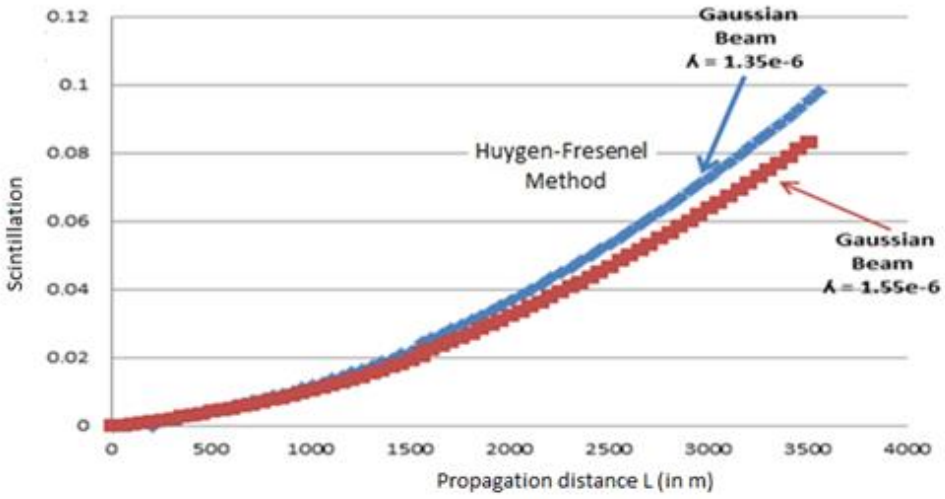

Figure 17: Scintillation behavior of the Gaussian beam against the propagation distance using the Huygens-Fresnel method for λ = 1.35 µm and λ = 1.55 µm

7.3.3. SI Results using the Random Phase Screen Method

The source field expression was explained in Eq. (6.1), which is able to generate a Gaussian beam. In the present work, we concentrate on the random phase screen to

compute the aperture averaged scintillation for the Gaussian beam as per Figures 18 and 19. We explore the aperture averaged scintillation of the Gaussian beam with a wavelength of operation at $\lambda = 1.35\mu$m and $\lambda = 1.55\mu$m,$C_n^2 = 10^{-15}$ m$^{-2/3}$, and a source size of $\alpha_s = 1$ cm. Applications of random phase screen to specific beam types have also appeared in the literature. Selecting the appropriate grid spacings and number of grid points, in turn, depends on source beam profile, diffractive beam properties and turbulence induced spreading of the propagation medium. In this process, the number of intermediate phase screen plates that are to be placed between the transmitter and the receiver is also determined. The detailed guidelines for such computations and constraints are stated in Ref. [120]. A comparison was made between the data available in Fig. 19 and those of the mentioned Fig. 6 in Ref. [120], a good agreement was found between the two cases. Figure 20 shows the aperture averaged scintillation of the GB with wavelengths of operation of $\lambda = 1.35\mu$m and $\lambda = 1.55\mu$m together, and it is clear that the that with $\lambda = 1.55\mu$m is better than the SI with $\lambda = 1.35\mu$m.

In the previous sections, we presented the numerical results obtained for scintillation characteristics in atmospheric turbulence for the Gaussian beam at various propagation distances using the Rytov, Huygens Fresnel, and Random Phase Screen methods. From the graphical outputs in Figures 21 and 22, it can be observed that the Random Phase Screen method exhibits less scintillation and it is nearer to the experimental method. From the above three tests, we deduce that the designed random phase screen setup can safely and reliably be used to estimate the scintillations of the Gaussian beam.

Finally, we collected the results in an article that had been accepted for publication in a science journal [121].

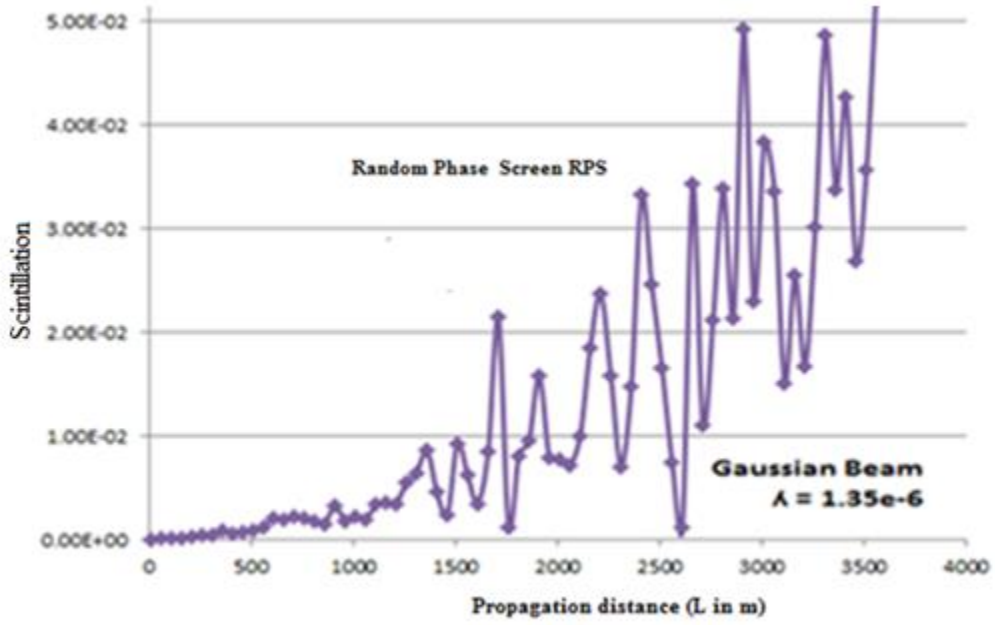

Figure 18: Scintillation behavior of the Gaussian beam against the propagation distance using the Random Phase Screen method for λ = 1.35 μm

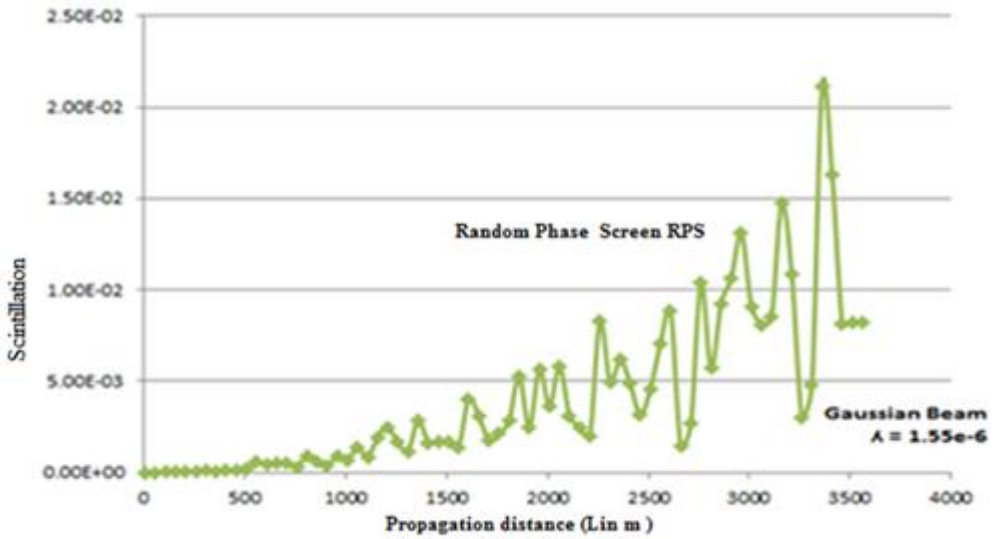

Figure 19: Scintillation behavior of the Gaussian beam against the propagation distance using the Random Phase Screen method for λ = 1.55 μm

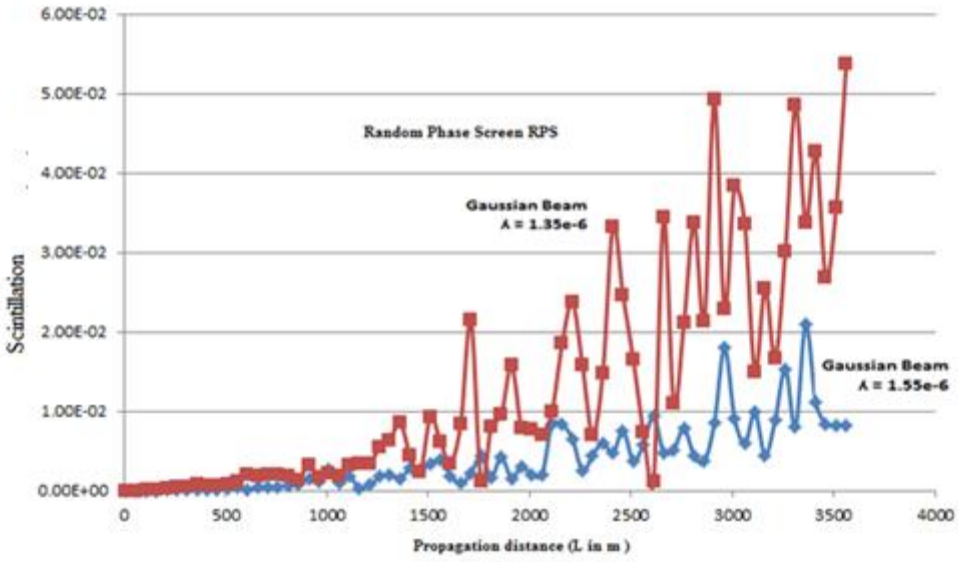

Figure 20: Scintillation behavior of the Gaussian beam against the propagation distance using the Random Phase Screen method for λ = 1.35 μm and λ = 1.55 μm

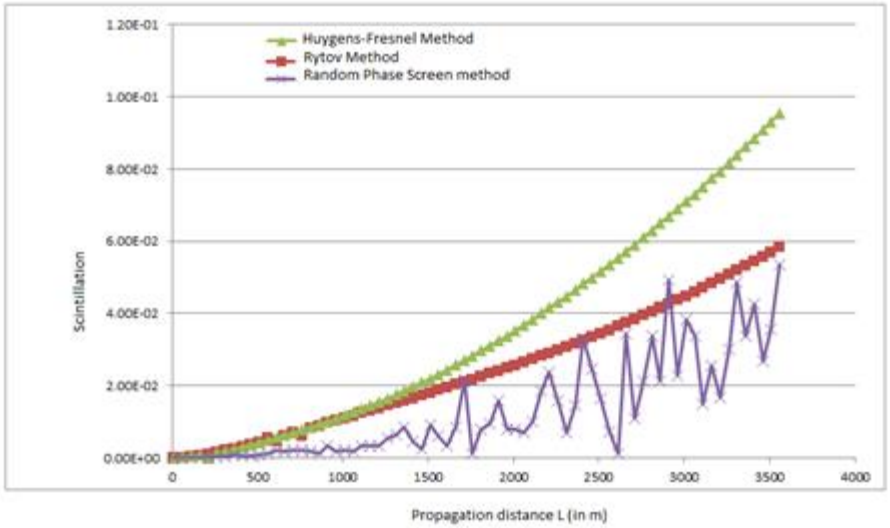

Figure 21: Scintillation behavior of the Gaussian beam against the propagation distance using the Rytov, Huygens-Fresnel and Random Phase Screen methods for λ = 1.35 μm

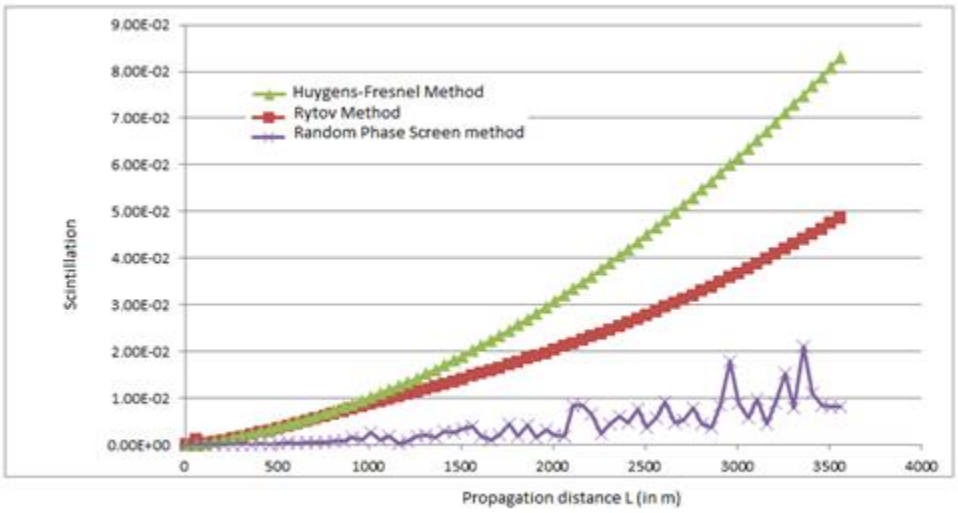

Figure 22: Scintillation behavior of the Gaussian beam against the propagation distance using the Rytov, Huygens-Fresnel and Random Phase Screen methods for λ = 1.55 μm

7.4. Results of the Scintillation Index for LGVB

7.4.1. Topological Charge for LGVB Being Constant

In this section, we discuss the values of the SI when an m for the LGVB is constant.

To begin with, m is adjusted as a constant value and made equal to 1, 3 or 7 for each

case and we set the degree of the polynomial (n) to different values such as 0, 1, 3, 4, 5 and 6.

7.4.1.1. Topological Charge (m = 1)

In this case, we set $(L_0^1, L_1^1, L_2^1, L_3^1, L_4^1, L_5^1, L_6^1)$. Figure 23 explains the values of the SI as being increased with an increase in the polynomial degree and the propagation distance, and when L = 3.5 km, the highest value of the SI and for $m = 1$ and $n = 6$, L_6^1 is equal to 0.1746 $m^{-2/3}$.

7.4.1.2. Topological Charge (m = 3)

In this case, we set $(L_0^3, L_1^3, L_2^3, L_3^3, L_4^3, L_5^3, L_6^3)$. Figure 24 shows the values of the SI increasing with an increase in the polynomial degree and the propagation distance. However, in this case, the values of the SI are greater than those in Section 7.4.1.1, and when L = 3.5 km, the highest value of the SI and for $m = 3$ and $n = 6$, L_6^3 is equal to 0.1864 $m^{-2/3}$.

7.4.1.3. Topological Charge (m = 5)

In this case, we set $(L_0^5, L_1^5, L_2^5, L_3^5, L_4^5, L_5^5, L_6^5)$. Figure 25 shows the values of the SI increasing with an increase in the polynomial degree and the propagation distance. However, in this case, the values of the SI are greatest in Sections 7.4.1.1 and 7.4.1.2, and when $L = 3.5$ km, the highest value of the SI and for $m = 5$ and $n = 6$, L_6^5 is equal to 0.2433 $m^{-2/3}$.

It can be seen from the results from the previous sections (7.4.1.1, 7.4.1.2 and 7.4.1.3) that the values of the scintillation index increased with an increase in the values of the *n* and *m* parameters.

7.4.2. Polynomial Degree for the LGVB Being Constant

In this section, we discuss the values of the SI when the degree of the polynomial for the LGVB is constant. To begin, n is adjusted as a constant value and made equal to 1 or 5 for each status. We set the topology charge (*m*) to different values, such as 0, 1, 3, 4, 5 and 6.

7.4.2.1. Polynomial Degree for LGVB (n = 1)

In this case, we set $(L_1^0, L_1^1, L_1^2, L_1^3, L_1^4, L_1^5, L_1^6)$. Figure 26 shows the values of the SI increasing with an increase in the topological charge (*m*) and the propagation distance. When L = 3.5 km, the highest value of the SI and for $n = 1$ and $m = 6$, L_1^6 is equal to 0.08238 $m^{-2/3}$.

7.4.2.2. Polynomial Degree for LGVB (n = 3)

In this case, we set $(L_3^0, L_3^1, L_3^2, L_3^3, L_3^4, L_3^5, L_3^6)$. Figure 27 explains the values of the SI increasing with an increase in the m and the propagation distance. When L = 3.5 km, the highest value of the SI and for $n = 3$ and $m = 6$, L_3^6 is equal to 0.1249 $m^{-2/3}$.

7.4.2.3. Polynomial Degree for LGVB (n = 5)

In this case, we set $(L_5^0, L_5^1, L_5^2, L_5^3, L_5^4, L_5^5, L_5^6)$. Figure 28 shows the values of the SI increasing with an increase in the m and the propagation distance. When

$L = 3.5$ km, the highest value of the SI and for $n = 5$ and $m = 6$, L_5^6 is equal to 0.1889 $m^{-2/3}$.

It can be seen from the results from the previous sections (7.4.2.1, 7.4.2.2 and 7.4.2.3) that the value of the scintillation index increased with an increase in the values of the *n* and *m* parameters.

Finally, the values of the scintillation index for the LGVB are near to each other in the case of changing the degree of the polynomial (n) when the (m) is fixed to 1, 3 or 5. In contrast, these values of the SI are far from each other in the case of the degree of the polynomial being fixed to 1 or 5 and with a change of the m. Therefore, for a good state of transmission, it is recommended that the degree of the polynomial be made equal to $n = 1$ and the topological charge numbers equal to 0, 1, 2, 3, 4, 5 and 6, such that $(L_1^0, L_1^1, L_1^2, L_1^3, L_1^4, L_1^5, L_1^6)$. In the end, we prepared an article for submission to a science journal.

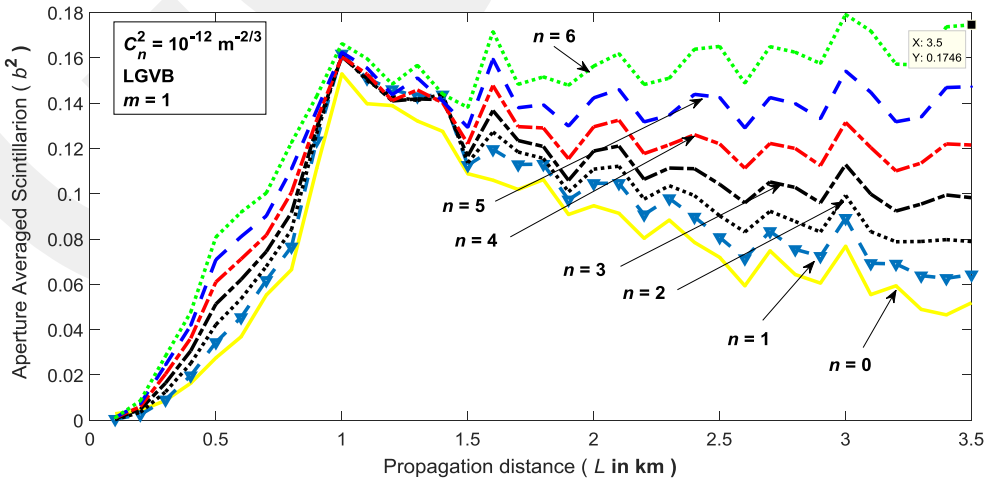

Figure 23: Scintillation variation of the LGVB with the degree of the polynomial when the topological charge is fixed to $m = 1$ against the propagation distance.

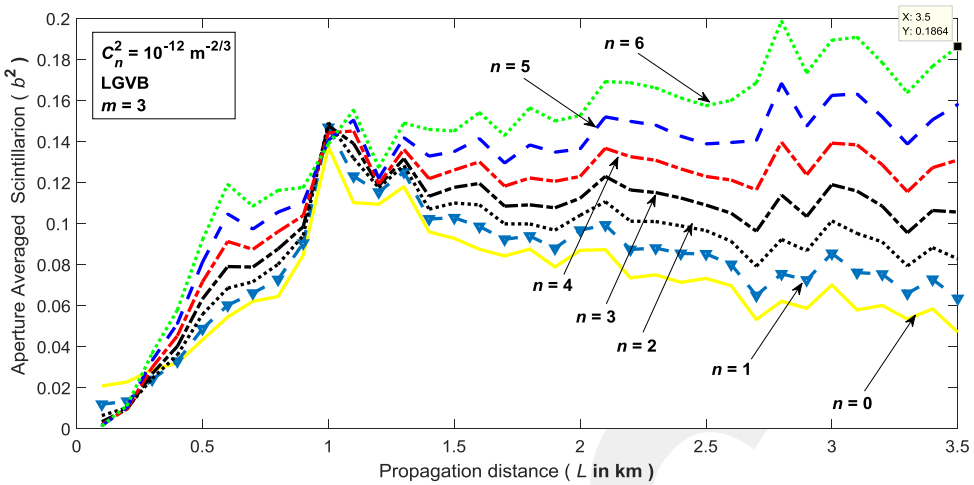

Figure 24: Scintillation variation of the LGVB with the degree of the polynomial when the topological charge is fixed to $m = 3$ against the propagation distance

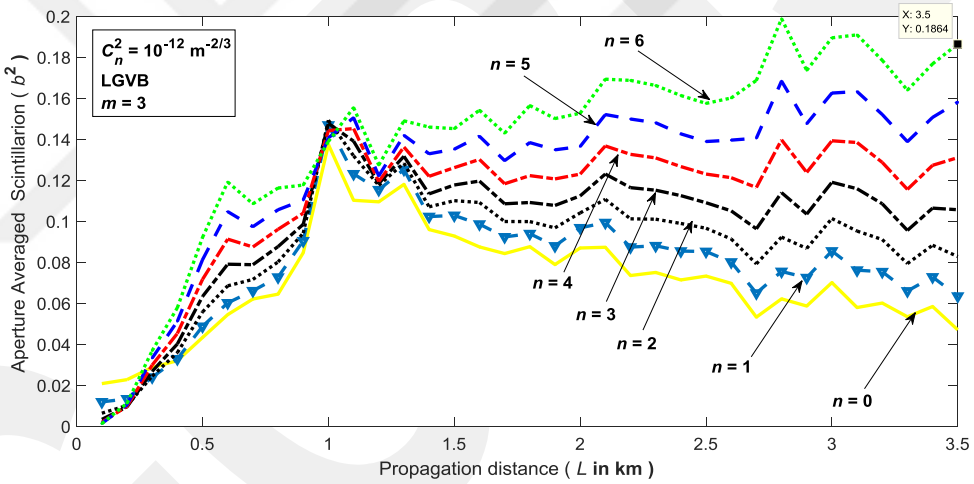

Figure 25: Scintillation variation of the LGVB with the degree of the polynomial when the topological charge is fixed to $m = 5$ against the propagation distance.

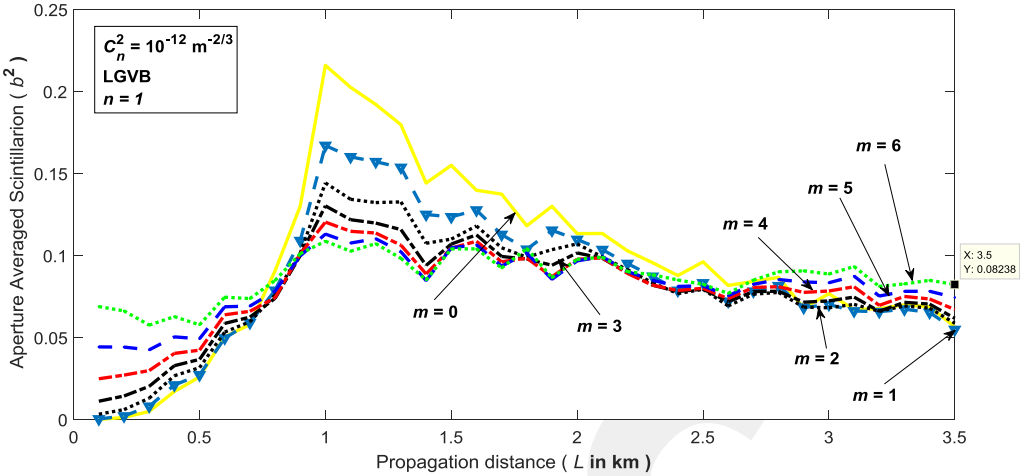

Figure 26: Scintillation variation of the LGVB with the topological charge when the degree of the polynomial is fixed to n = 1 against the propagation distance

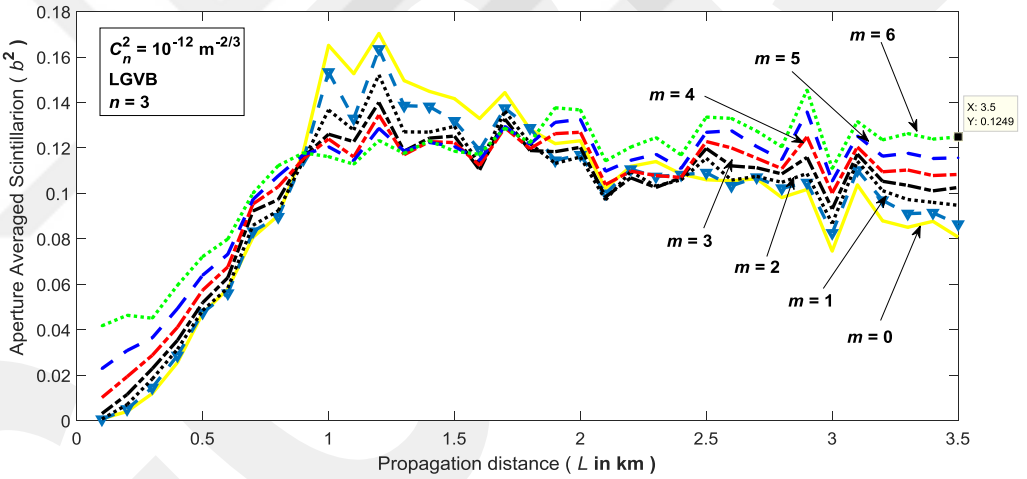

Figure 27: Scintillation variation of the LGVB with the topological charge when the degree of the polynomial is fixed to n = 3 against the propagation distance

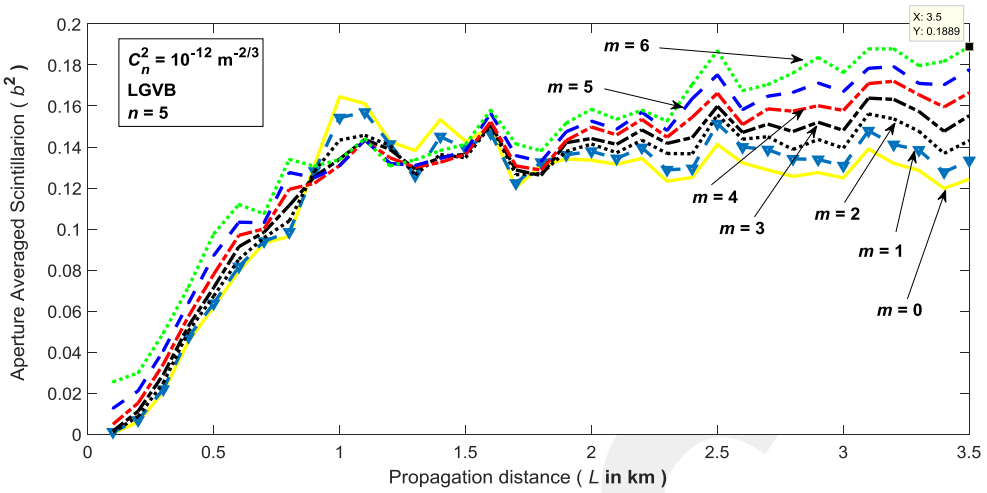

Figure 28: Scintillation variation of the LGVB with the topological charge when the degree of the polynomial is fixed to $n = 5$ against the propagation distance

7.5. Comparisons between Gaussian, Elliptical, Laguerre and Bessel Vortex Beams

Four types of beam, namely Gaussian, Elliptical, Laguerre and Bessel vortex beams were selected and measurements of the SI were taken for different values of the n and m parameters for their beams by using Eqs. 6.14, 6.15, 6.16 and 6.17. Then, we compared among them to select the most suitable. Finally, it was found that the Elliptical beam with m equaling 7 and 3 were best. Figures 29, 30, 31, 32 and 33 show the changes of the SI taking a variety of values of the n and m parameters for multi-types of beam. Tables 2 and 3 show the effect of varying the n and m parameters on the values of the SI for the four types of beam.

Table 2: Variation of values of SI between Gaussian vortex (GVB) and Elliptical Gaussian vortex (EGVB) beams

Item	**Propagation Distance** (L in *m*)	**GVB** (*n* = 6, *m* = 3)	**GVB** (*n* = 5, *m* = 3)	**EGVB** (*m* = 7)	**EGVB** (*m* = 3)
1	1.00E−01	0.05946	0.0661	0.0856	0.02625
2	0.2	0.05479	0.07976	0.08123	0.03512
3	0.3	0.04365	0.0721	0.05658	0.03913
4	0.4	0.04085	0.0724	0.04804	0.03915
5	0.5	0.03872	0.06531	0.04817	0.0436
6	0.6	0.05416	0.07979	0.05591	0.05362
7	0.7	0.07204	0.09244	0.05736	0.05715
8	0.8	0.07648	0.0978	0.07266	0.0738
9	0.9	0.08401	0.1011	0.08576	0.09309
10	1	0.09241	0.103	0.114	0.1221
11	1.1	0.1112	0.1242	0.09577	0.1008
12	1.2	0.1266	0.1247	0.08237	0.08821
13	1.3	0.1342	0.1328	0.087	0.09165
14	1.4	0.1372	0.1445	0.06883	0.07232
15	1.5	0.1164	0.1251	0.07162	0.07637
16	1.6	0.1327	0.134	0.06887	0.07552
17	1.7	0.1224	0.1163	0.06825	0.0703
18	1.8	0.1162	0.118	0.0647	0.06932
19	1.9	0.1011	0.1109	0.0567	0.05996
20	2	0.1073	0.1118	0.04563	0.04896
21	2.1	0.102	0.1134	0.04401	0.04685
22	2.2	0.1097	0.1221	0.04986	0.05275
23	2.3	0.09474	0.1044	0.04175	0.04397
24	2.4	0.09702	0.1023	0.0445	0.04697
25	2.5	0.09235	0.1046	0.0453	0.04761
26	2.6	0.0886	0.09811	0.04542	0.05053
27	2.7	0.0994	0.107	0.03658	0.03895
28	2.8	0.08796	0.09735	0.0378	0.03976
29	2.9	0.07913	0.08766	0.03971	0.04179
30	3	0.07845	0.0924	0.03883	0.04116
31	3.1	0.08672	0.1055	0.03158	0.03354
32	3.2	0.06932	0.08092	0.03834	0.03929
33	3.3	0.06604	0.08197	0.03081	0.03394
34	3.4	0.08956	0.09745	0.03385	0.03659

Table 3: Variation of values of SI between Laguerre Gaussian vortex (LGVB) and Bessel Gaussian vortex (BGVB) beams

Item	**Propagation Distance** (L in *m*)	**LGVB** (*n* = 6, *m*= 3)	**LGVB** (*n* = 5, *m*= 3)	**BGVB** (*m* = 7)	**BGVB** (*m*= 3)
1	1.00E−01	0.05668	0.003523	0.07746	0.05359
2	0.2	0.06001	0.005602	0.08652	0.06002
3	0.3	0.04849	0.01492	0.07328	0.05576
4	0.4	0.0622	0.03112	0.07055	0.05731
5	0.5	0.05899	0.04701	0.06224	0.05408
6	0.6	0.06095	0.05674	0.07573	0.07005
7	0.7	0.07485	0.07757	0.0891	0.08556
8	0.8	0.07601	0.09473	0.09366	0.08997
9	0.9	0.09803	0.1139	0.09628	0.09581
10	1	0.09829	0.1223	0.09934	0.0981
11	1.1	0.09853	0.1286	0.1188	0.1232
12	1.2	0.0988	0.1121	0.1216	0.1262
13	1.3	0.09262	0.1195	0.1301	0.1357
14	1.4	0.08425	0.1082	0.1394	0.1428
15	1.5	0.08832	0.1024	0.1204	0.1212
16	1.6	0.08117	0.0959	0.1299	0.1363
17	1.7	0.08706	0.09938	0.112	0.1201
18	1.8	0.08397	0.09956	0.1157	0.1171
19	1.9	0.06802	0.08396	0.1063	0.1071
20	2	0.08262	0.09383	0.1075	0.11
21	2.1	0.08218	0.09174	0.1075	0.1096
22	2.2	0.07437	0.09449	0.1169	0.1191
23	2.3	0.07117	0.07852	0.09963	0.1015
24	2.4	0.07138	0.08126	0.09772	0.1015
25	2.5	0.07566	0.08211	0.09938	0.099
26	2.6	0.06991	0.07306	0.09332	0.09427
27	2.7	0.06126	0.06805	0.1027	0.1031
28	2.8	0.06694	0.06942	0.09185	0.0939
29	2.9	0.06076	0.06712	0.0828	0.08426
30	3	0.06242	0.06594	0.08715	0.08831
31	3.1	0.06076	0.06513	0.09954	0.09798
32	3.2	0.06077	0.0652	0.0762	0.07644
33	3.3	0.06603	0.06882	0.07671	0.07546
34	3.4	0.05866	0.06331	0.09335	0.09302

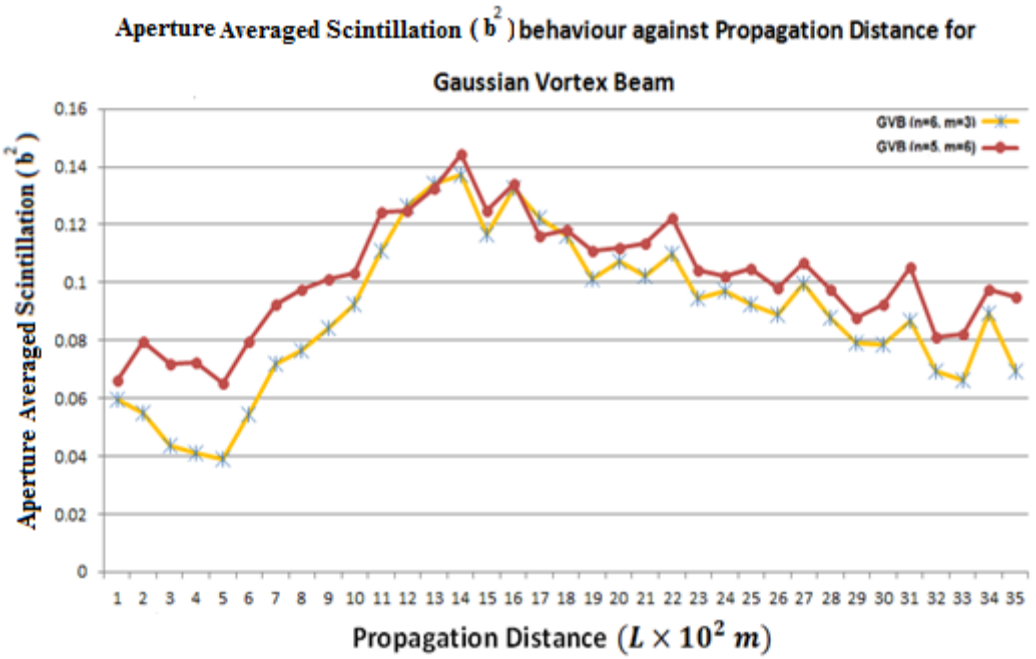

Figure 29: Aperture Averaged Scintillation variation of GVB with the topological charges equal to 3 and 6, and the degrees of the polynomial equal to 6 and 5 against the propagation distance

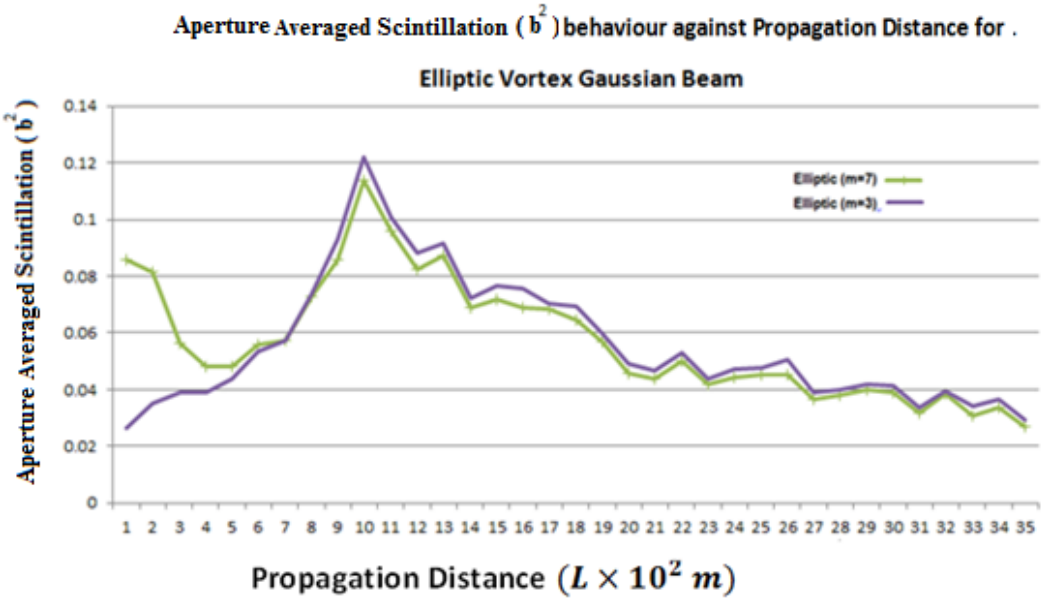

Figure 30: Aperture Averaged Scintillation variation of the Elliptic beam with the topological charges equal to 7 and 3 against the propagation distance

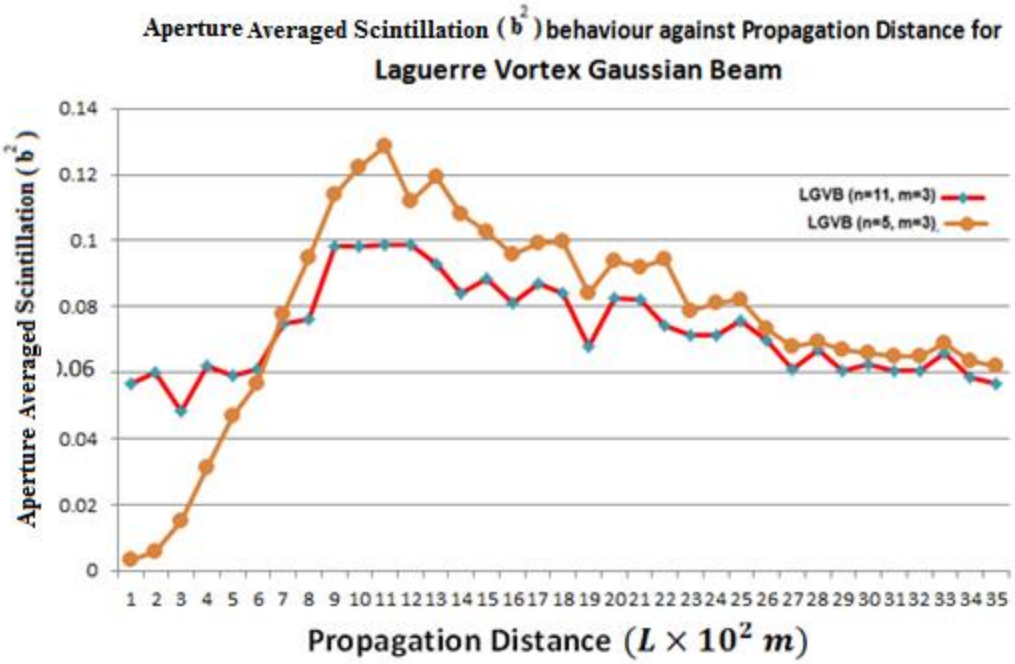

Figure 31: Aperture Averaged Scintillation variation of the LGVB with the topological charges equal to (m 3) and the degrees of the polynomial equal to 11and 5 against the propagation distance

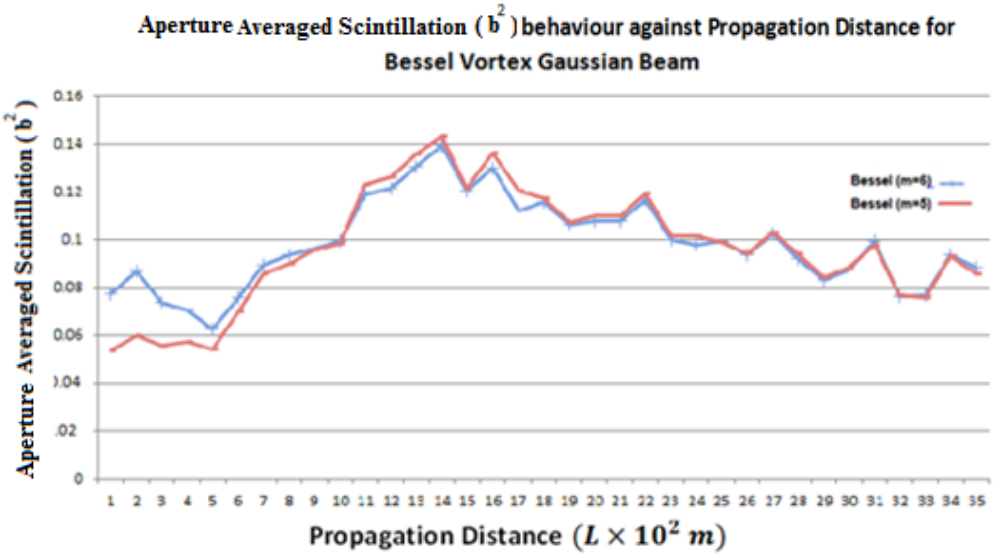

Figure 32: Aperture Averaged Scintillation variation of the BGVB with topological charges equal to 6 and 5 against the propagation distance (L in km).

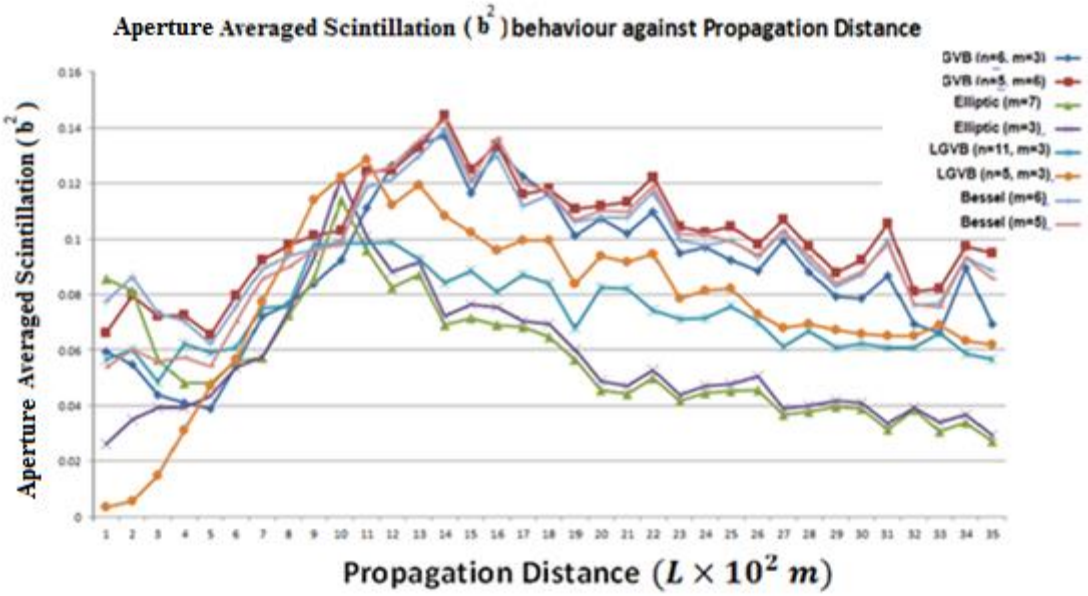

Figure 33: Changes in the Aperture Averaged Scintillation taking a variety of values of the *n* and *m* parameters for multi-types of beams against the propagation distance.

7.6 Comparison between Gaussian and Vortex Gaussian Beams

Two types of beam, namely the Gaussian (GB) and Gaussian vortex beams (GVB), were selected and measurements of the SI were taken for different values of the *n* and *m* parameters of the GVB. Then, it was shown that the GVB with a degree of the polynomial and topological charge being fixed to $n = 6$, $m = 3$ and $n = 5$, $m = 6$ were better than the GB. Figures 34 and 35 explain the change in the SI taking a variety of values of the *n* and *m* parameters for the Gaussian (GB) and Gaussian vortex beams (GVB) beams. It is clear that the SI for the Gaussian vortex beams (GVB) is better than the SI for the Gaussian vortex beams (GVB) with the same set of simulation parameters.

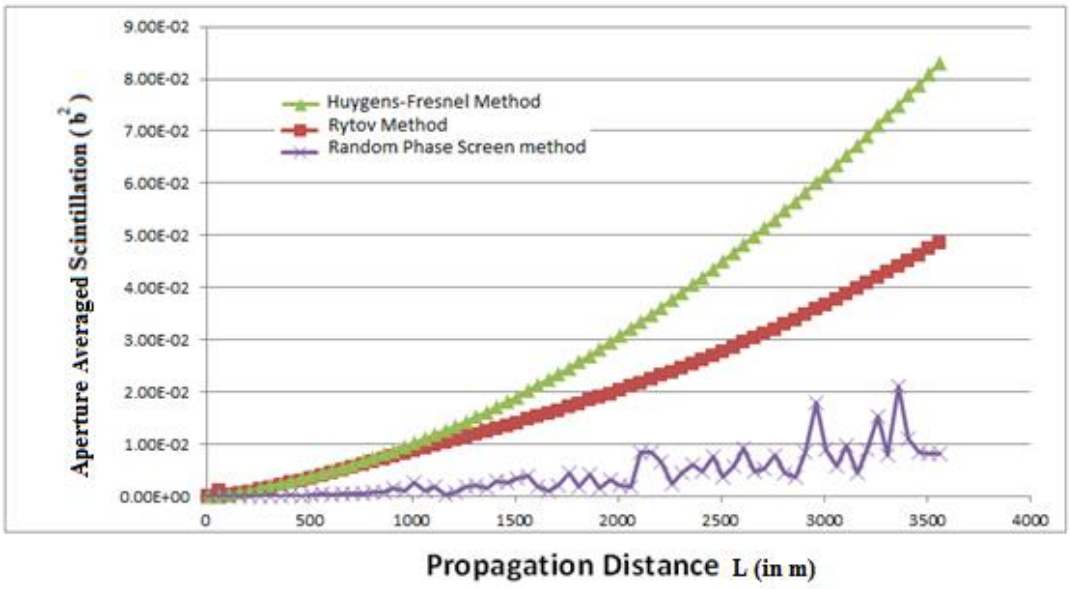

Figure 34: Changes of the SI taking a variety of values of the *n* and *m* parameters for GB beams against the propagation distance

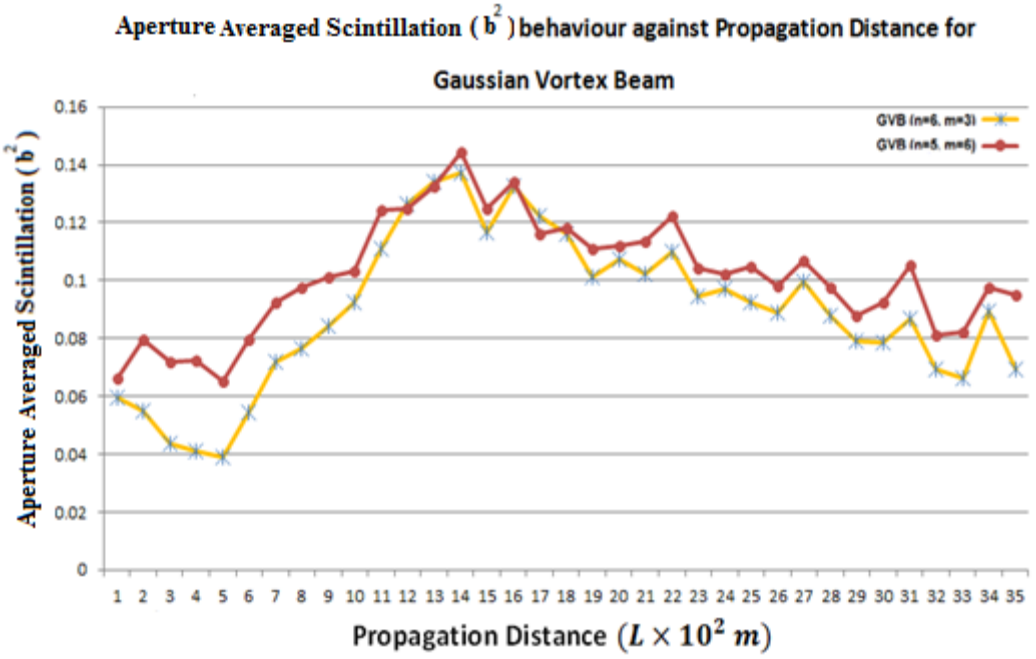

Figure 35: Changes in the SI taking a variety of values of the *n* and *m* parameters for GVB beams against the propagation distance

7.7. The effect of Turbulence on the Average Intensity of the Laguerre Beam

In this section, we explain the variation of values of the receiver intensity in free-space and in turbulence for the Laguerre Gaussian vortex beam with topology charge ($m = 1$, 3, 5 and 7) and degree of polynomial ($n = 1$), Figures 36 and 37 illustrate the behavior of intensity of LGVB against the receiver plane (r_x, r_y) in free-space and in turbulence.

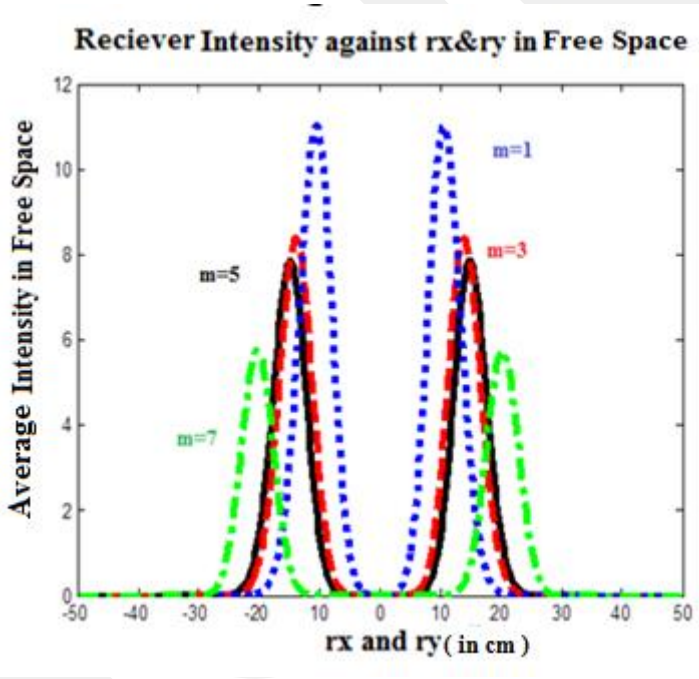

Figure 36: Average Receiver Intensity against r_x and r_y in free space

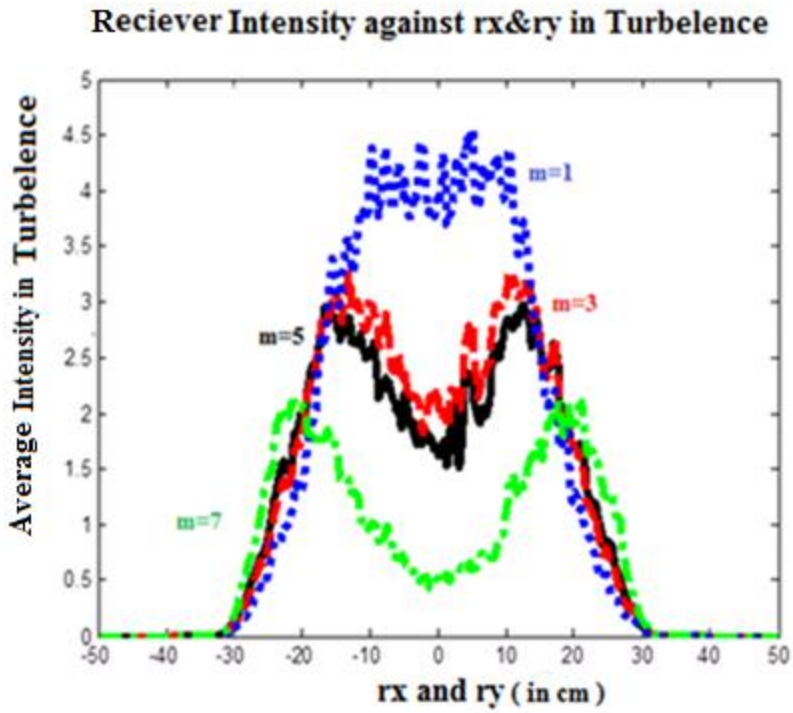

Figure 37: Average Receiver Intensity against r_x and r_y in turbulence

7.8. Effect of Polynomial Parameters of LGVB on Intensities of the Receiver in Free Space.

In this section, we discuss the effect of Laguerre polynomial parameters on free space receiver intensities where, $Irfs1$, $Irfs2$, $Irfs3$ and $Irfs4$ are the free space receiver intensities. To begin, n is adjusted as a constant value and equal to 1, 3, 5 and 7 for each status and set m into different values such as 1, 3, 5 and 7 for each individual case. Tables 4, 5, 6 ,7 and 8 show the effect of the Laguerre polynomial parameters on receiver intensities in free space to yield acceptable values when n = 1 with m = 1, 3, 5 and 7 as shown in Table 4 , n = 7 with m = 1, 3, 5 and 7 as seen in Table 5, and when m = 1 with n = 1, 3, 5 and 7 in Table 6; and n = 7 with m = 1, 3, 5 and 7 in Table 7. Finally, n = 1, 3, 5 and 7 with m = 1, 3, 5, 7 represent the best case in Table 8. Figures 38, 39, 40, 41 and 42 show the variation of receiver intensities of LGVBs in free space by changes in the polynomial parameters of the

Laguerre beam. It becomes evident that when the n and m parameters are the same, the receiver intensities of LGVBs become more separated.

Table 4: Effect of Laguerre polynomial parameters ($n = 1$ and $m = 1, 3, 5$ and 7) on receiver intensities in free space.

Receiver Intensities of LGVBs in Free Space					
Item		$Irfs1$	$Irfs2$	$Irfs3$	$Irfs4$
1	$Irfs1$	**1.0000**			
3	$Irfs2$	**0.6350**	**1.0000**		
5	$Irfs3$	**0.2211**	**0.7316**	**1.0000**	
7	$Irfs4$	**0.0542**	**0.3359**	**0.7882**	**1.0000**

Table 5: Effect of Laguerre polynomial parameters (n = 7 and m = 1, 3, 5 and 7) on receiver intensities in free space

Receiver Intensities of LGVBs in Free Space					
Item		$Irfs1$	$Irfs2$	$Irfs3$	$Irfs4$
1	$Irfs1$	**1.0000**			
3	$Irfs2$	**0.2356**	**1.0000**		
5	$Irfs3$	**0.8987**	**0.9136**	**1.0000**	
7	$Irfs4$	**0.4417**	**0.7172**	**0.9268**	**1.0000**

Table 6: Effect of Laguerre polynomial parameters (n = 1 and m = 1, 3, 5 and 7) on receiver intensities in free space

Receiver Intensities of LGVBs in Free Space					
Item		$Irfs1$	$Irfs2$	$Irfs3$	$Irfs4$
1	$Irfs1$	**1.0000**			
3	$Irfs2$	**0.2356**	**1.0000**		
5	$Irfs3$	**0.0131**	**0.4468**	**1.0000**	
7	$Irfs4$	**0.0004**	**0.0692**	**0.5782**	**1.0000**

Table 7: Effect of Laguerre polynomial parameters (n = 7 and m = 1, 3, 5 and 7) on receiver intensities in free space

Receiver Intensities of LGVBs in Free Space					
Item		*Irfs* 1	*Irfs* 2	*Irfs* 3	*Irfs* 4
1	*Irfs* 1	**1.0000**			
3	*Irfs* 2	**0.5209**	**1.0000**		
5	*Irfs* 3	**0.1099**	**0.6315**	**1.0000**	
7	*Irfs* 4	**0.0143**	**0.2093**	**0.7215**	**1.0000**

Table 8: Effect of Laguerre polynomial parameters (m = n = 1, 3, 5 and 7) on receiver intensities in Free Space

Receiver Intensities of LGVBs in Free Space					
Item		*Irfs* 1	*Irfs* 2	*Irfs* 3	*Irfs* 4
1	*Irfs* 1	**1.0000**			
3	*Irfs* 2	**0.0604**	**1.0000**		
5	*Irfs* 3	**0.0004**	**0.2556**	**1.0000**	
7	*Irfs* 4	**0.0000**	**0.0138**	**0.4446**	**1.0000**

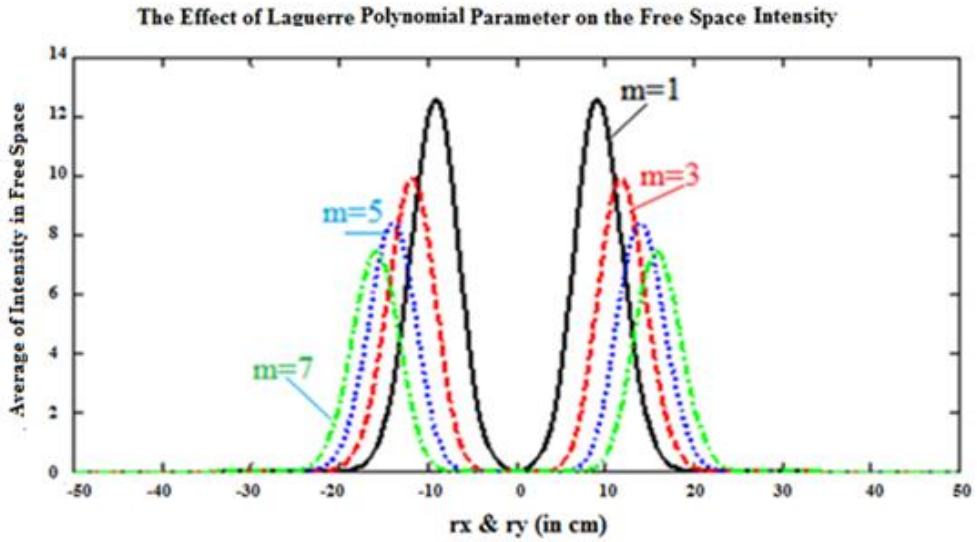

Figure 38: A two-dimensional view of receiver plane intensities of Laguerre Gaussian vortex beam with n = 1 and m = 1, 3, 5 and 7

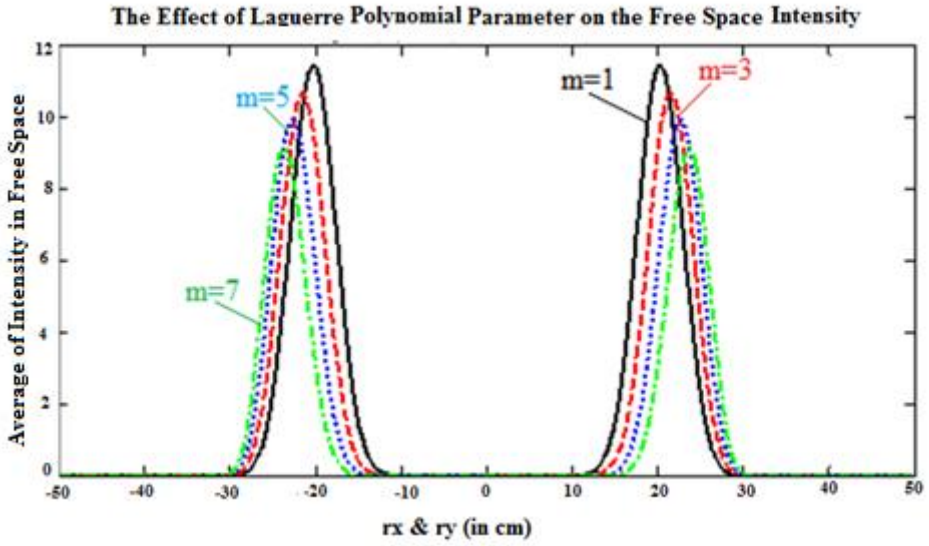

Figure 39: A two-dimensional view of receiver plane intensities of Laguerre Gaussian vortex beam with n = 7 and m = 1, 3, 5 and 7

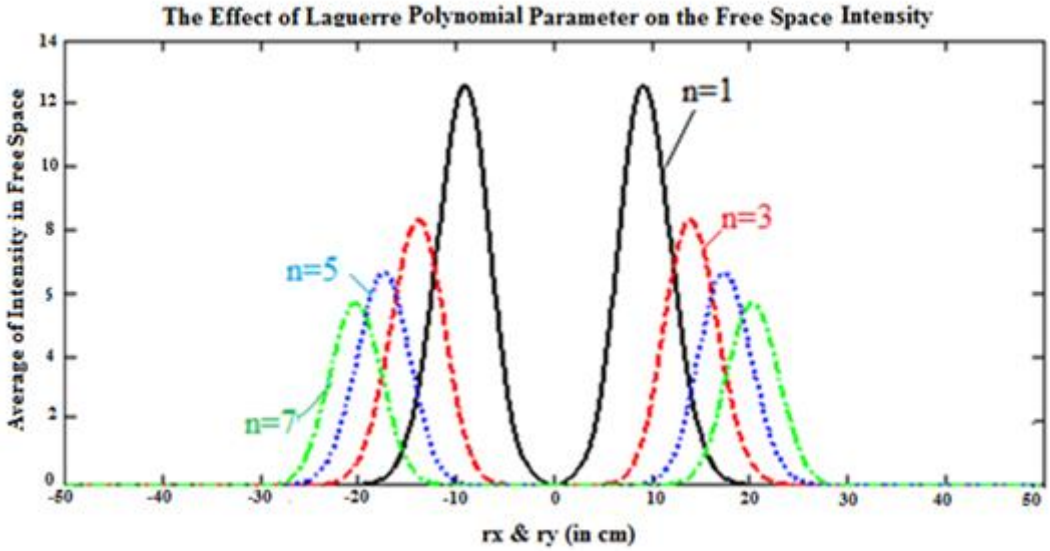

Figure 40: A two-dimensional view of receiver plane intensities of Laguerre Gaussian vortex beam with n = 1, 3, 5 and 7 and m = 1

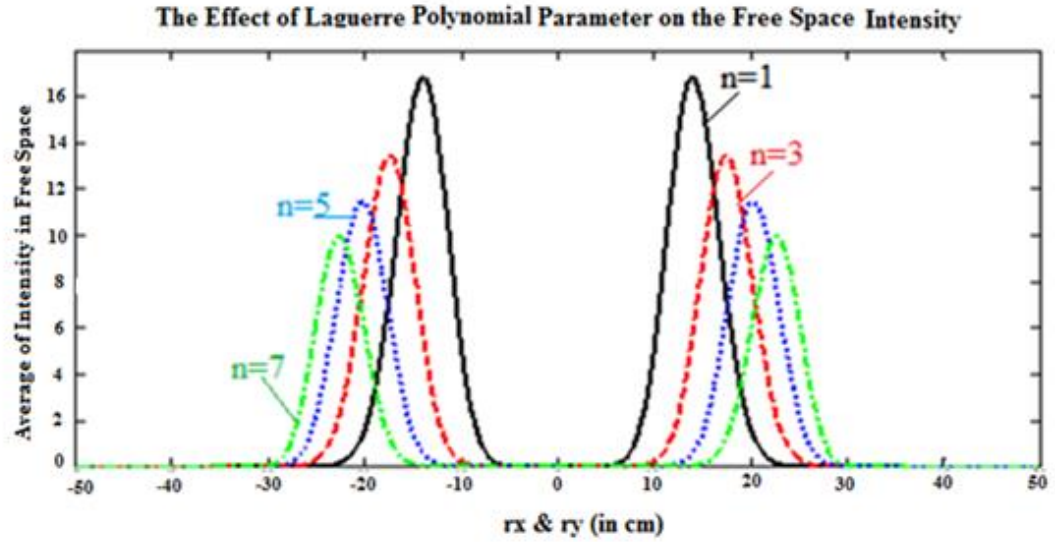

Figure 41: A two-dimensional view of receiver plane intensities of Laguerre Gaussian vortex beam with n = 1, 3, 5, and 7 and m = 7

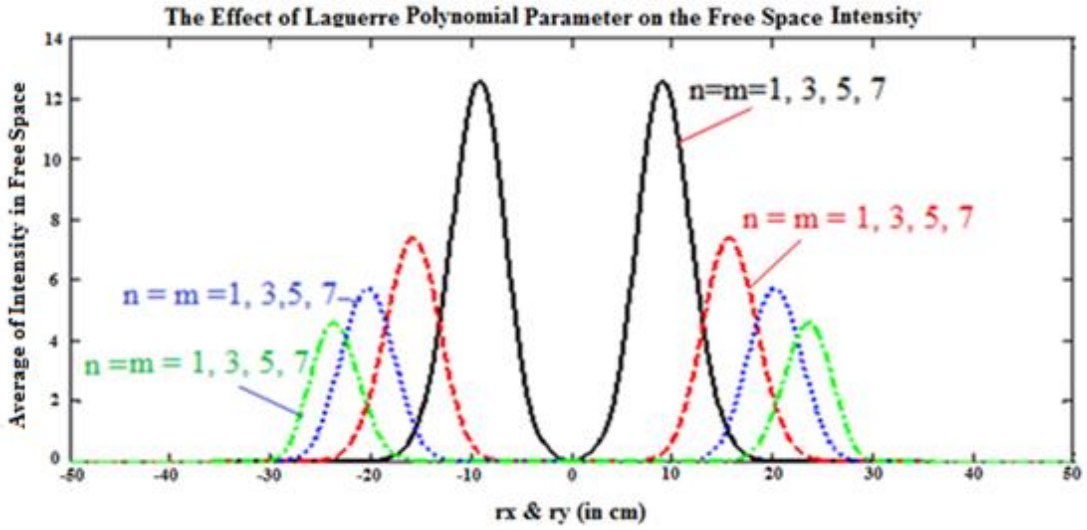

Figure 42: A two-dimensional view of receiver plane intensities of Laguerre Gaussian vortex beam with n = 1, 3, 5, and 7 and m = 1, 3, 5, and 7

7.9. Behavior of the Symbol Error Rate of the Gaussian Vortex Beam for 8-Mary

In this section, we discuss the behavior of Symbol Error Rate of Gaussian vortex beam for 8-Mary. It is clear from Figure 43 that the SER increases when the value of

C_n^2 increases. Finally, we can plot the SER in semi-log against C_n^2. Figure 44 illustrates the behavior of the SER against C_n^2 in semi-log format.

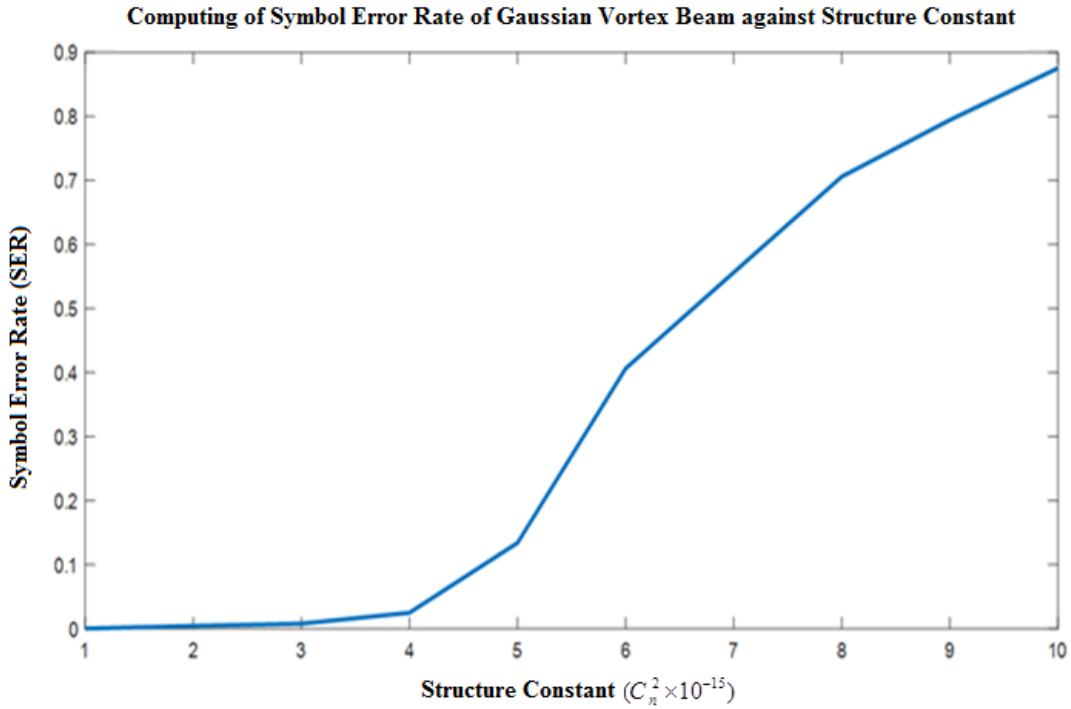

Figure 43: Symbol error rate against the structure constant C_n^2 for 8-Mary

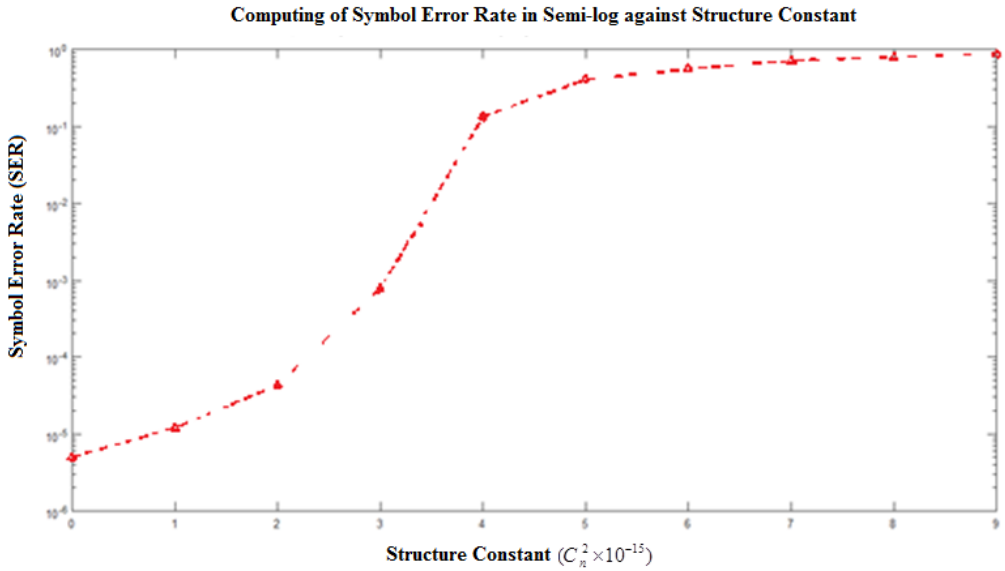

Figure 44: Symbol error rate in semi-log format plotted against the structure constant C_n^2 for 8-Mary.

CHAPTER 8

CONCLUSION AND FUTURE WORK

8.1 Conclusion

Firstly, we used the Gaussian vortex, Elliptical Gaussian vortex and the Laguerre-Gaussian vortex beams in this part of the study as related to the phase distribution approach of the transmitter and receiver. Therefore, computer modeling of the phase distributions of vortex beams were investigated by means of the numerical simulation of propagation through free space. It is expected that these results would be beneficial to optical links, and this work has assisted us to know the phase distribution receiver by changing the numbers of the topological charge, which helps to predict receiver messages in photodetector devices.

Secondly, the scintillation index formulation for the Gaussian beam on a propagation length in a turbulent atmosphere was evaluated. The scintillation index methods were compared so as to select the best approach to describe the phenomenon. The properties of each method, namely Rytov, Huygens-Fresnel and Random Phase Screen, were closely examined. From the graphical outputs, it was observed that the Random Phase Screen method produces an acceptable value of scintillation index

which is near to practical and thus can be regarded as advantageous in the case of a GB, in particular at long propagation lengths.

Thirdly, we constructed and tested the behavior of the scintillation index mechanism, which was devised for an optical system operating with the 7-Mary symbols of the LGVB by changing the polynomial parameters of the Laguerre Function. Then, the random phase screen technique method was used to model the propagation medium of the turbulent atmosphere. Additionally, the Matlab program was used to test any scintillation variation of the LGVB with the degree of the polynomial when the topological charge was fixed to m = 1, 3 and 7 for each case. It can be seen from the results from the previous sections (7.4.1.1, 7.4.1.2 and 7.4.1.3) that the value of the scintillation index increased with an increase in the values of the n and m parameters. In addition, the Matlab program was run again to test the scintillation variation of the LGVB with the topological charge when the degree of the polynomial was fixed to n = 1 and 5 for each case. It can be seen from the results from previous sections (7.4.2.1, 7.4.2.2 and 7.4.2.3) that the value of the scintillation index also increased with an increase in the values of the n and m parameters. Then, the values of the scintillation index variation of the Laguerre-Gaussian beam were near together in the case of changes in the topological charge (m) when the degree of the polynomial (n) was fixed and equal to 1, 3 or 5. In contrast, these values of the SI are far from each other in the case of the topological charge being fixed to m = 1, 3 or 5 and changing the degree of the polynomial (n). In conclusion for this part of the result, the topology charge (m) had a greater effect than the degree of the polynomial (n) on the SI values. Therefore, for a good state of transmission, it is recommended to make the degree of the polynomial n = 1 and the topological charge number change

to 0, 1, 2, 3, 4, 5 and 6 values. Therefore, for a good state of transmission, it is recommended that the degree of the polynomial be made equal to $n = 1$ and the topological charge numbers equal to 0, 1, 2, 3, 4, 5 and 6, such that $(L_1^0, L_1^1, L_1^2, L_1^3, L_1^4, L_1^5, L_1^6)$.

Fourthly, four types of beam, namely the Gaussian, Elliptical, Laguerre and Bessel vortex beams, were selected and measurements of the SI were taken for different values of the *n* and *m* parameters for their beams. Then, we compared among them to select one that would be suitable. Finally, it was found that the Elliptical beam with topological charge equaling 7 and 3 was best.

Fifthly, two types of beams, namely GB and GVB, were chosen and measurements of the SI were taken for the different values of the n and m parameters of the GVB. Then, it was shown that the GVB with the degree of the polynomial and the topological charge equaling values of $n = 6$, $m = 3$ and $n = 5, m = 6$ were better than the GB. Although the SI values of the GB were increasing with an increasing propagation distance, the SI values of the GVB remained between 0.04 and 0.14 with increasing propagation distance.

Sixthly, receiver intensities for LGVB in free space are affected by changes in the polynomial parameters of Laguerre beam. It becomes evident that when n and m are the same, the receiver intensities of LGVB become more separate.

Finally, the SER for GVB for 8-Mary against structure constant is computed, and it has appeared that the SER is increased by the increasing structure constant parameter.

8.2 Future Work

The result of this study presented and established a solid foundation for much future work in the area of optical beam propagation in weak and strong turbulence. However, achieving the desired beam without an SI is still a difficult problem. Some studies may prove fruitful in establishing classes of beam sources that prove more robust while propagating through oceanic turbulence. Other studies have been proposed to satisfy the high value of SNR. Further continuous studies are included in work on the wave structure function in addition to studies on the bit error rate (BER) of a communication channel and enhanced backscatter in laser radar systems.

REFERENCES

[1] Henniger S.D., Epple H.B., Moore C.I., Rabinovich W., Sova R., Young D., (2008), *"Requirements and Challenges for Tactical Free-Space Lasercomm",* IEEE Journals, INSPEC Accession Number 10457523

[2] Juarez J.C., Sluz J.E., Nelson C., Airola M.B., Fitch M.J., Young D.W., Terry D., F.M. Davidson, Rottier J.R., Sova R.M., (2010), *"Free-space optical channel characterization in the maritime environment",* In Proc. SPIE 7685.

[3] Sharma S., (2012), *"A Simplified free-space adaptive optics system against atmospheric turbulence",* International Journal of Electronic, Vol.99, Iss. 3, 417-436.

[4] Al-Habash M.A., (2000), *"The aperture averaged scintillation of the intensity of a Gaussian laser beam propagated through strong optical turbulence and reflected various targets",* USA, Florida.

[5] Lambert S.G., Casey W.L., (1995), *"Laser Communications in Space"*, Artech House, Boston.

[6] **Edelson B.L., Hyde G., (1996)** *"A report of the IEEE-USA Aerospace Policy Committee on laser satellite communications, programs, technology and applications",* IEEE.

[7] **Andrews L.C., Phillips R.L., (2005),** *"Laser Beam Propagation through Random Media",* 2nd. Ed. SPIE, Washington.

[8] **R. Guenther, (1990),** *"Modern Optics",* John Willey & Sons, New York.

[9] **Andrews L.C., Phillips R.L., (1998),** *"Laser beam propagation through random media",* SPIE Press, Bellingham, Washington.

[10] **Zhao Z., Liao R., Lyke S., Roggemann M., (2010),** *"Direct detection free-space optical communications through atmospheric turbulence",* in Proceedings of IEEE Aerospace Conference, Big Sky, Montana, USA, Mar. 6.13, pp. 1-9.

[11] **Bloom S., Korevaar E., Schuster J., Willebrand H., (2003),** *"Understanding the performance of free-space optics [invited]",* Journal of Optical Networking, vol. 2, no. 6, pp. 178-200, [Online]. Available: http://jon.osa.org/abstract.cfm. Last access: 02.01.2018.

[12] **Acampora A., (2002),** *"Last mile by laser",* Scientific American, vol. 287, No. 1, pp. 32-7.

[13] **Hemmati H., (2006),** *"Deep Space Optical Communications",* Hoboken, NJ: John Wiley & Sons.

[14] Kim I.I., Stieger R, Koontz J.A., Moursund C., Barclay M., Adhikari P., Schuster J., Korevaar E., (1998) "*Wireless optical transmission fast Ethernet, FDDI, ATM, and ESCON protocol data using the Terra link laser communication system",* Optical Engineering, Society of Photo-Optical Instrumentation Engineers. Vol. 32, No. 12, pp. 3143-3155.

[15] Kim I.I., Mitchell M., Korevaar E., (1999), *"Measurement of scintillation for free space laser communication at 785nm and 1550nm",* Optical Wireless Communication II, Proc. SPIE. Vol.3850, pp 49-62.

[16] Boucouvalas A.C., (2005), *"Challenges in Optical Wireless Communications",* in Optics & Photonics News, Vol. 16, No. 5, 36.39.

[17] Smolyaninov I.I., Wasiczko L., Cho K., Davis C.C., (2002), *"Long Distance 1.2 Gb/s Optical Wireless Communication Link at 1550 nm in Free-Space Laser",* Proc. SPIE 4489, Free-Space Laser Communication and Laser Imaging, doe: 10.1117/12.453237.

[18] Davis C.C., Smolyaninov I.I., (2002), *"Effect of atmospheric turbulence on bit-error rate in an on-off-keyed optical wireless system",* In Free-Space Laser. *Proc. SPIE* 4489, Free-Space Laser Communication and Laser

[19] Carson M.K., (2007), *"Alexander Graham Bell: Giving Voice to the World",* Sterling Biographies. New York: Sterling Publishing. pp. 76-78. ISBN 978-1-4027-3230-0.

[20] Alexander G.B. (1880), *"On the Production and Reproduction of Sound by Light",* American Journal of Science, Third Series XX (118): 305-324.

[21] Robert O., (1967), *"On Processing Optical Images Propagated Through the Atmosphere",* IEEE Journals & Magazines**.**

[22] Gebhart M., Leitgeb E., Bregenzer J. (2003), *"Atmospheric effects on optical wireless links",* IEEE Journals, INSPEC Accession Number **8106427**

[23] Baykal Y., Eyyuboğlu H.T., (2006), *"Scintillation index of flat-topped-Gaussian beams",* Appl. Opt. 45, 3793-3797.

[24] Eyyuboğlu H.T., (2008), *"Propagation and coherence properties of higher order partially coherent dark hollow beams in turbulence",* Opt. Laser Technol. **40**, 156-166.

[25] Clint T. (2007). *"A 173-mile 2-way all electronic optical contact",* Modulated light web site.

[26] Eyyuboğlu H.T., (2009), *"Concept of area scintillation",* Appl. Phys. B **96**, 301.

[27] Gurvich A.S., Vorob'ev V.V., Fedorova O.V., (2010), *"Strong scintillation spectra behind the atmosphere with large- and small-scale in homogeneities",* Springer.

[28] Pan P., Zhang B., Qiao N., Dan Y., (2011), *"Propagation properties of flat-topped beams in a turbulent atmosphere",* Journal of Modern Optics.

[29] Gilberto K., Vítor G., Cruz A.R., (2013), *"Evaluation of the strong turbulence impact over free-space optical links",*vol. 305, pp. 42-47.

[30] Yang, L., Gao X., Slim M., (2014), *"Performance Analysis of Free-Space Optical Communication Systems with Multiuser Diversity Over Atmospheric Turbulence Channels",* IEEE, Vol 6, No. 2.

[31] Xiumin G., Jian W., Lingling S. *"Hyperbolic-cosine-Gaussian beam focusing with a non-spiral vortex and a spiral vortex",*

[32] Mansour A., Mesleh R., Abaza M., (2017), *"New challenges in wireless and free space optical communications",* ScienceDirect, Vol 89, pp. 1-202.

[33] Siegman A., (1986), *"Lasers",* University Science, Mill Valley, Calif.

[34] Eyyuboğlu, H.T., *"Free space propagation notes",* [Online]. Available: http://ece635.cankaya.edu.tr/uploads/files/ECE%20635_Free%20space%20propagation%20notes_Eylul%202011_HTE.pdf, Last access: 02.01.2018.

[35] Eyyuboğlu, H.T., *"Theoretical Formulations and Simulations",* [Online]. Available:http://ece646.cankaya.edu.tr/uploads/files/Notes%20of%20ECE%20646_HTE_Bahar%202012.pdf, Last access: 25.01.2018.

[36] Andrews L.C., Miller W.B., (1995), "*Single-pass and double-pass propagation through complex paraxial optical systems",* J. Opt Soc. Am. A 12, 137-150.

[37] Kampen V., (1976), *"Stochastic differential equations", Physics* Reports, Section C of Physics Letters, 24, 171-228.

[38] Strohbehn J.W., (1978), *"Laser Beam Propagation in the Atmosphere",* Springer, New York.

[39] Sobczyk K., (1985), *"Wave Propagation",* Elsevier, Amsterdam.

[40] Chernov L.A., (1960), *"Wave Propagation in a Random Medium",* McGraw-Hill, New York, trans. by R.A. Silverman.

[41] Ishimaru A., (1997), *"Wave Propagation and Scattering in Random Media",* IEEEPress, Piscataway, New Jersey, previously published as Vols I & II by Academic, New York.

[42] Rytov S.M., Kravtsov Yu. A., Tatarskii V.I., (1989), *"Principles of statistical radio physics in Wave Propagation through Random Media",* Springer, Berlin, Vol. 4.

[43] Parry G., Pusey P.N., (1979), *"K distributions in atmospheric propagation of laser light",* J. Opt. Soc. Am. 69, 796-798.

[44] Rytov S.M., (1937), *"Diffraction of light by ultrasonic waves",* Izvestiya Akademii Nauk SSSR, Seriya Fizicheskaya (Bulletin of the Academy of Sciences of the USSR, Physical Series) 2, 223-259.

[45] Obukhov A.M., (1953), *"Effect of weak in homogeneities in the atmosphere on sound and light propagation",* Izv. Acad. Nauk SSSR, Ser. Geofiz, 2, 155-165.

[46] Tatarskii V.I., (1971), *"The Effects of the Turbulent Atmosphere on Wave Propagation",* trans. from the Russian and issued by the National Technical Information Office, U.S. Dept. of Commerce, Springfield.

[47] Yura H.T., Sung C.C., Clifford S.F., Hill R.J., (1983), *"Second-order Rytov approximation",* J. Opt. Soc. Am. 73, 500-502.

[48] Tatarskii V.I., (1961), *"Wave Propagation in a Turbulent Medium",* McGraw-Hill, New York.

[49] Yura H.T., Hanson S.G., (1989), *"Second-order statistics for wave propagation through complex optical systems",* J. Opt. Soc. Am. A **6**, 564-575.

[50] Lawrence R.S., Strohbehn J.W., (1970) *"A survey of clear-air propagationeffects relevant to optical communications",* Proc. IEEE 58, 1523-1545.

[51] Prokhorov A.M., Bunkin F.V., Gochelashvily K.S., Shishov V.I., (1975) *"Laser irradiance in turbulent media",* Proc. IEEE 63, 790-809.

[52] Fante R.L., (1975), *"Electromagnetic beam propagation in turbulent media",* Proc. IEEE 63, 1669-1692.

[53] Fante R.L., (1980), *"Electromagnetic beam propagation in turbulent media: An update",* Proc. IEEE 68, 1424-1443.

[54] Uscinski B.J., (1977), *"The Elements of Wave Propagation in Random Media",* McGraw-Hill, New York.

[55] Zuev V.E., (1982), *"Laser Beams in the Atmosphere",* Consultants Bureau, New York.

[56] Tatarskii V.I., Ishimaru A., Zavorotny V.U., eds., (1993), *" Wave Propagation in Random Media (Scintillation)",* (SPIE Optical Engineering Press, Bellingham, Wash.; Institute of Physics Pub., Techno House, Bristol, England

[57] Sasiela R.J., (1994), *"Electromagnetic Wave Propagation in Turbulence",* (Springer, New York,).

[58] Andrews L.C., Phillips R.L., Hopen C.Y., (2001), *"Laser Beam Scintillation with Applications",* (SPIE Press, Bellingham,).

[59] Wheelon A.D., (2001), *"Electromagnetic Scintillation I. Geometrical Optics",* (Cambridge University Press, Cambridge, UK,).

[60] Wheelon A.D., (2003), *"Electromagnetic* Scintillation II. Weak Scattering*",* (Cambridge University Press, Cambridge, UK,).

[61] Eyyuboğlu H.T., Arpali C., Baykal Y.K., (2006), *"Flat topped beams and their characteristics in turbulent media",* Opt. Express **14**(10), 4196-4207.

[62] Eyyuboğlu H.T., (2007), *"Propagation of higher order Bessel-Gaussian beams in turbulence",* Appl. Phys. B **88**(2), 259-265.

[63] Cai Y., (2006), *"Propagation of various flat-topped beams in a turbulent atmosphere",* J. Opt. A, Pure Appl. Opt. **8**(6), 537-545.

[64] Cai Y., He S., (2006), *"Propagation of a partially coherent twisted anisotropic Gaussian Schell-model beam in a turbulent atmosphere",* Appl. Phys. Lett. **89**(4), 041117-0411173.

[65] Eyyuboğlu H.T., Baykal Y., Sermutlu E., (2006), *"Convergence of general beams into Gaussian intensity profiles after propagation in turbulent atmosphere",* Opt. Com. **265**(2), 399-405.

[66] Cai Y., He S., (2006), *"Average intensity and spreading of an elliptical Gaussian beam propagating in a turbulent atmosphere",* Opt. Lett. **31**(5), 568-570.

[67] Alavinejad M., Ghafary B., Kashani F.D., (2008), *"Analysis of the propagation of flat-topped beam with various beam orders through turbulent atmosphere",* Opt. Lasers Eng. **46**(1), 1-5.

[68] Yuan Y., Cai Y., Qu J., Eyyuboğlu H.T., Baykal Y., (2009), *"Average intensity and spreading of an elegant Hermite-Gaussian beam in turbulent atmosphere",* Opt. Express **17**(13), 11130-11139.

[69] Gibson G., Courtial J., Padgett M., Vasnetsov M., Pas'ko V., S. Barnett, Franke-Arnold S., (2004), *"Free-space information transfer using light beams carrying orbital angular momentum",* Opt. Express **12**(22), 5448-5456.

[70] Paterson C., (2005), *"Atmospheric turbulence and orbital angular momentum of single photons for optical communication",* Phys. Rev. Lett. **94**(15), 153901.

[71] Čelechovský R., Bouchal Z., (2007), *"Optical implementation of the vortex information channel",* N.J. Phys. **9**(9), 328-333.

[72] Gbur G., Tyson R.K., (2008), *"Vortex beam propagation through atmospheric turbulence and topological charge conservation",* J. Opt. Soc. Am. A **25**(1), 225-229.

[73] Ji X., (2008), Opt. Com. 281, 3407.

[74] Cai Y., He S., (2006), Opt. Express 14, 1353.

[75] Ji X., Huang T., Lu B., (2006), Acta Phys. Sin. 55, 978.

[76] Eyyuboğlu H.T., Baykal Y., (2004), Opt. Express 12 4659.

[77] Polynkin P., Peleg A., Klein L., Rhoadarmer T., Moloney J., (2007), Opt. Lett 32 885.

[78] Cai Y., Lin Q., Baykal Y., Eyyuboğlu H.T., (2007), Opt. Com. 278, 157.

[79] Du X.Y., Zhao D.M., Korotkova O., (2007), Opt. Express 15, 16909.

[80] Eyyuboğlu H.T., Sermutlu E., Baykal Y., Cai Y., Korotkova O., (2008), Appl. Phys. B 93, 605.

[81] Eyyuboğlu H.T., Baykal Y., E. Sermutlu, Cai Y., (2008), Appl. Phys. B 92, 229.

[82] Chavez G.V., Dholakia K., Lee W.M., (2006), Opt. Express 14 7436.

[83] Helseth L.E., (2004), Opt. Com. 229, 85.

[84] Gbur G., Visser T.D., (2006), Opt. Com. 259, 428.

[85] Rao L., Pu J., (2007), Chin. Phys. Lett. 24, 1252.

[86] Xie Q., Zhao D., (2008), Opt. Com. 281, 7.

[87] Sztul H.I., Alfano R.R., (2006), Opt. Lett. 31, 999.

[88] Dennis M.R., O'Halloran K., (**2009)**. *"Singular optics: optical vortices and polarization singularities",* Progress in Optics. 293-363.

[89] Aksenov V.P., Pogutsa, Ch.E., (**2008),** *"Fluctuations of the orbital angular momentum of a laser beam, carrying an optical vortex, in the turbulent atmosphere",* Quantum Electron., 38(4), 343-348.

[90] Gbur, G., (**2008)**, *"The evolution of vortex beams in atmospheric turbulence",* Proc. SPIE 6878, 687804.

[91] Wang T., Pu J., Chen Z., (2009), *"Beam-spreading and topological charge of vortex beams propagating in a turbulent atmosphere",* Opt. Com. 282(7), 1255-1259.

[92] Gracheva, M.E., Gurvich, A.S., (1965) *"Strong fluctuations in the intensity oflight propagated through the atmosphere close to the earth*", Izvestiya VUZ. Radiofizika **8**, 717-724.

[93] Vetelino F.S., Andrews L.C., (2004).), *"Annular Gaussian beams in turbulent media",* in Free-Space Laser Communication and Active Laser Illumination III, Proc. SPIE 5160, 86-97

[94] Patrushev G. Ya., (1978), *"Fluctuations of the field of a wave beam on reflection in a turbulent atmosphere",* Sov. J. Quantum Electron. 8, 1315-1318.

[95] Miller W.B., Ricklin J.C., Andrews L.C., (1994), "*Effects of the refractive index spectral model on the irradiance variance of a Gaussian beam",* J. Opt. Soc. Am. A. 11, 2719-2726.

[96] Andrews L.C., Phillips R.L., Hopen C.Y., Al-Habash M.A., (1999), "*Theory of optical scintillation",* J. Opt. Soc. Am. A 16, 1417-1429.

[97] Andrews L.C., Al-Habash M.A., Hopen C.Y., Phillips R.L., (2001), "*Theory of optical scintillation: Gaussian-beam wave model",* Waves Random Media 11, 271-291.

[98] Ricklin J.C. Davidson F.M., (2003), "*Atmospheric optical communication with a Gaussian-Schell beam",* J. Opt. Soc. Am. A 20, 856-866.

[99] Vetelino F.S., Young C., Andrews L.C., Grant K., Corbett K., Clare B., (2005), *"Scintillation: theory vs. experiment in Atmospheric Propagation II",* Proc. SPIE 5793, 166-177.

[100] Korotkova O., (2006), *"Control of the intensity fluctuations of random electromagnetic beams on propagation in weak atmospheric turbulence",* in Free-Space Laser Communication Technologies XVIII, Proc. SPIE 6105, 61050V.

[101] Ishimaru A., (1978), "Wave Propagation and Scattering in Random Media*",* (Academic,), Vol. 2.

[102] Herman B.J., Strugala L.A., (1990), *"Method for inclusion of low-frequency contributions in numerical representation of atmospheric turbulence",* Proc. SPIE 1221, pp. 183.192.

[103] Johansson E.M., Gave D.T. l, (1994), *"Simulation of stellar speckle imaging",* Proc. SPIE 2200, pp. 372.383.

[104] Sedmak G., (1998), *"Performance analysis of and compensation for aspect-ratio effects of fast-Fourier-transform-based simulations of large atmospheric wave fronts",* Appl. Opt. 37, pp. 4605.4613.

[105] Belmonte A., (2000), *"Feasibility study for the simulation of beam propagation: consideration of lidar performance",* Applied Optics; 39(30): 5426-45.

[106] Schmidt J.D., (2010), *"Numerical Simulation of Optical Wave Propagation with examples in MATLAB",* Washington: SPIE Press.

[107] Voelz D., (2011), *"Computational Fourier Optics A MATLAB Tutorial",*Washington: SPIE Press.

[108] Eyyuboğlu, H.T., *"Notes on the use of Angular Spectrum Model and Random Phase Screen",* [Online]. Available: http://ece646.cankaya.edu.tr/upload/files/ECE%20646_Notes%20on%Angular%20 Spectrum%20and%20RPS_HTE_Bahar%202014.pdf, Last access: 04.02.2018.

[109] Beijersbergen M.W., Coerwinkel R.P.C., Kristensen M., Woerdman J.P. (**1994**), *"Helical-wave front laser beams produced with a spiral phase plate",* Opt.Com.112-321B

[110] Kang M., Chen J.; Wang X.L., Wang H.T., (2012), *"Twisted Vector Field from an Inhomogeneous and Anisotropic Metamaterial",* J. Opt. Soc. Am. B. 29 (4): 572-576.

[111] Yan Y., (2014), *"High-capacity millimeter-wave communications with orbital angular momentum multiplexing",* Nature Communications. **5**: 4876.

[112] Chen Z., Li C., Ding P., Pu J. (2012), Appl. Phys. B. 107, 469-472.

[113] Lukin V.P., Konyaev P.A., Sennikov V.A. (2012), Appl. Opt.51, C84-C87

[114] Wang T., Pu, J., Chen, Z. (2009), Opt. Com., 282, 1255-1259.

[115] Liu X., Pu J. (2011), Opt. Exp. 19, 26444-26450.

[116] Liu D., Wang Y., Yin H. (2015), Appl. Opt. 54, 10510-10516.

[117] Dheyab A.A., (2018), *"Phase Distribution Behavior with Multi-Values of Topology Charge of Vortex Beams",* Ciencia e Tecnica Vitivinicola, ISSN: 0254-0223.

[118] Eyyuboğlu, H.T., Baykal Y., (2007), *"Scintillation characteristics of cosh-Gaussian beams",* Appl. Opt. (46), 1099-1106.

[119] Eyyuboğlu, H.T., Baykal Y., Cai Y., (2010), *"Scintillation calculations for partially coherent general beams via extended Huygens-Fresnel integral and self-designed Matlab function",* Appl. Phys. B100: 597-609.

[120] Eyyuboğlu, H.T., (2013), *"Estimation of aperture averaged scintillations in weak turbulence regime for annular, sinusoidal and hyperbolic Gaussian beams using random phase screen",* Op. & Laser Tech. 52: 96-102

[121] Dheyab A.A., (2018), *"Studying Methods of Computing the Scintillation Index of Gaussian Beam",* Ciencia e Tecnica Vitivinicola, ISSN: 0254-0223.

APPENDIX

CURRICULUM VITAE

PERSONAL INFORMATION

Name, Surname: ALI ABDULRAHMAN DHYEAB AL-SAJEE

Date and Place of Birth: 11 July 1970, Iraq/Baghdad

Marital Status: Married

Phone: +90 531 913 86 89

Email: alidiab70@yahoo.com

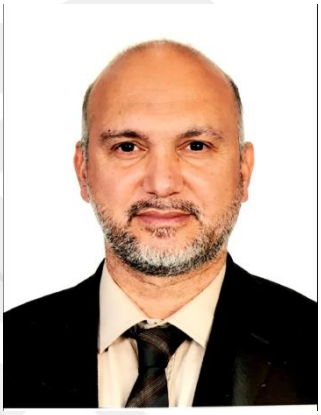

EDUCATION

Degree	Institution	Year of Graduation
M.Sc.	Technology Univ., Electrical and Electronic Department, Baghdad, Iraq.	2005
B.Sc.	University of Baghdad, Engineering College, Iraq, Baghdad	1994
High School	Al-Karkh Secondary School	1988

WORK EXPERIENCE

Year	Place	Enrollment
1994-2003	Saad Company / Engineering Design Center	Official Job
2003-2006	General System Company	Designer
2006-2018	Ministry of Higher Education & Scientific Research	Lecturer

FOREIGN LANGUAGES:

Arabic Native, Advanced English and Turkish

PROJECTS:

Fiber optics, Networks, GIS and CISCO

HOBBIES:

Reading, Swimming, Travelling, Boxing and Fitness